MEASUREMENT AND MODELING OF THERMODYNAMIC AND KINETIC DATA OF MEMBRANE-FORMING SYSTEMS

A Thesis Submitted to
The Graduate School of Engineering and Science of
İzmir Institute of Technology
in Partial Fulfillment of the Requirements for the Degree of

MASTER OF SCIENCE

in Chemical Engineering

by
Mine Özge ARSLAN

September 2007
İZMİR

We approve the thesis of **Mine Özge ARSLAN**

Date of Signature

……..... **14 September 2007**

Assoc. Prof. Dr. Sacide ALSOY ALTINKAYA

Supervisor

Department of Chemical Engineering

İzmir Institute of Technology

……..... **14 September 2007**

Assoc. Prof. Dr. Funda TIHMINLIOĞLU

Department of Chemical Engineering

İzmir Institute of Technology

……..... **14 September 2007**

Assoc. Prof. Dr. Metin TANOĞLU

Department of Mechanical Engineering

İzmir Institute of Technology

……..... **14 September 2007**

Prof. Dr. Devrim BALKÖSE

Head of Department

İzmir Institute of Technology

……

Prof. Dr. M. Barış ÖZERDEM

Head of Graduate School

ACKNOWLEDGEMENTS

I would like to thank to my advisor, Assoc. Prof. Dr. Sacide ALSOY ALTINKAYA for her guidance, encouragement, trust, support and neverending optimism during my thesis study. I have learned a lot of things from her, not only academically. She means more than an advisor for me.

My special thanks go to Yılmaz Yurekli. Without his help, I would never able to finish my studies. I would like to thank him for his support, help and especially for his patience.

I also express my special thanks to Seyhun Gemili and İsa Atik Doğan for their valuable technical help and friendship.

I would like to express my special thanks to Dane Ruscuklu, Diren Kacar and Gözde Genc for their encouragement, support and neverending friendship during not only my thesis but also my whole life.

I also would like to thank to my friends Senem Yetgin, Hasan Demir, Ali Emrah Çetin, Rojda Aslan, Seçil Çoban, Selahattin Umdu, Alev Güneş, Filiz Yaşar Mahliçli, Ahmet Kuru and Ülger Erdal for their unconditional help, friendship, encouragement and motivation.

And finally, I would like to thank to my family for their unconditinal support during my thesis and my life. I would like to thank them, especially to my father for letting met to draw my own way in my life and always supporting me.

ABSTRACT

MEASUREMENT AND MODELING OF THERMODYNAMIC AND KINETIC DATA OF MEMBRANE-FORMING SYSTEMS

Phase inversion process involving a ternary system (nonsolvent/solvent/ polymer) is frequently used to prepare porous and asymmetric polymeric membranes. The thermodynamic and kinetic data for the ternary system are required to understand membrane formation mechanisms, change the preparation conditions and predict the final structure of the membranes. In this study, cloud point curves for polysulfone (PSf)/1-methyl-2-pyrrolidinone (NMP)/water, PSf/tetrahydrofurane (THF)/water, PSf/NMP/ ethanol, PSf/THF/ethanol, polymethyl methacrylate (PMMA)/acetone/water, PMMA/ THF/water, PMMA/acetone/formamide and PMMA/THF/formamide systems were measured by titrating polymer solutions with nonsolvents until the onset of turbidity. Binodal curves were calculated by using the Flory Huggins theory with constant interaction parameters. Theoretical ternary phase diagrams were found to be in good agreement with experimental cloud point data. In addition to liquid liquid equilibrium data, sorption isotherms and diffusion coefficients of water, ethanol and chloroform were measured by using a magnetic suspension balance. Results of kinetic studies have shown that water sorption in PSf films exhibits Fickian diffusion while anomalous diffusion is observed for ethanol and chloroform sorption. The kinetic data for water sorption was analyzed using a simple Fickian diffusion model to determine the diffusion coefficients. On the other hand, anamalous sorption kinetics were interpreted by a mathematical model involving independent contributions from Fickian diffusion and polymer relaxations. The model successfully fits non-Fickian anomalies including sorption overshoot and allows to determine diffusion coefficients and relaxation times. Diffusivities of penetrants in PSf was found to decrease in the following order: Water > Chloroform > Ethanol. Equilibrium sorption isotherms of ethanol and chloroform are well described by classical Flory Huggins thermodynamic theory with constant interaction parameters. A modified version of this theory for concentration dependent interaction parameter is used to correlate the sorption isotherm of water. Vrentas Duda free volume theory is able to correlate diffusivity data of water collected at 30°C and 40°C while the theory fails to correlate the diffusivities of ethanol and chloroform both of which were determined from diffusion-relaxation model.

ÖZET

MEMBRAN OLUŞTURAN SİSTEMLERİN KİNETİK VE TERMODİNAMİK VERİLERİNİN ÖLÇÜLMESİ VE MODELLENMESİ

Gözenekli ve asimetrik polimerik membranların hazırlanmasında, üçlü sistemleri (çözücü olmayan/çözücü/polimer) de içeren faz dönüşümü yöntemi kullanılır. Üçlü sistemler için termodinamik ve kinetik data, membran oluşum mekanizmalarının anlaşılması, membran hazırlama koşullarının değiştirilmesi, ve membran yapılarının tahmin edilebilmesi için gereklidir. Bu çalışmada, polisülfon (PSf)/1-metil-2-pirolidinon (NMP)/su, PSf/tetrahidrofuran (THF)/su, PSf/NMP/etanol, PSf/THF/etanol, polimetilmetakrilat (PMMA)/aseton/su, PMMA/THF/su, PMMA/aseton/formamid ve PMMA/THF/formamid sistemlerine ait bulanım noktaları, polimer çözeltilerinin, çözücü olmayan bileşenler ile çözeltide bulanıklık gözlemlenene kadar titrasyonuyla ölçülmüştür. Binodal eğrileri, sabit etkileşim parametreleri kullanılan Flory Huggins teorisiyle hesaplanmıştır. Teorik olarak hesaplanan binodal eğrilerinin, deneysel bulanım noktaları ile uygunluk gösterdiği bulunmuştur. Sıvı sıvı denge datasına ilaveten; su, etanol ve kloroformun denge izotermleri ve difüzyon katsayıları manyetik askılı terazi kullanılarak bulunmuştur. Kinetik çalışmaların sonucu göstermiştir ki, suyun polisülfon içindeki difüzyonu Fickian difüzyon göstermektedir; öte yandan etanol ve kloroformun difüzyonunda non-Fickian difüzyon gözlenmiştir. Difüzyon katsayılarını elde etmek için, su sorpsiyonuna ait kinetik data, Fickian difüzyon modeli kullanılarak analiz edilmiştir. Non-Fickian sorpsiyon kinetikleri ise polimer rölaksasyonları ve Fickian difüzyonunu içeren matematiksel bir modelle yorumlanmıştır. Sorpsiyon overshootlarını da içeren non-Fickian sorpsiyonu başarılı bir şekilde modellenmiştir ve model, difüzyon katsayılarının ve rölaksasyon zamanlarının elde edilebilmesini sağlamıştır. Penetrantların polisülfon içindeki difüzivitelerinin şu sırada azaldığı bulunmuştur: Su > Kloroform > Etanol. Etanol ve kloroformun denge izotermleri, sabit etkileşim parametreleri kullanılan klasik Flory Huggins termodinamik teorisi ile başarılı bir şekilde tanımlanmıştır. Bu teorinin konsantrasyona bağımlı etkileşim parametreleri için modifiye edilmiş versiyonu, suya ait denge izotermlerinin ilişkilendirilmesinde kullanılmıştır. Vrentas Duda free volume teorisi, 30°C ve 40°C'deki suya ait difüzyon datasına uygulanabilmiştir fakat etanol ve kloroformun difüzyon datasına uygulanabilirliği başarılı olmamıştır.

TABLE OF CONTENTS

LIST OF FIGURES

LIST OF TABLES

LIST OF SYMBOLS

V^*	Minimum hole size into which molecule can jump
V^f	The average hole free volume per sphere
A	The proportionality constant
γ	The overlap factor to account for the overlap between free volume elements
D_1	Solvent self diffusion coefficient in a polymer solution (cm^2/s)
D_0	Constant preexponential factor
D	Mutual diffusion coefficient (cm^2/s)
E	Activation energy per mole that a molecule needs to overcome attractive forces holding it to its neighbors (J/mole.K)
$\hat{V}_i^*$	Specific critical hole free volume required for a diffusive jump of the component i (cm^3/g)
R	Universal gas constant (cal/mol.K)
$\hat{V}_{FH}$	Specific hole free volume of the polymer-solvent mixture (cm^3/g)
Tg_i	Glass transition temperature of component i (K)
Q	Thermodynamic factor
$\hat{V}_1^*$, $\hat{V}_2^*$	Specific volumes of the solvent and polymer at 0 K (cm^3/mol)
K_{11}	Solvent free volume parameter ($cm^3/g.K$)
K_{21}	Solvent free volume parameter (K)
K_{12}	Polymer free volume parameter ($cm^3/g.K$)
K_{22}	Polymer free volume parameter (K)
C_{12}^{WLF}, C_{22}^{WLF}	WLF constants
a_t	Shift factor
G′	Loss modulus
G″	Storage modulus
$\tilde{V}_1^\circ(0)$, $\tilde{V}_{2j}^*$	Solvent molar volume at 0 K and the molar volume of the polymer jumping unit
M_1	Molecular weight of the solvent (g/mol)
$\tilde{V}_c$	Molar volume of the solvent at its critical temperature (cm^3/mol)
$\hat{V}_1$	Molar volume of the pure solvent (cm^3/g)
P_1	Vapor pressure of the solvent at T (atm)

P_1^{sat}	Saturation vapor pressure of the solvent at the column temperature (atm)
Δf	Crystal frequency shift
K	Proportionality constant
χ_{13}	Flory Huggins nonsolvent/polymer interaction parameter
χ_{23}	Flory Huggins solvent/polymer interaction parameter
g_{12}	Flory Huggins nonsolvent/solvent interaction parameter
ν_i	Molar volume of component i
δ_2 , δ_3	Solubility parameter of solvent and polymer ($cal^{1/2}/cm^{3/2}$)
M_t, M_∞	Penetrant mass uptake at time t and at equilibrium (g)
L	Film thickness (cm)
C_0	Concentration of the penetrant in the polymer at time t = 0 (g/cm^3)
C_{eq}	Concentration of the penetrant at the surface at time t > 0 (g/cm^3)
$M_{\infty,i}$	Equilibrium sorption due to the *i*th relaxation process (g)
k_i	First-order relaxation constant of the *i*th relaxation process
α_R	Fraction of weight uptake controlled by polymer relaxation
τ_R	Time constant characterizing the long time drift in mass uptake toward equilibrium (sec)
t_D	Delay factor associated with a delay in the beginning of structural relaxation (sec)
β	Inverse of the characteristic time for attaining saturation at the surface
λ_m	Relaxation time for the polymer-solvent systems
θ_D	Characteristic diffusion time
De	Deborah number
η_1, η_2	Viscosity of the solvent and polymer (g/cm.s)
ξ	Ratio of molar volume of the solvent jumping unit to that of the polymer jumping unit
ωi	Weight fraction of the component i
ϕi	Volume fraction of the component i
μi	Chemical potential of the component i
N_a, N_b	Mole fraction of component a and b
k_a, k_b	Uptake rate constants for pure liquid a or b
t	Time (sec)

CHAPTER 1

INTRODUCTION

Polymeric membranes are widely used in pharmaceutical, chemical, biomedical, food and biotechnology industries for different separation purposes. Several methods are used for producing polymeric membranes, however phase inversion method invented by Loeb and Sourirajan in 1962, is the most common method. In this method, an initially homogeneous polymer solution thermodynamically becomes unstable due to different external effects and phase separates into polymer lean and polymer rich phases.

The kinetics and thermodynamics of the phase separation process have important roles in determining the final structure of the membranes. Depending on the evaporation/quenching conditions, initial thickness and composition of the polymer solution, various membrane stuctures ranging from dense to highly asymmetric ones can be obtained. Membrane preparation conditions, thus, membrane formation process and morphology can be optimized by using reliable mathematical models which require both thermodynamic and diffusivity data (Alsoy Altinkaya and Ozbas 2004). Information about ternary phase diagrams describing the equilibrium behavior of liquid-liquid phase separation is also important and needed for studying membrane formation mechanisms (Lai et al. 1998).

Experimentally, phase diagrams are constructed using cloud point curves. The method of titrating polymer solutions with nonsolvents is generally in use for the determination of cloud point curves (onset of turbidity as function of composition) (Schneider et al. 2002). The amounts of nonsolvents required to bring the onset of turbidity are measured and at the onset of turbidity, the volume fractions of nonsolvent, solvent and polymer represent the cloud points in a ternary phase diagram. Various techniques have been used for the measurement of diffusivity of polymer solvent systems such as inverse gas chromatography (IGC), pressure decay method, FTIR-ATR spectrophotometry and sorption measurements either gravimetric or piezoelectric. Kleinrahm and Wagner (1986) developed a unique balance, so-called a magnetic suspension balance (MSB), which is one of the most reliable and sensitive apparatus among other gravimetric sorption equipments such as quartz spring balance or Cahn

electrobalance. By using this device, the measuring force is transmitted contactlessly from the measuring chamber to the microbalance. The weight change of the sample is obtained in the range of micrograms as a function of time.

In this study, polysulfone (PSf) and polymethylmethacrylate (PMMA) have been selected due to their excellent chemical resistance, mechanical strength, thermal stability and transport properties, hence, their frequent use as membrane materials. There are a few reports presenting the experimental phase diagrams in ternary mixtures of PSf/solvent/water (Altena and Smolders 1982, Kim et al. 1997, Barth and Wolf 2000). The solvents studied are dimethylacetamide (DMAc), NMP, dimethylformamide (DMF) and THF. It was observed that for all systems small amount of water is required to achieve phase separation due to hydrophobic nature of PSf. Lai et al. (1998) constructed the ternary phase diagrams of PMMA/acetone/water, PMMA/n-butyl acetate/n-hexane and PMMA/acetone/n-hexane systems at 25°C. Kinetic studies for PSf/solvent or PSf/nonsolvent pairs are very limited. Only in a few studies, diffusivities and sorption isotherms of water in polysulfone were measured (Swinyard et al. 1990, Schult and Paul 1996a, Schult and Paul 1996b, Karimi et al. 2005).

The main objective of this study is to collect thermodynamic and kinetic data for two most commonly used membrane forming materials, PSf and PMMA. For this purpose, the diffusivity and equilibrium isotherms of water, ethanol and chloroform in PSf were determined by using a magnetic suspension balance. In addition, experimental cloud points of PSf/NMP (1-methyl-2-pyrrolidinone)/water, PSf/THF (Tetrahydrofuran)/water, PSf/NMP/ethanol, PSf/THF/water, PMMA (Polymethylmethacrylate)/acetone/water, PMMA/THF/water, PMMA/acetone /formamide and PMMA/THF/formamide systems were determined by the titration of homogeneous polymer solutions (8-22 w%) with nonsolvents until the onset of turbidity. Theoretically, binodal curves were calculated by using nonsolvent/polymer (χ_{13}), solvent/polymer (χ_{23}) and nonsolvent/solvent (χ_{12}) interaction parameters and agreement between experimental cloud points and theoretical binodal curves were investigated. A correlation that describes diffusivity of water in polysulfone as a function of temperature and concentration was obtained by using Vrentas and Duda free volume theory and all equilibrium isotherms were correlated by Flory Huggins theory (Flory 1953).

This thesis consists of nine sections. After giving a brief introduction in the first part, in the second part, information about membrane materials are given. Free volume

theory, sorption isotherms and previous diffusion and equilibrium studies on polysulfone are reviewed in the third section. Methods developed for the measurement of diffusivities in polymer-solvent systems are discussed in the fourth section while methods for measurement of cloud point curves and construction of ternary phase diagrams are given in the fifth section. In the sixth section, information about modeling process are reviewed. Materials and methods are given in seventh section, while in the eighth section, results are shown and discussed. Finally in the ninth section, conclusions are given.

CHAPTER 2

MEMBRANE MATERIALS AND PROPERTIES

Sorption and diffusion data are related to a variety of applications including membrane separation of gases and vapors; packaging and coating technology; controlled drug release systems, and materials for biomedical applications (Rodriguez et al. 2003). Typical membrane applications are microfiltration, ultrafiltration, gas permeation and dialysis. Each application needs specific requirements on the membrane material (van de Witte 1996).

In order to use membranes in these applications, some requirements are needed for membrane materials. The most important membrane material requirements are high selectivity, high permeability, mechanical strength, temperature stability and chemical resistance (Rautenbach and Albrecht 1989).

Membrane materials can be classified as “modified natural products” and “synthetic products”. Modified natural products are cellulose derivatives such as cellulose acetate, cellulose acetobutyrate, cellulose nitrate etc. Polyamide, polymethylmethacrylate (PMMA), polysulfone, polyfuran, polycarbonate, polyethylene, polypropylene and polyethersulfone can be given as examples for synthetic products. Commercial membranes are usually produced from polymers due to their low cost and performance. However, ceramic membranes are prefered in case of high temperature applications due to their thermal stability at higher temperatures. Typical materials used in membrane fabrication are shown in Table 1. Among these materials, polysulfone and polymethylmethacrylate are widely used as membrane materials.

Table 2.1. Membrane materials

(Source: Rautenbach and Albrecht 1989)

Modified natural products Cellulose acetate (cellulose-2-acetate, cellulose-2,5-diacetate, cellulose-3-acetate), cellulose acetobutyrate, cellulose regenerate, cellulose nitrate
Synthetic products Polyamide (aromatic polyamide, copolyamide, polyamide hydrazide), polybenzimidazole, polysulfone, vinyl polymers, polyfuran, polycarbonate, polyethylene, polypropylene, PVA, PAN, polyethersulfone, polyolefins, polyhydantoin, (cyclic polyurea), polymethylmethacrylate
Miscellaneous Polyelectrolyte complex, porous glass, graphite oxide, ZrO_2-polyacrylic acid, ZrO_2-carbon, oils, Al_2O_3

2.1. Polysulfone Based Membranes

According to their chemical, mechanical, thermal, hydrolytic stability and excelllent insulative capabilities, polysulfones are of practical interest as membrane materials (Tweddle et al. 1983). Polysulfone is a high performance polymer used for numerous applications across the membrane separation processes. Polysulfone films have the advantage of applicability to a wide range of pH and temperature (Oğuzer 2004). Polysulfones also have high permeability and permselectivity that make them attractive as membrane polymers in gas separation (Fried 1995). The inert and sulfone backbone functionalities supply resistance against hydrolysis and chemical attack by acid and bases. This characteristic feature makes polysulfone valuable in medical and food contact applications. Polysulfone membranes are used in ultrafiltration, reverse osmosis and hemodialysis (artificial kidney) units. Gas separation membrane technology was developed in the 1970s based on polysulfone hollow-fiber membranes (Mark 2004). There are several examples for the commercial use of polysulfone in gas permeation processes such as separating CO_2-CH_4 and recovery of H_2 (Rautenbach and Albrecht 1989). Polysulfone-based membranes are also used recently for plazma separation from blood (WEB_1 2007). Some physical and chemical properties of polysulfone are given in Table 7.2.

Polysulfones are characterized by the presence of the para-linked diphenylenesulfone group as part of their backbone repeat units (Mark 2004). Polysulfone repeat unit is given in Figure 2.1.

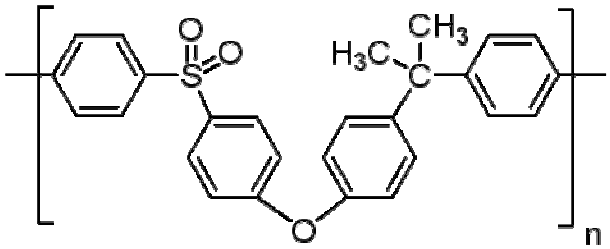

Figure 2.1. Polysulfone molecular structure

(Source: WEB_2 2007)

2.2. PMMA Based Membranes

PMMA is an amorphous polymer with high light transparency and good resistance to acid and environmental deterioration (Fried 1995). PMMA is used in contact lenses. The successful lens product must provide appropriate water content and oxygen permeability. Comport and on-eye movement depend on water content and water transport properties (Rodriguez et al. 2003). Among the variety of polymeric membranes for gas separation, PMMA possess high solubility in a large number of organic solvents. Many researchers have studied PMMA to elucidate how the casting solvent affect the performance of the gas separation membrane (Tung et al. 2006).

The repeated unit of PMMA is given in Figure 2.2, while its physical and chemical properties are given in Table 7.2.

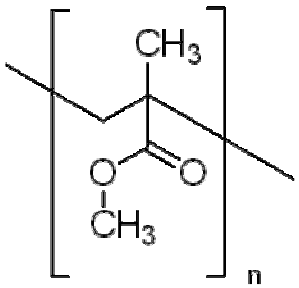

Figure 2.2. PMMA molecular structure

(Source: WEB_2 2007)

CHAPTER 3

DIFFUSION AND THERMODYNAMIC BEHAVIOR OF POLYMER/SOLVENT MIXTURES

By the invention of the phase inversion technique, it became the most popular method to prepare asymmetric polymeric membranes. Asymmetric membranes consist of a very thin dense layer and a porous sublayer. The permeability and high selectivity is provided by the dense layer while the mechanical strength is imparted by the porous sublayer. According to the desired application and operating costs, structural characteristics of the membrane can be adjusted by optimizing the membrane preparation conditions. Prediction of membrane formation mechanisms and morphology can overwhelm time consuming trial and error experimentation (Alsoy Altinkaya and Ozbas 2004).

The polymer rich phase forms the matrix of the membrane, while, the polymer lean phase, rich in solvents and nonsolvents, fills the pores. After the polymer solidifies, the liquid in the pores is extracted. The phase inversion techniques can be classified into four groups based on the external effects: immersion precipitation (wet-casting), vapor-induced phase separation, thermally induced phase separation and dry-casting (Ozbas 2001).

3.1. Prediction of Diffusivities of Small Molecules in Polymers

3.1.1. Free Volume Theory

Free volume theory was first introduced by Cohen and Turnbull in 1954. According to Cohen and Turnbull, the small molecules are assumed as hard spheres, and if one of the spheres moves to another direction and leaves a space behind it, another sphere may jump to this vacancy. A molecule is able to move if the following two conditions are fulfilled: (1) a sufficiently large hole opens up next to the molecule due to a fluctuation in local density, and (2) the molecule has sufficient energy to break away from its neighbors. Such displacements result in diffusive motion. However, the

diffusional transport will be completed only if another molecule jumps into the hole before the first molecule returns to its initial position. Hence, the diffusion constant can be related to the average number of jumps per unit time and the jump distance. According to this theory, diffusion coefficient is proportional to the probability of finding a hole that is sufficiently large for the molecule. The following equation shows the relationship between self diffusion and free volume (Cohen and Turnbull 1954).

$$D_1 = A \times \exp\left[\frac{-\gamma V^*}{V^f}\right] \tag{3.1}$$

where V^* is the minimum hole size into which molecule can jump, V^f is the average hole free volume per sphere, the proportionality constant A is related to the gas kinetic velocity and γ is the overlap factor to account for the overlap between free volume elements.

Many researchers have extended Cohen and Turnbull's free volume theory to describe molecular transport in polymer solutions. Among these studies, the most successful one was derived by Vrentas and Duda (1977).

3.1.2. Vrentas Duda Free Volume Theory

In Vrentas Duda free volume theory, total volume of the liquids is divided into two parts: *occupied volume* which is taken by the molecules themselves and *free volume* between the molecules. Total free volume also consists of two parts: hole free volume and interstitial free volume. When two molecules come close to each other, the repulsive forces can not be negligible, so the free volume within a system is not accessible for molecular transport. Due to usual random thermal fluctuations, some of this free volume is continuously being redistributed and is called as *hole free volume* where molecular transport takes place in this part of the free volume. The remaining part of the free volume, which is not being continuously redistributed is called *interstitial free volume* and is not available for molecular migration. The specific volume/temperature relationship was given in Figure 3.1.

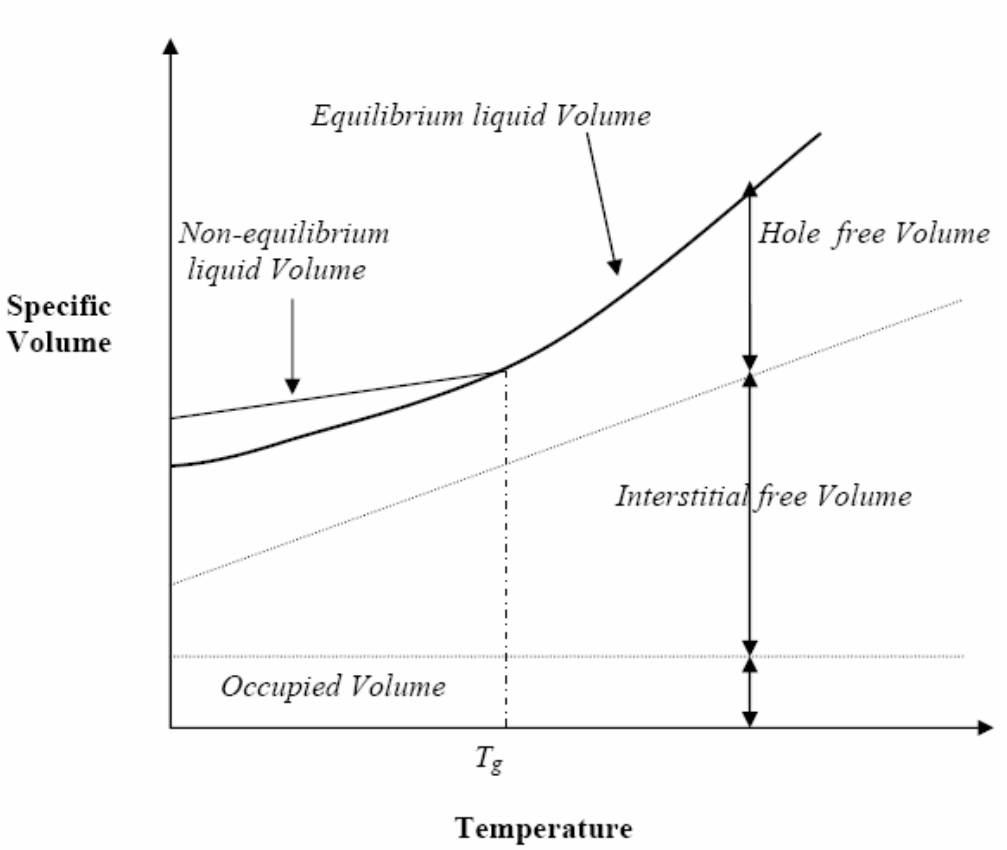

Figure 3.1. Vrentas Duda concept of free volume of a polymer above and below the glass transition temperature T_g (Source: Mohammadi 2005)

Vrentas and Duda extended this theory to binary polymer-solvent systems and derived the following expression for solvent self diffusion coefficient in a polymer solution, D_1:

$$D_1 = D_0 \exp\left[\frac{-E}{RT}\right] \times \exp\left[-\frac{\left(\omega_1 \hat{V}_1^* + \omega_2 \hat{V}_2^* \xi\right)}{\frac{\hat{V}_{FH}}{\gamma}}\right] \tag{3.2}$$

Here D_0 is a constant preexponential factor, E is the activation energy per mole that a molecule needs to overcome attractive forces holding it to its neighbors (J/moleK), $\hat{V}_i^*$ is the specific critical hole free volume required for a diffusive jump of the component i, R is the universal gas constant, γ is an overlap factor, and ω_i is the weight fraction of the component i. In Equation (3.2), $\hat{V}_{FH}$ is the specific hole free volume of the polymer-solvent mixture given by:

$$\hat{V}_{FH} = \omega_1 K_{11}(K_{21} - T_{g1} + T) + \omega_2 K_{12}(K_{22} - T_{g2} + T) \tag{3.3}$$

where K_{1i} and K_{2i} are free volume parameters and Tg_i is the glass transition temperature of component i.

Incorporating the work of Bearman (1961), following relationship to express the mutual diffusion coefficient, D by the self diffusion coefficient is proposed by Duda et al. (1982):

$$D = D_1 Q \tag{3.4}$$

where Q is the thermodynamic factor and is defined as:

$$Q = \frac{\omega_1 \omega_2}{RT}\left(\frac{\partial \mu_1}{\partial \omega_1}\right)_{T,P} \tag{3.5}$$

If chemical potential is calculated from a modified version of the Flory Huggins equation which includes concentration dependent χ parameter

$$\frac{\mu_1 - \mu_1^0}{RT} = \ln a_1 = \ln \phi_1 + \phi_2 + \chi \phi_2^2 + \phi_1 \phi_2^2 \frac{d\chi}{d\phi_1} \tag{3.6}$$

then Equation (3.5) is rewritten as follows:

$$Q = \phi_2^2 \left[(1 - 2\chi\phi_1) + 2\phi_1(\phi_2 - \phi_1)\frac{d\chi}{d\phi_1} \right] \tag{3.7}$$

For a constant interaction parameter, combining Equation (3.4) and (3.5) leads to the following equation which is the most widely used form of the mutual diffusion coefficient

$$D = D_1 \phi_2^2 (1 - 2\chi\phi_1) \tag{3.8}$$

Then, the expression for the mutual diffusion coefficient become

$$D_1 = D_0 \exp\left(\frac{-E}{RT}\right) \exp\left(\frac{-\left(\omega_1 \hat{V}_1^* + \omega_2 \xi \hat{V}_2^*\right)}{\omega_1\left(\frac{K_{11}}{\gamma}\right)\left(K_{21} - T_{g1} + T\right) + \omega_2\left(\frac{K_{12}}{\gamma}\right)\left(K_{22} - T_{g2} + T\right)}\right) \quad (3.9)$$

3.1.2.1. Estimation of Free Volume Parameters

There are 13 independent parameters to be evaluated in Equation (3.9). Grouping some of them means that only 10 parameters need to be determined to estimate the mutual diffusion coefficients. The free volume parameters can be estimated if chemical structure of both solvents and polymers, viscosity of each pure component at different temperatures, critical molar volume of the solvents and glass transition temperature of the polymer are known.

$\hat{V}_1^*$ and $\hat{V}_2^*$

The two critical volumes, $\hat{V}_1^*$ and $\hat{V}_2^*$ are the specific volumes of the solvent and polymer at 0 K. Molar volumes at 0 K can be estimated by using group contribution methods developed by Sugden (1927) and Biltz. Haward (1970) has summarized these methods, and a corrected version of his summary is presented in Table 3.1.

Table 3.1. Group Contribution Methods to Estimate Molar Volumes at 0 K

(Source: Hong 1995)

Component	Sugden (cm^3/mol)	Biltz (cm^3/mol)
H	6.7	6.45
C (aliphatic)	1.1	0.77
C (aromatic)	1.1	5.1
N	3.6	
N (in ammonia)	0.9	
O	5.9	
O (in alcohol)	3.0	
F	10.3	
Cl	19.3	16.3
Br	22.1	19.2
I	28.3	24.5
P	12.7	
S	14.3	

(cont. on next page)

Table 3.1. (cont.)

Triple bond	13.9	16.0
Double bond	8.0	8.6
3-membered ring	4.5	
4-membered ring	3.2	
5-membered ring	1.8	
6-membered ring	0.6	
OH (alcoholic)		10.5
OOH (carboxyl)		23.2

K_{11}/γ and $K_{21}-T_{g1}$ (Solvent free volume parameters)

An empirical equation to describe the viscosity-temperature relationship was proposed by Vogel in 1921. Doolittle then, described that viscosity should be related to the amount of free volume in a system and derived the equation of Vogel in terms of free volume concepts (Doolittle 1951). The relationship between the viscosity of the solvent, η_1 and the free volume parameters are given by the following equation (Hong 1995).

$$\ln \eta_1 = \ln A_1 + \frac{(\gamma \hat{V}_1^* / K_{11})}{(K_{21} - T_{g1}) + T} \tag{3.10}$$

where A is a constant. Hence, K_{11}/γ and $K_{21}-T_{g1}$ can be determined from a nonlinear regression of Equation (3.10) using viscosity-temperature data.

K_{12}/γ and $K_{22}-T_{g2}$ (Polymer free volume parameters)

The free volume parameters of polymer can also be evaluated from the nonlinear regression of Doolittle's expression if the viscosity of the polymer is measured at glass transition temperature and 100°C above the T_g. However, viscosity data near the glassy region are generally not available. An alternate form of the Doolittle expression is developed by William, Landel and Ferry which is a commonly used relationship in correlating viscosity with temperature for pure polymers as shown in Equation (3.11).

$$\log\left(\frac{\eta_2(T)}{\eta_2(T_{g2})}\right) = \frac{-C_{12}^{WLF}(T - T_{g2})}{C_{22}^{WLF} - T_{g2} + T} \tag{3.11}$$

where η_2 is the viscosity of the polymer and C_{12}^{WLF}, C_{22}^{WLF} are the WLF constants. The free volume parameters for polymer are obtained from WLF constants as follows (Hong 1995):

$$K_{22} = C_{22}^{WLF} \tag{3.12}$$

$$\frac{K_{12}}{\gamma} = \frac{\hat{V}_2^*}{2.303\, C_{12}^{WLF}\, C_{22}^{WLF}} \tag{3.13}$$

Values of C_{12}^{WLF} and C_{22}^{WLF} for a large number of polymers have been published by Ferry (1970). When these constants are not available for the polymer of interest, they can be obtained from experimental measurements of shift factor, a_t. The proper relationship between the shift factor and the temperature can be obtained by measuring loss modulus, G′; and storage modulus, G″ as a function of frequency at several temperatures. Master curve is obtained from loss modulus and storage modulus as a function of temperature of ω (rad/s) and shift factor can be obtained by shifting the data until they overlap. The relationship between the shift factor and the temperature in terms of WLF constants are given by the following equation:

$$\log a_T = -\frac{C_{12}(T - T_{ref})}{C_{22} + T - T_{ref}} \tag{3.14}$$

ξ, D_0 and E

The parameter ξ is the ratio of molar volume of the solvent jumping unit to that of the polymer jumping unit. Binary experimental diffusivity data are the correlation source for D_0, ξ and E. These free volume parameters can be evaluated from the experimental diffusion data by nonlinear regression analysis. These parameters can also be predicted if no diffusivity data are available. Assuming that solvent molecule moves as a single unit, then it may be expressed as:

$$\xi = \frac{\tilde{V}_1^{\circ}(0)}{\tilde{V}_{2j}^*} = \frac{\hat{V}_1^* M_1}{\hat{V}_2^* M_{2j}} \tag{3.15}$$

where $\tilde{V}_1^{\circ}(0)$ and $\tilde{V}_{2j}^{*}$ are the solvent molar volume at 0 K and the molar volume of the polymer jumping unit, respectively. M_1 and M_{2j} are the molecular weights of the solvent and the polymer jumping unit, respectively. Zielinski (1992) assumed that the size of the polymer jumping unit is independent of the solvent and proposed a linear relationship between ξ and the solvent molar volume at 0 K as given by the Equation (3.16):

$$\frac{\gamma \hat{V}_2^{*} \xi}{K_{12}} = \beta \tilde{V}_1^{\circ}(0) \tag{3.16}$$

where β is a constant. According to this relationship, once β is known for a specific polymer the ξ parameter for any solvent in a polymer can be determined. β values have been reported for various polymers (Ju et al. 1981a, Ju et al. 1981b).

In addition, D_0 and E can be estimated by combining the Dullien equation (Dullien 1972) for the self diffusion coefficient of pure solvents with the Vrentas Duda free volume equation in the limit of pure solvents (Hong 1995).

$$\ln\left(\frac{0.124\times10^{-16}\tilde{V}_c^{2/3}RT}{\eta_1 M_1 \tilde{V}_1}\right) = \ln D_0 - \frac{E(\omega_1 \to 1)}{RT} - \frac{\frac{\gamma \hat{V}_1^{*}}{K_{11}}}{K_{21} - T_{g1} + T} \tag{3.17}$$

where $\tilde{V}_c$ (cm^3/mol) is the molar volume of the solvent at its critical temperature, 0.124 $\times 10^{-16}$ is a constant and η_1 (g/cm.s) and $\hat{V}_1$ (cm^3/g) are the viscosity and the molar volume of the pure solvent, respectively, and are the only temperature dependent parameters in the expression. Since solvent free-volume parameters have been determined previously from Equation (3.10), D_0 and E can be determined from the nonlinear regression (Hong 1995). According to Equation (3.17), D_0 is a solvent property and independent of the polymer.

3.2. Prediction of Sorption Isotherms of Polymer/Solvent Systems

The dependence of penetrant concentration on the penetrant pressure is described by a sorption isotherm. There are four general isotherms that describe

sorption of small molecules in a polymer matrix as shown in Figure 3.2. These isotherms are known as the (a) Henry's Law, (b) Dual Mode, (c) Flory Huggins, and (d) Generalized isotherms. Among these isotherms, Flory Huggins theory has been successfully used to correlate sorption isotherms of polymer/solvent systems.

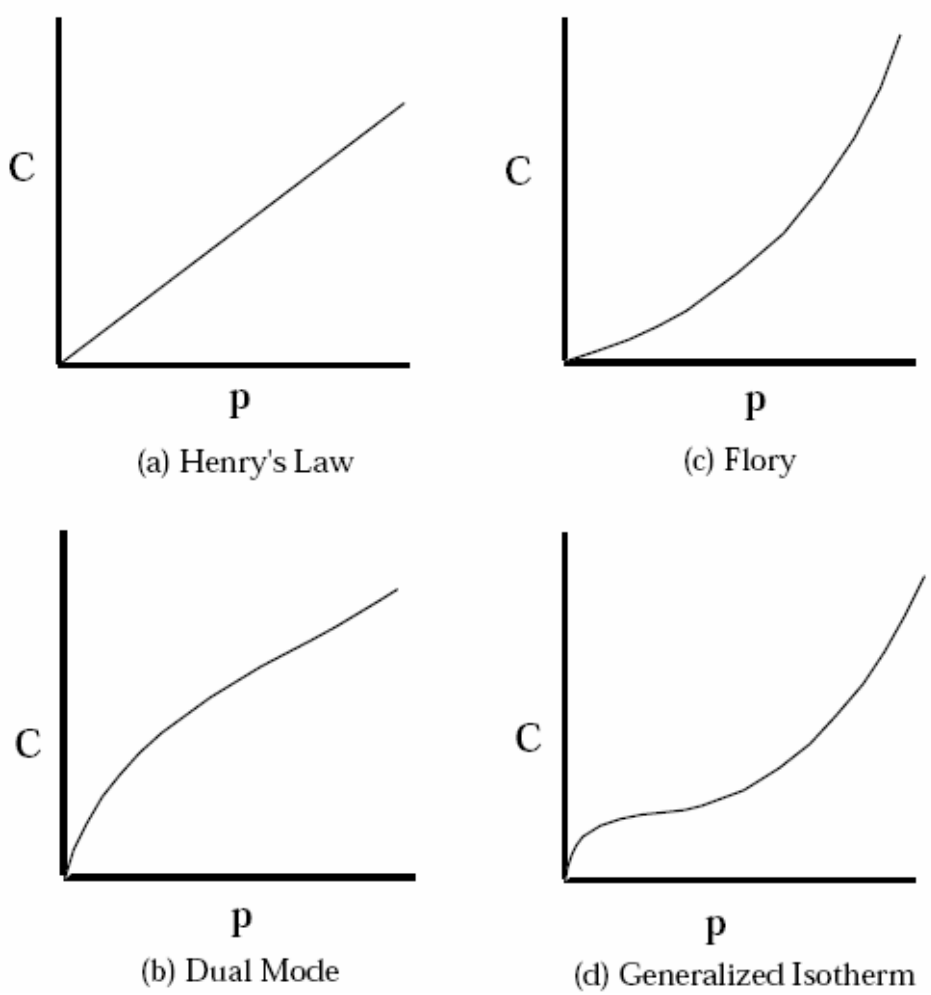

Figure 3.2. Sorption isotherms of vapors in polymers
(Source: McDowell 1998)

During a typical sorption experiment, when the penetrant vapor reaches an equilibrium with the polymer, then

$$\mu_{penetrant}^{vapor} = \mu_{penetrant}^{polymer} \tag{3.18}$$

If vapor pressure of the polymer is neglected and ideal gas of pure solvent is assumed, then activity of the penetrant is calculated as follows:

$$a_1 = \frac{P_1}{P_1^{sat}} \tag{3.19}$$

where P_1 is the pressure of the solvent measured and P_1^{sat} is the saturation vapor pressure of the solvent at the column temperature. If the interaction parameter χ is constant, then, Equation (3.6) combined with Equation (3.19) is written as follows:

$$\ln \frac{P_1}{P_1^0} = \ln \phi_1 + \phi_2 + \chi \phi_2^2 \tag{3.20}$$

χ parameter is regressed from Equation (3.20) by minimizing the difference between the experimental and theoretical activity data. Experimental data usually collected as the weight fraction of penetrant is converted into volume fraction through following expressions:

$$\phi_1 = \frac{\omega_1 \hat{V}_1}{\omega_1 \hat{V}_1 + \omega_2 \hat{V}_2} \tag{3.21}$$

where subscripts 1 and 2 refer to penetrant and polymer, respectively.

The strength of the polymer-penetrant interaction is characterized by the magnitude of Flory-Huggins parameter. The correlation between the solvation power of a penetrant in a given polymer and χ has been given as follows (Feng 2001):

1. if $\chi < 0$, there is strong interaction between polymer and penetrant, water will not cluster
2. if χ is between 0 and 0.5, it is a good solvent for that polymer
3. if χ is greater than 0.5, penetrant can not completely dissolve the polymer
4. if $\chi > 1$, water tends to cluster

3.3. Previous Diffusion and Equilibrium Studies with Polysulfone

Schult and Paul (1996a) have measured diffusion coefficients of water in polysulfone at 30, 40 and 50°C. The diffusion coefficients were obtained as 9.5×10^{-8} at activity equals to 0.5 and 8.9×10^{-8} at activity 1 (Figure 3.3).

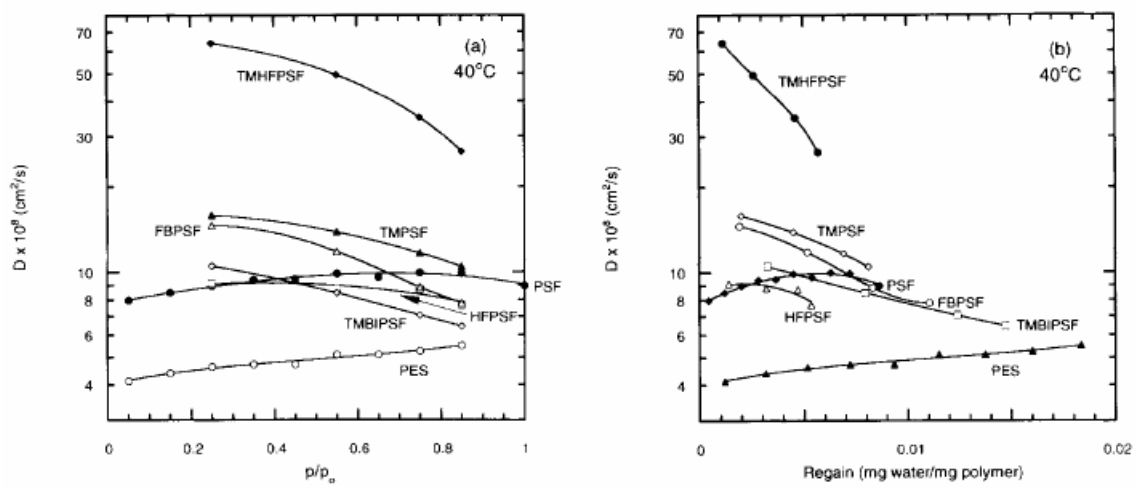

Figure 3.3. Diffusion coefficients for the various polysulfones at 40°C calculated from the sorption kinetic data plotted versus (a) average water activity and (b) average water concentration (Source: Schult and Paul 1996a)

They have also measured equilibrium isotherms were at 30°C, 40°C and 50°C. Figure 3.4 shows the equilibrium isotherm at 40°C. The isotherms were represented in terms of the weight of water sorbed by the film at a given water vapor activity divided by the dry weight of the polymer.

A Cahn balance was used to measure both the equilibrium and the kinetics of water vapor sorption. The initial slope method was used to determine the diffusion coefficients from sorption data. Authors claimed that Fickian sorption kinetics with a mildly concentration-dependent diffusion coefficient was obtained. It was observed that at low activities diffusion coefficients of water in PSf increase with activity, and decreases at high activitities. Such decrease at high activity was attributed to self-hydrogen bonding of water molecules to form clusters and clustering became more pronounced at activities above 0.5.

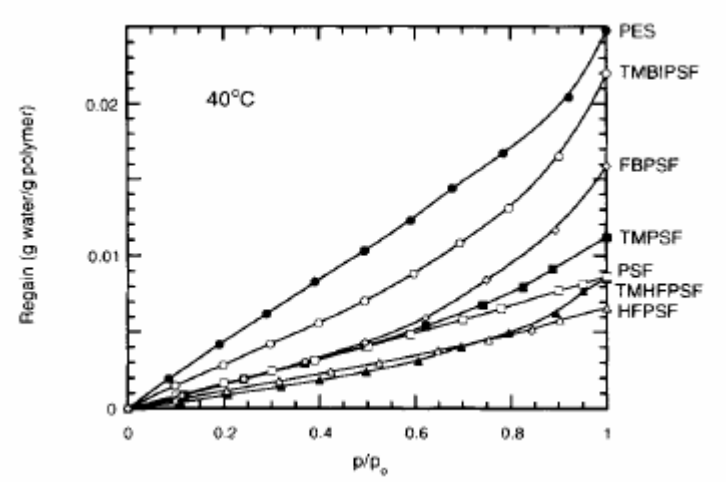

Figure 3.4. Equilibrium water vapor isotherms for polysulfones at 40°C. Water concentration was measured in terms of the regain, which is the weight of the water sorbed at the given activity divided by the dry weight of the polymer (Source: Schult and Paul 1996a)

In the study of Karimi et al. (2005), sorption isotherms of water in polysulfone were determined at 25°C by use of magnetic suspension balance. It is observed that in the water activity range of 0.20-0.95, the water uptake is linear with water vapor pressure.

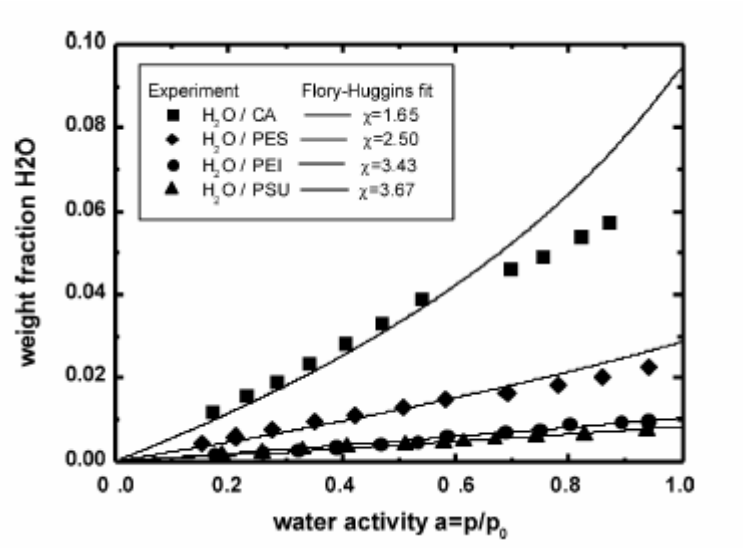

Figure 3.5. Sorption isotherms for water in CA, PES, PEI and PSU at 25°C. The curves represent fits with the Flory Huggins theory (Source: Karimi et al. 2005).

CHAPTER 4

METHODS DEVELOPED FOR THE MEASUREMENT OF DIFFUSIVITIES IN POLYMER-SOLVENT SYSTEMS

Various techniques have been used for the measurement of diffusivity of polymer solvent systems such as inverse gas chromatography (IGC), pressure decay method, FTIR-ATR spectrometry and sorption measurements either gravimetric or piezoelectric.

4.1. Inverse Gas Chromatography (IGC)

Inverse gas chromatography has been used to study sorption and diffusion in polymer-solvent systems accurately (Surana et al. 1996, Tihminlioglu et al. 2000, Balashova et al. 2001, Davis et al. 2004a). Gray and Guillet (1973) are the first researchers developing gas chromatography for the diffusion measurements by the IGC method. In a typical IGC experiment, a polymeric stationary phase is placed inside an empty column. The polymeric stationary phase can be in the form of a capillary column or packed column. In capillary column inverse gas chromatography (CCIGC), inside of a capillary column is coated with a thin film of polymer while in packed column inverse gas chromatography (PCIGC), the polymer is coated on support particles and these coated particles are then packed into the column. The first IGC studies done for measuring diffusion coefficients of penetrates in polymers used packed columns. A new mathematical model was proposed by Romdhane and Danner (Romdhane 1994) for describing the chromatographic process in packed columns. Because of the difficulties in knowing the geometry and morphology of the stationary phase, some problems had been observed in getting reliable diffusion data. The morphology of the stationary phase can differ according to the nature of the polymer and the amount of polymer needed for preparing the column. These problems were solved with capillary columns with a uniformly distributed polymeric stationary phase by Pawlisch et al (1987). However, the preparations of such uniform morphology in capillary columns present some difficulties in elastomeric polymers or polymers with low glass transition temperature.

The principle of IGC method is based on to measure the residence time of a volatile solvent in the carrier gas (mobile phase) dissolving and passing the polymer (stationary phase) inside a GC column (Krüger et al. 2006). A pulse of solvent is injected and vaporized into the column by a carrier gas flowing through the column. Due to the mass transfer resistance in the polymer phase, the solute is swept through the column. The concentration front traveling down the packed column is then measured by a detector. The data collected are the solvent concentration in the carrier gas at the column's outlet as a function of time. The shape of the elution profile reflects the properties of the polymer-solvent system. The fundamental property measured by IGC from which most of these properties are derived is known as the retention volume, a parameter that gives information about the thermodynamics of a polymer-solvent system. IGC allows us to calculate thermodynamic magnitudes such as partition or activity coefficients and the Flory-Huggins interaction parameter. Figure 4.1 shows the experimental set-up for a capillary column inverse gas chromatography experiment (Tihminlioglu and Danner 2000). IGC is a very fast, accurate and reliable technique, however diffusion coefficients measured by this method is not precise because it is difficult to ensure a constant coating thickness within the IGC column (Krüger et al. 2006). This is the case when preparing the column by handwork but this problem is eliminated when columns are prepared by corporations.

IGC is commonly used for measurements at infinite solvent dilution. This is achieved by injecting a very small amount (<1 μL) of solvent into a stream of an inert gas (Danner and High, 1993). In the past, this technique has been limited to measurements in the infinite dilution region but it has been extended to measure diffusion coefficients at the finite concentration region. (Tihminlioglu and Danner 2000). This is achieved by doping the carrier gas with a solvent by passing the carrier gas through a saturator maintained at constant temperature. The disadvantage of IGC is the limitation of solvent concentration. The data show deviations in the finite concentration because of baseline fluctuations arising from the presence of solvent in the carrier gas. The baseline fluctuations are large, making results questionable at high activities (Tihminlioglu and Danner 2000).

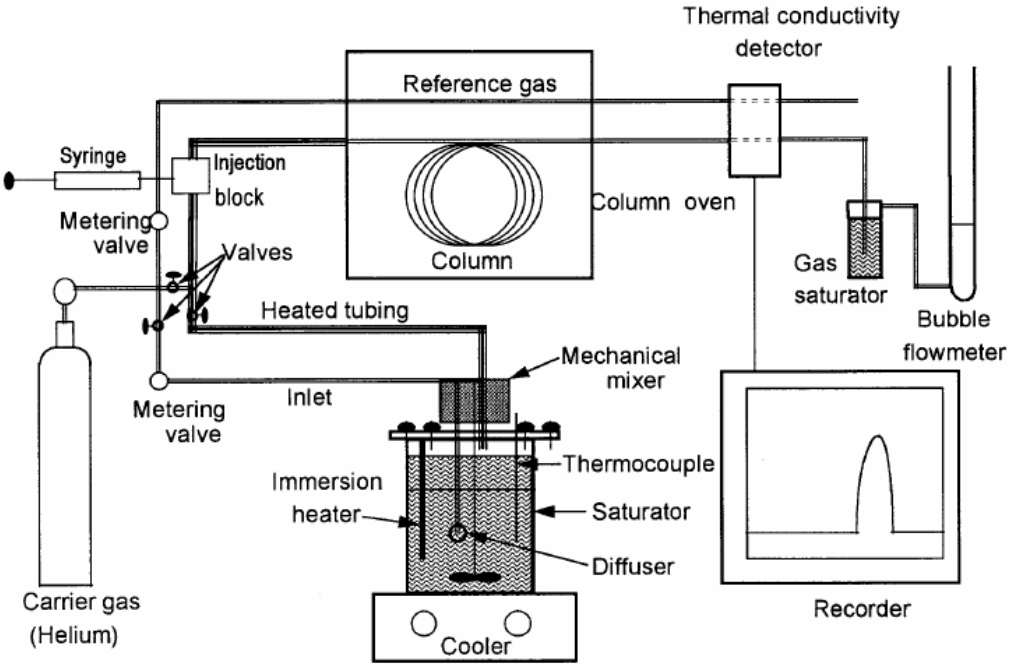

Figure 4.1. Experimental Set-up of IGC System

(Source: Tihminlioglu and Danner 2000)

4.2. Piezoelectric Crystal

Quartz crystal resonators are easy and precise tool for determining the weight of the thin films. When a thin film is cast onto one of the electrodes of a thickness-shear resonator, its acoustical resonance frequencies change due to the weight of the film. Piezoelectric method allows the detection as little as 10 nanograms of solvent using a 10 MHz crystal (Saby-Dubreuil 2001). It operates by using the frequency response of a quartz crystal to measure the weight of solvent captured on the polymer. Sensing is achieved by correlating acoustic wave-propagation variations to the amount of solvent captured at the surface. This sensor using acoustic waves was first introduced by King in 1964. After extensive researches, the quartz crystal has been known as a sensitive mass detecting device (Chang et al. 2000).

Figure 4.2 illustrates the experimental set-up of piezoelectric crystal sorption system. First, the polymer film cast onto the quartz crystal resonator is located inside a vacuum chamber. Then, the chamber is connected through electronic valves to a solvent reservoir in which the solvent vapor pressure is equal to the saturated vapor pressure of pure solvent. Experiments are carried out with slow ramps of increasing pressure. The

pressure step changes are chosen small enough to allow diffusion equilibrium at all times. Finally, frequency is recorded as a function of time.

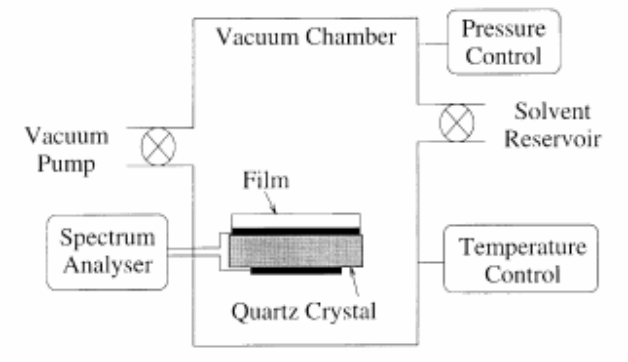

Figure 4.2. Experimental set-up of piezoelectric crystal sorption system
(Source: Saby-Dubreuil et al. 2001)

According to Sauerbery equation, the linear relationship between the mass uptake (Δm) on the coated crystal and the quartz crystal frequency shift (Δf) is described below:

$$\Delta m = K\Delta f \tag{4.1}$$

Here, K is the proportionality constant, corresponds to known properties of the quartz crystal. Two characteristic frequency shifts are measured for determining sorption levels in thin polymer films. The first is the frequency shift associated with the mass of polymer deposited on the crystal, $\Delta f_{polymer}$. The second is the incremental frequency shift resulting from the sorption of vapor at any specific pressure or activity, $\Delta f_{sorption}$. Using these characteristic values, the weight fraction of the sorbed vapor can be determined from the following relationship:

$$wt\% = \frac{m_{sorption}}{m_{polymer}} = \frac{\Delta f_{sorption}}{\Delta f_{polymer}} \tag{4.2}$$

The weight fraction can be converted into volume fractions with known properties of the polymer and vapor (Zhang et al. 2003). Although the quartz crystal microbalance is known to be a very precise and accurate tool, in some studies the

obtained results were far from the theoretical ones because of the various phenomena that affect weight determination (Dubreuil et al. 2003).

4.3. Pressure Decay Method

The pressure-decay method was first developed by Newitt and Weale in 1948 for studying the solubilities of gases in polystyrene. This method was latter improved for diffusion measurements by Lundberg et al. in 1963 (Davis et al. 2004b). The pressure decay experiment is carried out by isolating a polymer sample and solvent vapor in an autoclave. As the polymer absorbs the vapor, the amount of vapor absorbed is calculated by the pressure drop within the autoclave and is recorded as a function of time. Schematic representation of pressure decay equipment is shown in Figure 4.3. An equation of state is used to calculate the mass uptake from the pressure drop.

During the 1970 and 1980s, the method was extensively used to study the sorption of gases into glassy polymers (Davis et al. 2004). The pressure decay method was popular because the apparatus is simple and construction cost is not expensive. However, it is difficult to operate it with molten polymers at higher temperatures because no high-resolution sensor of pressure is available at the high temperature condition that is high enough to melt the polymer. Also, in this method, large amount of sample is needed, which results in long measurement times (Sato et al. 2001).

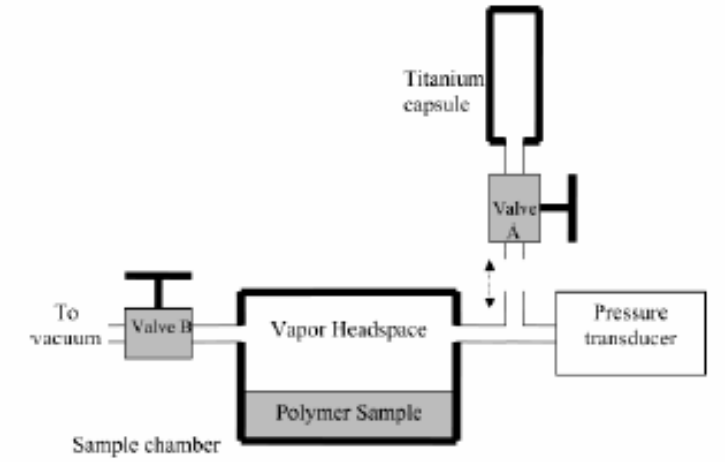

Figure 4.3. Diagram of the pressure decay instrument
(Source: Davis et al. 2004)

4.4. FTIR-ATR Spectrometer

Recently time-resolved FTIR (Infrared Spectroscopy with Fourier Transform) / ATR (Attenued Total Reflection) spectroscopy has been used to examine diffusion coefficients in polymers (Yossef et al. 2003, Baschetti et al. 2003). The FTIR-spectroscopy is based on the property of any material absorbing light at a determined wavelength due to its characteristic. ATR configuration is employed for mass transport applications. This technique allows for the analysis of diffusive transport of gases and liquids in polymeric films. Studying the diffusion of multicomponent systems, in particular of measuring the diffusion coefficients of each component of a mixture absorbed by a polymeric film and possibility to detect and analyze the swelling of penetrant in the polymer during sorption are the features of this technique.

The technique is based on the observation of total reflection where there is a penetration of the electromagnetic field in the less dense phase called “evanescent wave”. This wave is absorbed by the film and leaves its characteristic track in the light beam. The spectrometer records this track and yields an interferogram (intensity as a function of time). Then it is recomputed through a Fourier transform in order to obtain an absorption spectrum (absorbance as a function of wavelength) where one can enable to determine the peaks of the polymer and the penetrants. Concentration of the penetrant in the polymer and the diffusion coefficient can be easily determined from these peaks.

Figure 4.4 is a schematic representation of an FTIR-ATR experimental arrangement. Here, the IR beam is modulated by an interferometer and enters from one side of the ATR element. The IR radiation reflects and is absorbed at the polymer interface of the ATR element. Then it exits from the opposite side of the ATR element and recorded by a detector (Yossef et al. 2003).

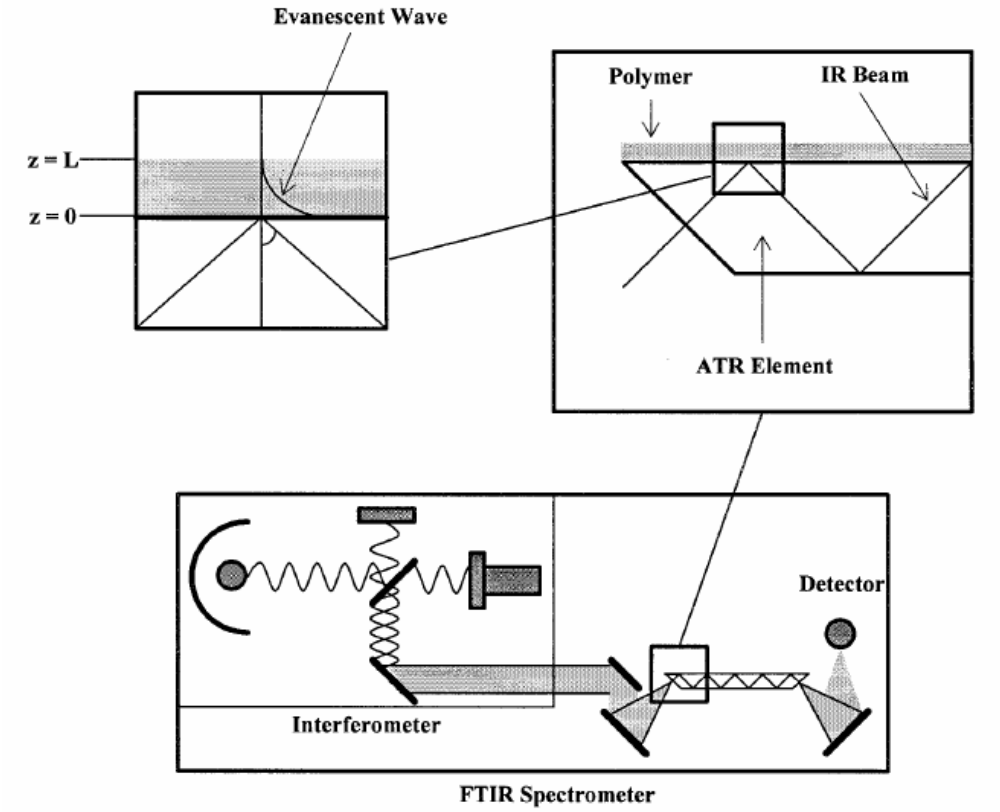

Figure 4.4. Schematic of the FTIR spectrometer and ATR attachment for the measurement of diffusion in the polymers (Source: Yossef et al. 2003).

FTIR-ATR spectroscopy is a robust, accurate and simple to use method and can provide reliable short-time data. The technique is also relatively inexpensive in comparison with other techniques (Yossef et al. 2003).

4.5. Gravimetric Sorption Techniques

Gravimetric sorption technique is the classical technique where a quartz spring, an electro balance or a magnetic suspension balance is used to measure the weight increase of a solid or non-volatile liquid sample in a solvent vapor or gas atmosphere due to absorption of vapor or gas in the sample.

4.5.1. Cahn Electro Balance

This apparatus is built to perform vapor sorption and diffusion experiments in polymers with a sensitivity of 0.1 μg. The sample is hanged at the balance left arm,

while an inert tare is suspended at the opposite arm (Figure 4.5). The polymer sample is maintained in a constant temperature chamber and the system is evacuated. The solvent vapor is produced by a vapor generator and is then introduced into the chamber at a fixed pressure and temperature (Doghieri et al. 1996). The sample weight is recorded and plotted as a function of time by a computer. Experiments are continued until a steady state is reached. Then the sample is totally degassed and a new pressure of vapor is introduced to the chamber to do a new experiment. The sorption experiments by a Cahn electrobalance cover a pressure range from 0 to 1 atm and a temperature range from 25 to 60°C (Uriarte et al. 1998). However, this experimental setup sometimes doesn't provide the desired activity instantaneously. This causes some difficulties in the determination of diffusion coefficients (Alfageme et al. 1999). In addition, the accuracy of the balance is affected by organic solvent vapors and the experiments can not be conducted at temperatures below 60°C.

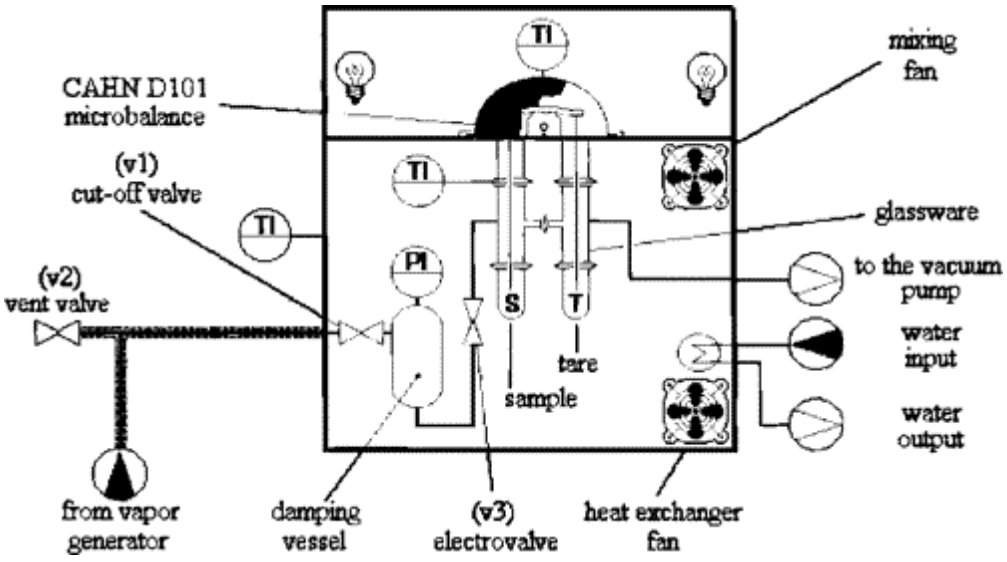

Figure 4.5. Experimental set-up of Cahn electrobalance

(Source: Doghieri et al. 1996)

4.5.2. Quartz Spring Balance

McBain spring balance is a widely used device for gravimetric sorption (Wang et al. 1999, Kamaruddin and Korros 2000, Huang et al. 2003, Piccinini et al. 2004, Dhoot 2004). The apparatus is based on a spring of quartz on which the polymeric sample is suspended and immersed in the penetrant phase. As penetrant sorbs into the

polymer, the load on the spring increases, and the spring extends. The elongation of the spring is monitored with a camera, directly connected to a computer and gives a measure of the weight change of the polymer due to the sorption of penetrant. The spring position data are converted to mass uptake values, M_t where M_t is the mass of penetrant sorbed by the polymer at time t per unit mass of dry polymer, and diffusion coefficients are extracted from the time dependence of M_t. A schematic diagram of this instrument is presented in Figure 4.6.

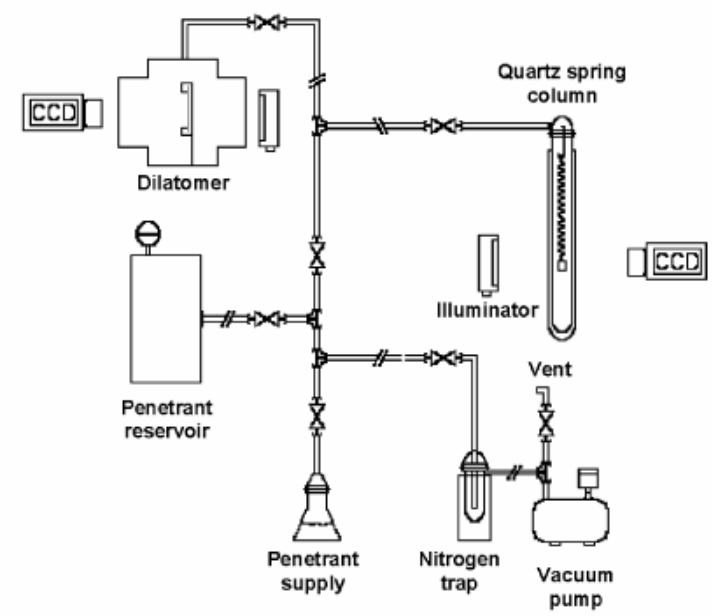

Figure 4.6. Schematic representation of quartz spring balance
(Source: Piccinini et al. 2004)

During a typical sorption experiment in quartz spring balance, the liquid penetrant is supplied from solvent flask and vaporized into a reservoir up to the desired pressure. The quartz spring is suspended in a glass column and its temperature is controlled by a water jacket through the experiment (Piccinini et al. 2004). Before starting the experiment, sorbed water vapor is removed from the polymer by evacuating the balance by a vacuum pump until there is no further spring displacement. Then the sample is exposed to penetrant at desired pressure. The pressure of penetrant is increased in a series of steps in case the sample is equilibrated after each step (Dhoot 2004). The sample elongation is observed through a CCD camera (Piccinini et al. 2004). The quartz spring balance is classical due to its high accuracy but the time required to reach equilibrium is too long (Huang et al. 2003). The solvent vapor requires days or

weeks to diffuse into the polymer and reach equilibrium due to low diffusivities of most solvents in the polymer. The main disadvantage of this system is the direct contact between the measuring atmosphere and the balance. The calibration of the balance can be affected through the long time experiments. Weight fractions of solvent up to 0.75 can be used in this method but the data become very unreliable in this range, and small fluctuations in temperature cause large swings in data (Danner and High, 1993).

4.5.3. Magnetic Suspension Balance (MSB)

Magnetic suspension balances have been widely used in a variety of applications such as sorption measurements of vapors in polymers (Mamaliga et al. 2004, Krüger and Sadowski 2005, Krüger et al. 2006), solubility of gases (Chaudhary and Johns 1998, Pfannschmidt and Michaeli 1998, Schnitzler and Eggers 1999, Sato et al. 2001, Areerat et al. 2002, Nalawade et al. 2006), adsorption measurements (Dreisbach et al. 1998, Dreisbach and Lösch 2000, Dreisbach et al. 2002, Kwapinski and Tsotsas 2004), and density measurements (Saleh and Wendland 2005, Hazeleger 2006). The list of applications for the magnetic suspension balance goes far beyond the fundamental research work. The device is also used in several industrial applications, including flue gas purification, the gasification of coal, soil detoxification, waste incineration, foodstuff manufacturing, plastic fabrication, supercritical fluid extraction, material synthesis, the storage of hydrogen and natural gas and the investigation of membranes for fuel cells (WEB_3 2007).

MSB has been first developed by Kleinrahm and Wagner (1986). The device has been recognized as one of the most reliable and sensitive apparatus among other gravimetric sorption equipments such as quartz spring balance or Cahn electrobalance.

The main problem when using conventional gravimetric instruments is the direct contact between the measuring atmosphere and the weighing instrument (Figure 4.7). The balance can be damaged or disturbed by the measuring atmosphere and the measuring atmosphere can be affected by flushing gases and pollution. The field of application of gravimetric measurements had been reduced by these restrictions in the past.

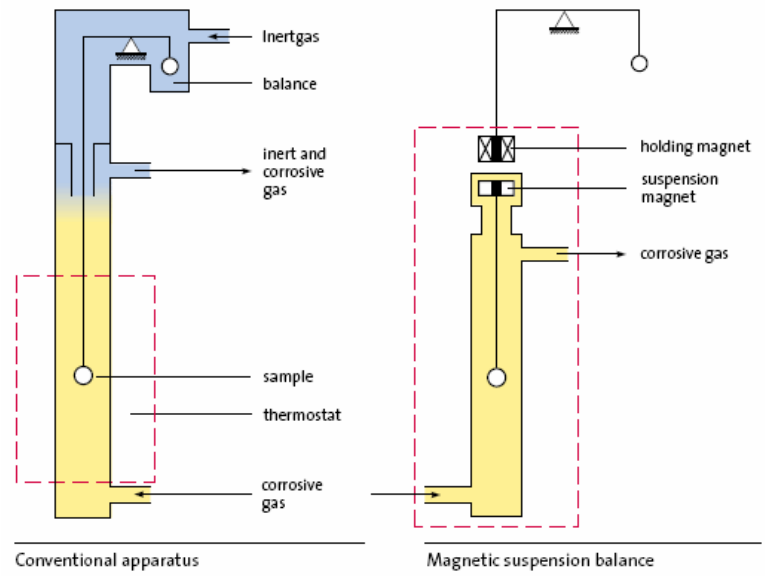

Figure 4.7. Comparison of gravimetric measurements with conventional apparatus and MSB (Source: WEB_4 2006)

The Magnetic suspension balance allows weighing samples contactlessly under nearly all conditions. The sample is linked to "suspension magnet" which consists of a permanent magnet, a sensor core and a device for decoupling the measuring-load (sample). An electromagnet, which is attached at the under floor weighing hook of a balance, maintains the freely suspended state of the suspension magnet via an electronic control unit. The suspended state is supplied by a direct analogous control circle (PID controller and position transducer). Suspension magnet achieves a constant vertical position by modulating the voltage on the electromagnet by the controlling unit (Figure 4.8). In this position the magnet and the sample are freely suspended and their mass is transmitted to the microbalance through the wall of the pressure vessel.

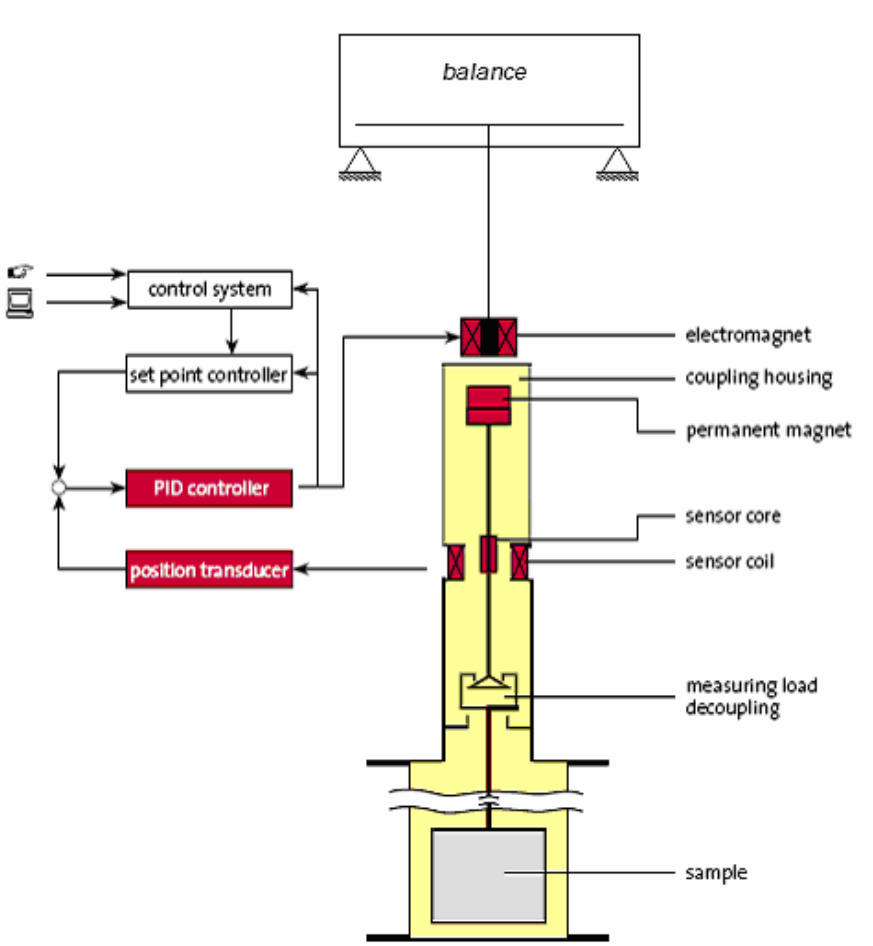

Figure 4.8. Operating principle of the magnetic suspension balance

(Source: WEB_4 2006)

Measuring force is transmitted contactlessly from the measuring chamber to the microbalance which is outside the chamber under atmospheric conditions by using the magnetic suspension coupling. Consequently, this set up eliminates almost all restrictions in gravimetric measuring instruments, and enlarges the application field.

The Magnetic suspension balance offers the possibility of lowering the suspension magnet to a second stationary position a few millimeters below the measuring position which is called “zero-point position” and corresponds to an empty balance pan in a normal weighing procedure and allows calibration of the balance at all times, even during recording measurements (Figure 4.9). At this position, the sample basket is set down on a support and the sample is decoupled from the balance (Sato et al. 2001). This feature can enhance the accuracy of the measurements considerably. (Dreisbach & Lösch 2000).

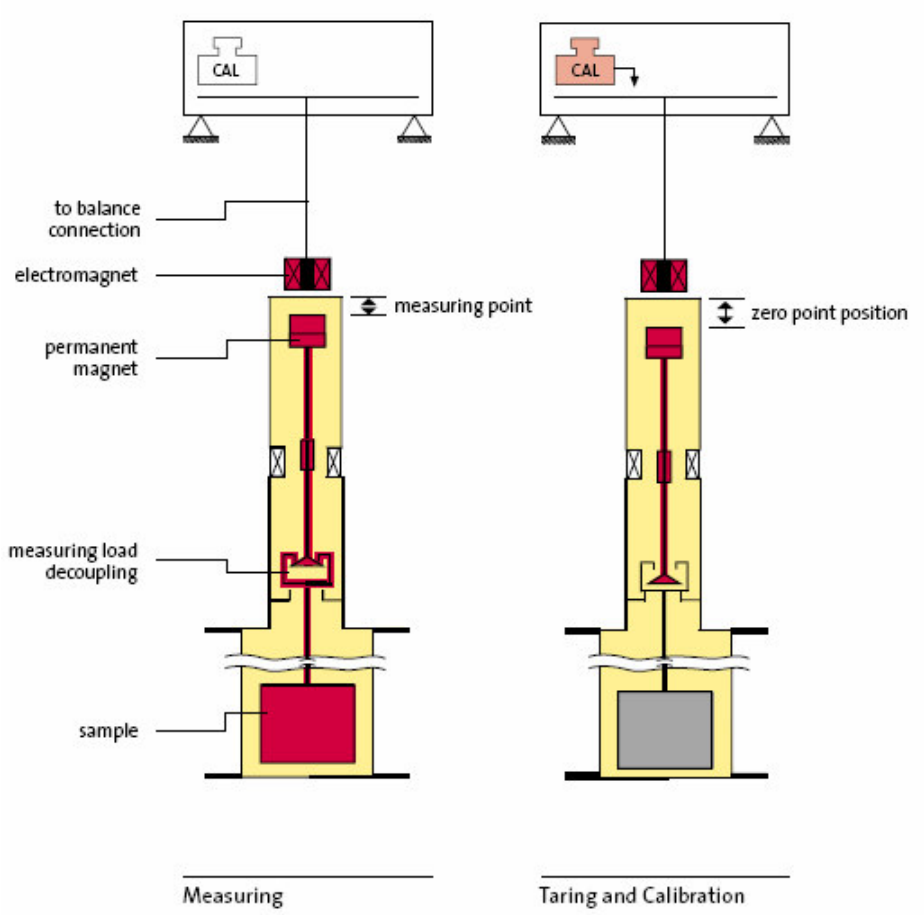

Figure 4.9. Automatic decoupling of the measurement load in order to tare and calibrate the balance (Source: WEB_4 2006)

The Magnetic Suspension Balance can be used in a pressure range of ultra high vacuum up to 500 bar and temperature range from -196°C to 350°C. A resolution of 1 µg with samples up to 30 g and a reproducibility of ± 2 µg can be obtained (WEB_5 2006).

The entire interior volume of the magnetic suspension balance can be thermostated to the same temperature (up to 620 K) as a thermal unit. This is achieved by means of double-walled thermostated jacket which completely surrounds the measuring cell.

The mass changes of any kind of sample materials caused by the adsorption or absorption of gases and vapors can be measured by using this instrument. Supercritical fluids and corrosive measuring atmospheres can also be used in this instrument without any problem (WEB_6 2007).

CHAPTER 5

MEASUREMENT OF CLOUD POINT CURVES AND CONSTRUCTION OF TERNARY PHASE DIAGRAMS

The membrane structure is affected both by thermodynamics and the kinetics of the system. The system thermodynamics is often demonstrated by a ternary phase diagram. The cloud point curve of liquid-liquid phase separation is an important factor affecting the membrane structure (Tsai et al. 2002). In the following sections, techniques used to determine cloud points experimentally and theoretically are given and previous studies are discussed.

5.1. Determination of Cloud Points Experimentally

5.1.1. Titration Method

The method of titrating polymer solutions with nonsolvents is in use for the determination of cloud point curves (onset of turbidity as function of composition), which are of great practical interest to quantify the limits of complete miscibility (Schneider et al. 2002). The cloud point curves are usually determined by a simple titration method. Polymer solutions at different concentrations are prepared by dissolving polymers in solvents at constant temperature. These homogeneous polymer solutions are titrated with nonsolvents. The amounts of nonsolvents required to bring the onset of turbidity are measured and at the onset of turbidity, the volume fractions of nonsolvent, solvent and polymer represent the cloud points in a ternary phase diagram.

5.1.2. Light Scattering Method

Another method used for the determination of cloud points is light scattering in which the intensity change transmitted through the homogeneous solution of polymer-solvent is followed by the addition of a nonsolvent. In the study of Schuhmacher et al. (2001), the ternary phase diagram of PMMA/THF/water was measured carried out using

a laser source (He-Ne, λ = 633 nm) with coupled photocell (Figure 5.1). The cloud points were determined when the value of intensity transmitted decreased 50% in comparison with the original homogeneous solution. With this procedure, the borderline between the unstable and stable region in the ternary phase diagram was determined (Figure 5.2).

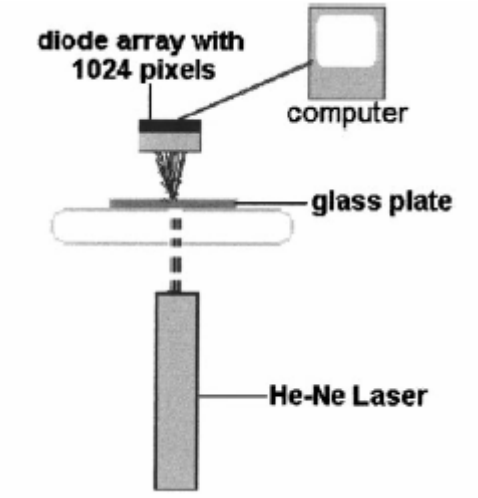

Figure 5.1. Diagram of the experimental system for light scattering measurements (Source: Schuhmacher et al. 2001)

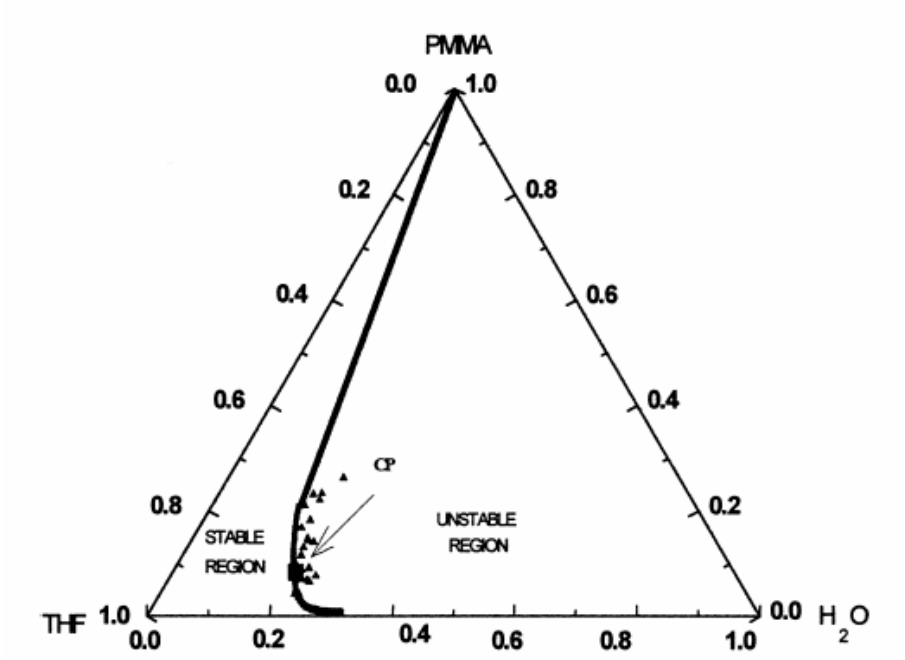

Figure 5.2. Phase diagram of PMMA/THF/water system. The solid triangles and the solid rectangle represent the cloud points and the critical point, respectively (Source: Schuhmacher et al. 2001)

5.1.3. Turbidity Measurements

Determination of cloud points with turbidity measurements is based on detecting the sudden change in the turbidity values (detected by a turbidimeter) while adding the nonsolvent slowly. This composition represents the transition concentration between one-phase and two-phase regions. With this data obtained, a ternary phase diagram can be constructed. Cheng et al. (1996) determined the cloud points of PMMA/Solvent/Nonsolvent systems at 25°C (Figure 5.3), using turbidity measurements.

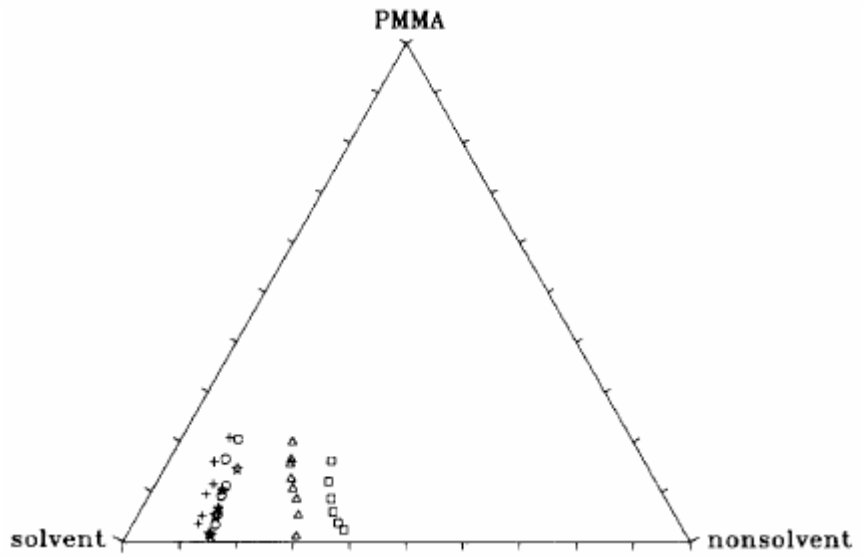

Figure 5.3. Ternary phase diagram of PMMA systems. Nonsolvent-solvent: (+) water-NMP; (○) water-acetone; (★) n-hexane-butyl acetate; (△) n-hexane-ethyl acetate; (□) n-hexane-acetone (Source: Cheng et al. 1996)

5.2. Ternary Phase Diagrams

The use of membranes were limited until Loeb and Sourirajan introduced the "phase inversion" technique in 1962. In phase inversion techniques, a homogeneous polymer solution consisting of solvent (s) and nonsolvent (s) is cast on a support and then evaporation of the casting solution takes place under convective conditions. During evaporation, the solution becomes thermodynamically unstable due to different external effects and phase separates into polymer lean and polymer rich phases. The successive solidification of the phase separated solution leads to a porous, asymmetric structure.

The ternary phase diagram of the polymer/solvent/nonsolvent system is needed to be constructed and kinetic aspect must be coupled with the thermodynamic one in order to predict the structures of the membrane formed. Therefore, the thermodynamics of ternary solutions will be discussed.

5.2.1. Thermodynamcis of Ternary Systems of Polymer/Solvent /Nonsolvent

Flory Huggins theory is generally used to describe the equilibrium behavior in a polymer/solvent/nonsolvent system. According to the theory of Tompa (1956), the Gibbs free energy of mixing in a ternary system can be described by the following equation:

$$\frac{\Delta G_m}{RT} = n_1 \ln \phi_1 + n_2 \ln \phi_2 + n_3 \ln \phi_3 + g_{12}(u_2) n_1 \phi_2 + \chi_{23} n_2 \phi_3 + \chi_{13} n_1 \phi_3 \qquad (5.1)$$

where R is the gas constant, T represents the absolute temperature, the subscripts refer to nonsolvent (1), solvent (2) and polymer (3). n_i and ϕ_i are the number of moles and the volume fraction of the component i, respectively. χ_{13} is the nonsolvent-polymer interaction parameter; χ_{23}, the solvent-polymer interaction parameter and g_{12} is the nonsolvent-solvent interaction parameter and it is assumed to be a function of u_2, $u_2 = \phi_2 / (\phi_2 + \phi_1)$.

Definition of chemical potential can be given as follows:

$$\frac{\Delta \mu_i}{RT} = \frac{\partial}{\partial n_i} \left(\frac{\Delta G_m}{RT} \right)_{n_{j, i \neq j}} \qquad (5.2)$$

5.2.2. Construction of Ternary Phase Diagrams

Construction of phase diagrams of ternary polymer solutions have been studied by several authors (Tompa 1956, Altena and Smolders 1982, Yilmaz and McHugh 1986). Altena and Smolders (1982), calculated the binodal and spinodal curves with concentration dependent solvent/nonsolvent interaction parameter and constant solvent/polymer and nonsolvent/polymer interaction parameters and investigated the

effect of interaction parameters on the phase diagrams of several cellulose acetate systems and PSf/DMF/water system. Yilmaz and McHugh (1986) studied the effect of constant variable interaction parameters and the molecular weight of the polymer on the shape of the phase diagram. In both studies, it was emphasized that nonsolvent/polymer interaction parameter has a critical role in predicting the phase diagrams of polymer solutions.

The phase diagram of a ternary system can be represented by a equilateral triangle as shown in Figure (5.4). Any point on this triangle represents a composition and the sum of the perpendicular distances from this point to all sides is unity. The corners of the triangle correspond to pure components whereas the points on the sides of the triangle represent the binary mixtures. The ternary phase diagram consist of binodal and spinodal lines, critical point, single phase, two phase and metastable phase regions. The position of the binodal and the spinodal curves are characteristic for each polymer/solvent/nonsolvent system.

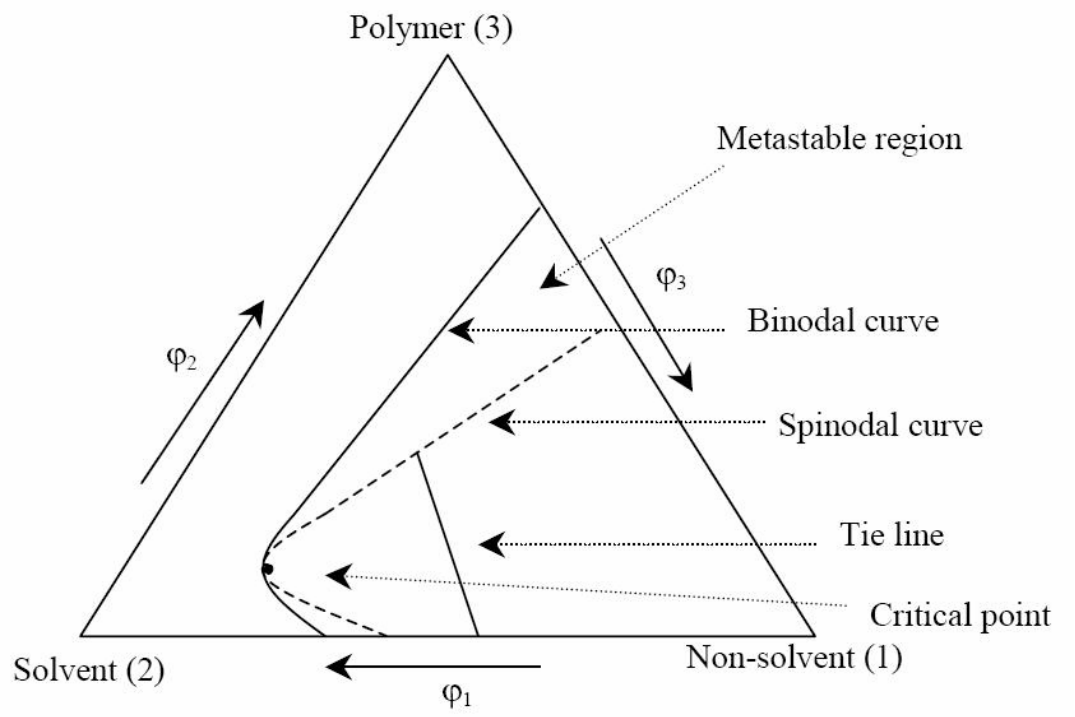

Figure 5.4. A representative phase diagram of a ternary mixture indicating the binodal, spinodal curves, the critical point (Source: Subrahmanyan 2003)

5.2.2.1. Binodal Curve

Binodal curve is the borderline between homogeneous phase region and two-phase region. Any two points on the binodal line correspond to compositions in two different phases that are in equilibrium. When homogeneous polymer solution phase separates into polymer-lean and polymer-rich phases, the composition of each component in both phases can be calculated by using the equations below:

$$\Delta\mu_i^L = \Delta\mu_i^R (i = 1,2) \qquad \sum_{i=1}^{3} \phi_{i,L} = 1 \qquad \sum_{i=1}^{3} \phi_{i,R} = 1 \tag{5.3}$$

$\Delta\mu_i$ and ϕ_i represent the chemical potential and the volume fraction of component "i" respectively. L and R denote the "polymer-lean" and "polymer-rich" phases. The subscripts refer to nonsolvent (1), solvent (2), and polymer (3).

The binodal composition is obtained under the equilibrium condition that the chemical potential $\Delta\mu_i = [\partial(\Delta G)/\partial n_i]_{T,P,n_{i\neq j}}$ of each component i in both phases is the same and the sum of the three component in each phase equals to one. Taking the composition in one phase as independent, five coupled nonlinear algebraic equations which consist of two material balances and the equilibrium condition for each component must be solved simultaneously in order to determine binodal compositions. The expressions for the chemical potentials are calculated by using Flory Huggins thermodynamic theory.

$$\frac{\Delta\mu_1}{RT} = \ln\phi_1 + 1 - \phi_1 - \phi_2(\nu_1/\nu_2) - \phi_3(\nu_1/\nu_3) + (\chi_{12}\phi_2 + \chi_{13}\phi_3)\times(\phi_2 + \phi_3) - \chi_{23}\phi_2\phi_3(\nu_1/\nu_2) \tag{5.4}$$

$$\frac{\Delta\mu_2}{RT} = \ln\phi_2 + 1 - \phi_2 - \phi_1(\nu_2/\nu_1) - \phi_3(\nu_2/\nu_3) + [\chi_{12}\phi_1(\nu_2/\nu_1) + \chi_{23}\phi_3] \times(\phi_1 + \phi_3) - \chi_{13}\phi_1\phi_3(\nu_2/\nu_1) \tag{5.5}$$

$$\frac{\Delta\mu_3}{RT} = \ln\phi_3 + 1 - \phi_3 - \phi_1(\nu_3/\nu_1) - \phi_2(\nu_3/\nu_2) + [\chi_{13}\phi_1(\nu_3/\nu_1) + \chi_{23}\phi_2(\nu_3/\nu_2)] \times(\phi_1 + \phi_2) - \chi_{12}\phi_1\phi_2(\nu_3/\nu_1) \tag{5.6}$$

where ν_i represents the pure molar volume of components i and χ_{ij} is the Flory Huggins interaction parameter between components i and j. The polymer concentration in polymer-lean phase is usually negligible, therefore it is assumed as zero. When the composition of the nonsolvent in the polymer-lean phase is set, then following equations are solved to construct binodal lines.

$$\Delta\mu_1^L = \Delta\mu_1^R \qquad \Delta\mu_2^L = \Delta\mu_2^R \qquad \phi_{1,R} + \phi_{2.R} + \phi_{3,R} = 1 \tag{5.7}$$

5.2.2.2. Spinodal Curve

Spinodal line forms a border between metastable and unstable two-phase regions and it is the line where all possible fluctuations lead to instability and phase separation occur spontaneously (Kim et al. 2001). The spinodal can be evaluated from the second derivative of the Gibbs free energy of mixing

$$G_{22}G_{33} = (G_{23})^2 \tag{5.8}$$

where

$$G_{ij} = \partial^2 \Delta G_m / \partial\phi_i \partial\phi_j \tag{5.9}$$

Spinodal composition can be calculated by choosing the concentration of nonsolvent as an independent variable. A single nonlinear equation is solved numerically with the variation of ϕ_1.

5.2.2.3. Critical Point

The binodal and spinodal lines coincide at a point called critical point, which is found by taking the third derivative of the Gibbs free energy of mixing given by the following equation:

$$\frac{\partial^3 \Delta G}{\partial x_B^3} = 0 \tag{5.10}$$

At any temperature above the critical point, mixtures exhibit a single phase at all compositions.

A Fortran program was written to solve nonlinear equations simultaneously. Three interaction parameters and molar volumes ν_i, i = 1, 2, 3 (1: nonsolvent, 2: solvent, 3: polymer) of three components need to be known in order to construct equilibrium binodal curve. The compositions of three components in the polymer-rich phase are obtained as an output and the binodal curve is plotted.

5.3. Determination of Binary Interaction Parameters

5.3.1. Nonsolvent/Polymer Interaction Parameter (χ_{13})

It was shown in literature that determination of nonsolvent/polymer interaction parameter (χ_{13}) is critical since this parameter has a considerable effect on the location of the miscibility gap in a ternary phase diagram (Karimi et al. 2005). Swelling and sorption experiments are generally used to determine χ_{13}.

5.3.1.1. Swelling-Equilibrium Experiment

χ_{13} can be determined from a swelling-equilibrium experiment based on the Flory-Rehner theory. In this experiment, a flask containing a polymer sample and nonsolvent is put in a cabinet in which the temperature is maintained constant. The swollen polymer sample is weighed every day until the reading reaches a constant value. Then, the nonsolvent/polymer interaction parameter is calculated by the following equation:

$$\chi_{13} = \frac{-\left[\ln(1-\phi_3)+\phi_3\right]}{\phi_3^2} \tag{5.11}$$

5.3.1.2. Sorption Experiment

χ_{13} parameter can also be determined from the solubility data in which equilibrium volume fraction of the nonsolvent in the polymer, ϕ_1 is known as a function of the vapor pressure of the nonsolvent, P_1. Using binary form of Flory Huggins equation:

$$Activity = \frac{P_1}{P_0} = \phi_1 \exp\left(\phi_3 + \chi_{13}\phi_3^2\right) \tag{5.12}$$

χ_{13} parameter is regressed from Equation (5.12) by minimizing the difference between the experimental and theoretical activities.

5.3.2. Solvent/Polymer Interaction Parameter (χ_{23})

The solvent/polymer interaction parameter (χ_{23}) is generally measured by using sorption data as explained in Section 5.3.1.2. χ_{23} can also be predicted by using Bristow's (Bristow and Watson 1958) semi-empirical equation given below by using the solubility parameters of the solvent, δ_2 and polymer, δ_3

$$\chi_{23} = 0.35 + \frac{V_2}{RT}(\delta_2 - \delta_3)^2 \tag{5.13}$$

Extensive tables for the solubility parameters of both polymers and solvents are reported in Polymer's Handbook (Brandrup et al. 1999).

5.3.3. Nonsolvent/Solvent Interaction Parameter (χ_{12})

5.3.3.1. Excess Gibbs Free Energy

The nonsolvent/solvent interaction parameter (χ_{12}) can be calculated by using the data of excess Gibbs free energy or activity coefficients available in the literature.

5.3.3.2. Vapor-Liquid Equilibrium Data

Vapor-liquid equilibrium data between solvent and nonsolvent, obtained as mole fraction in vapor phase versus mole fraction in liquid phase can also be utilized to calculate χ_{12}. For this purpose, data is converted to activity versus volume fraction and χ_{12} is regressed from the expression $activity = \phi_1 \exp(\phi_2 + \chi_{12}\phi_2^2)$ by minimizing the difference between the experimental and theoretical activities.

5.4. Previous Studies on Determination of Cloud Point Curves for PSf/Solvent/Nonsolvent Systems

There are only a few studies on the experimental ternary phase diagrams for PSf. Kim et al. (1997), determined the cloud point curves for PSf/1-methyl-2-pyrrolidinone (NMP)/water and PSf/Tetrahydrofuran(THF)/water systems by using a titration method. They found that small amount of water is needed to induce liquid-liquid demixing and homogeneous phase region is enlarged slightly with increasing temperature as shown in Figure 5.5. In addition, the homogeneous phase region was found to be larger when THF instead of NMP was used as solvent (Figure 5.5a and 5.5b). They also calculated phase diagrams by using constant interaction parameters as well as variable solvent-nonsolvent interaction parameter. Their calculation indicated that the phase behavior of PSf/solvent/water is significantly influenced by the nonsolvent-polymer interaction parameter, χ_{13}. By choosing concentration-dependent interaction S-NS parameter while other interaction parameters are constant, they were able to fit the calculated binodal curve with their experimental cloud point curve for PSf/THF/water. On the other hand, deviation between experimental data and calculation was observed for PSf/NMP/water system especially at high polymer concentrations. Authors have suggested using a concentration dependent solvent-polymer interaction parameter in order to explain the phase behavior of the PSf/NMP/water system.

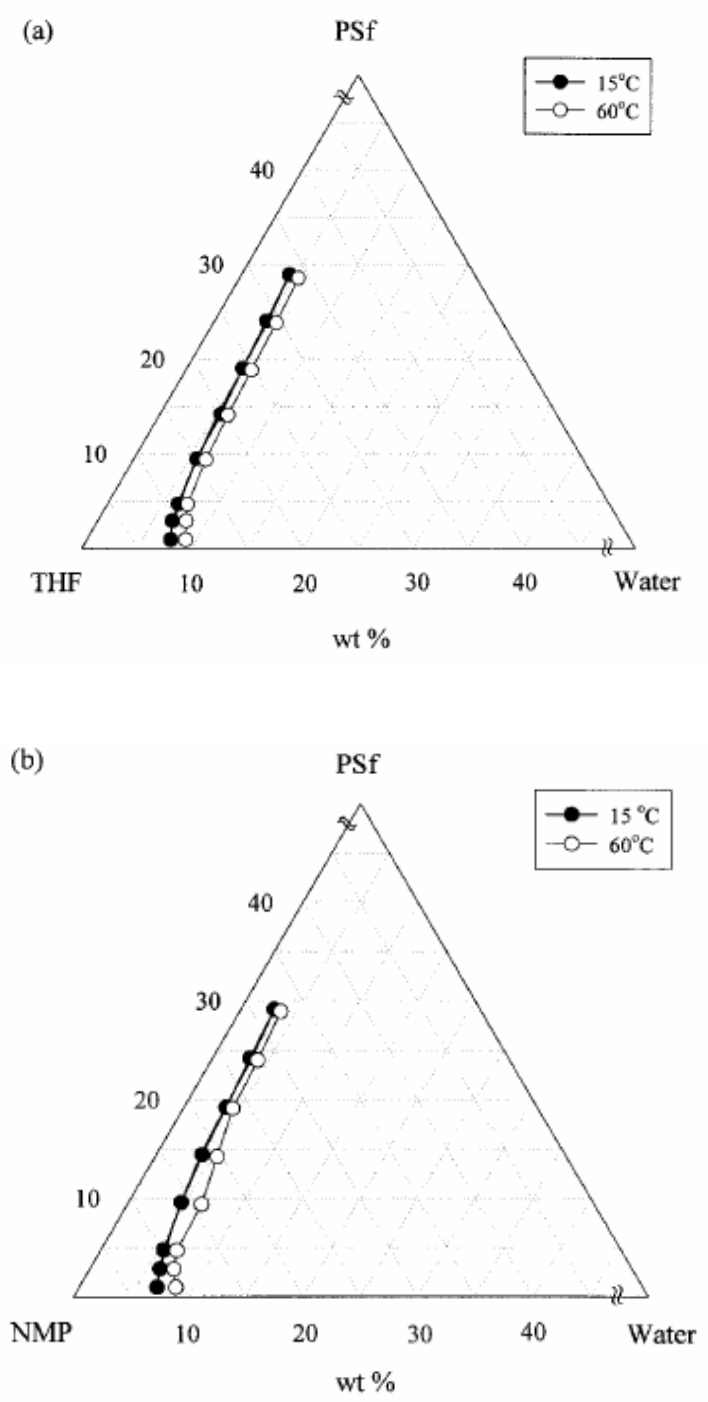

Figure 5.5. Cloud point curves of (a) PSf/THF/water and (b) PSf/NMP/water at 15°C and 60°C (Source: Kim et al. 1997)

In the study of Barth and Wolf (2000), the cloud point curves of PSf/DMF (Dimethylformamide)/water system at 20, 30, 40 and 50°C were determined by titration until turbidity could be detected visually. In the Figure 5.6, it was observed that the homogeneous phase was very small. Another observation was two phase regions change only little with temperature. The numbers in abbreviations indicate the weight average

molecular weight in kg/mol as determined by light scattering experiments in NMP at 30°C. The theoretical calculation of phase diagrams was performed by minimizing the Gibbs energy of mixing and using the binary interaction parameters which are experimentally determined by using Head space gas chromatography and swelling experiments. The binary interaction parameters for the systems DMF/water and DMF/PSf were determined as a function of composition and temperature.

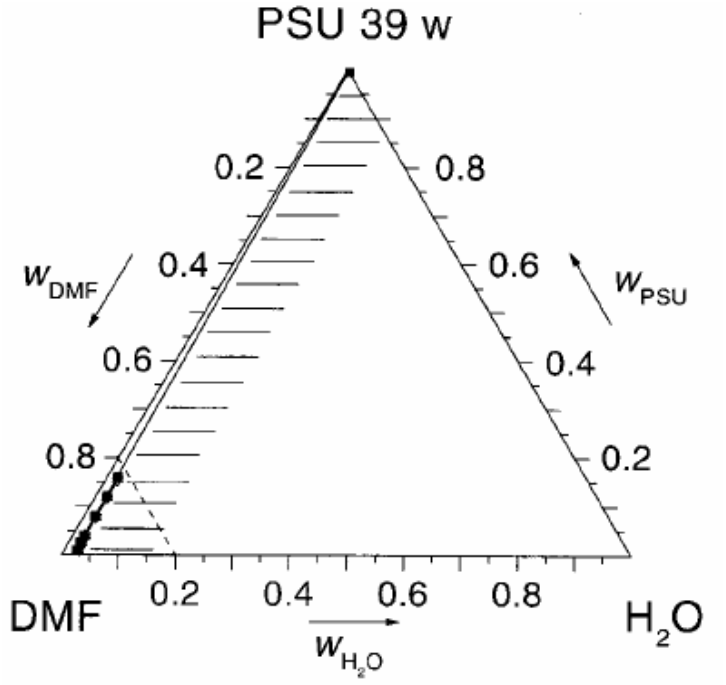

Figure 5.6. Cloud point curves of the system PSf/DMF/water
(Source: Barth and Wolf 2000)

In the study of Karimi et al. (2005), gravimetric water vapor sorption experiments carried out in order to determine sorption isotherms of water in polysulfone at 25°C by use of magnetic suspension balance. The Flory Huggins nonsolvent/polymer interaction parameter (χ_{13}) is found as 3.67 as by this sorption technique. In this study χ_{13} parameter is also determined by fitting experimental cloud point data of ternary polymer systems with the Flory Huggins theory and given as 2.5 for the PSf/NMP/water system and 3.2 for the PSf/THF/water system. χ_{12} and χ_{23} values and the data sets of experimental cloud points for the given ternary systems were taken from the literature. It was found that χ_{13} values obtained from sorption were larger than from fitting. According to this study, it was concluded that equilibrium water uptake techniques, like

sorption or swelling measurements could not give precise χ_{13} values for hydrophobic membrane polymers.

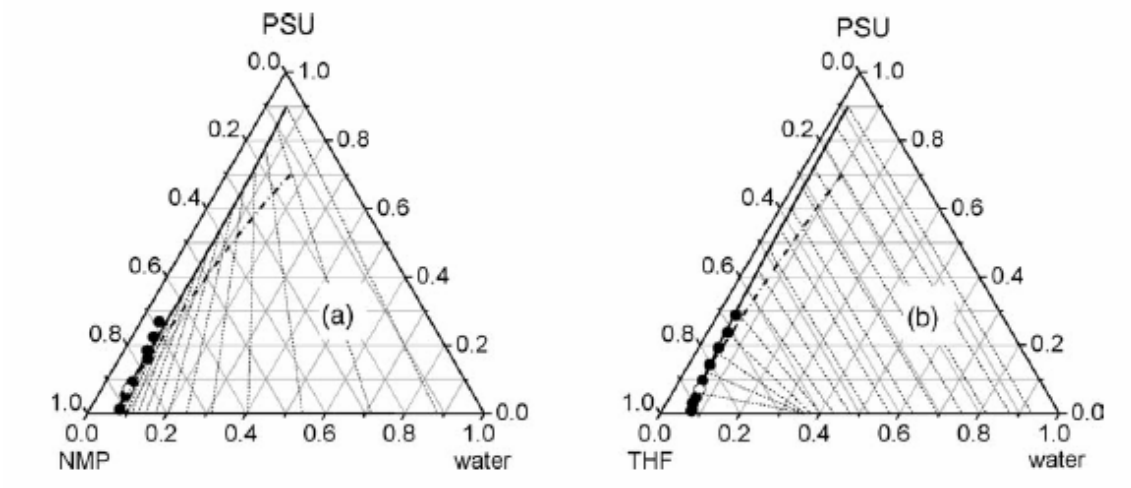

Figure 5.7. Calculated binodal curves obtained by fitting technique (full line) for (a) PSf/NMP/water and (b) PSf/THF/water systems in comparison with experimental cloud points (full circle) (Source: Karimi et al. 2005)

It was observed that experimental cloud points were in good agreement with the calculated binodal curves on the basis of the Flory Huggins model with a constant water/polymer interaction parameter.

Altena and Smolders (1982), calculated the binodal curves for polysulfone/solvent/water system. The Flory Huggins theory for three component systems was used. The values for the binary interaction parameters were taken from literature sources. Good agreement was found between calculated and experimentally found miscibility gaps when the solvent/nonsolvent parameter was taken to be concentration dependent and the other parameters, were kept constant (Figure 5.8). The interaction parameter χ_{13} was determined from equilibrium swelling measurements and reported as 3.7. It was observed that the demixing behavior was mainly determined by χ_{13}. Large variations in χ_{12} and χ_{23} only had a small effect on the ternary phase diagram. Small amount of water, a few percent, was needed to achieve phase separation.

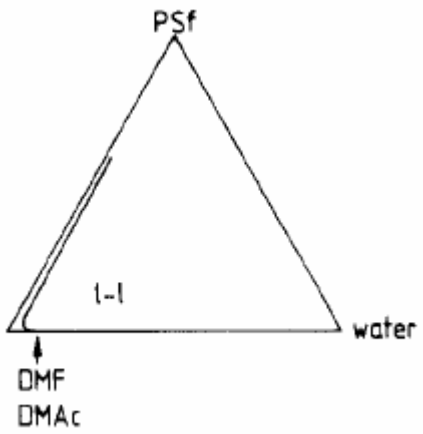

Figure 5.8. Approximate situation of the liquid-liquid (l-l) phase separataion gap in PSf/solvent/water membrane forming systems (Source: Altena and Smolders 1982)

Han (1999) investigated the effect of propionic acid (PA) in the casting solution on the characteristics of phase inversion polysulfone membranes. Cloud points were determined by titration of polysulfone-NMP and polysulfone-(NMP+PA) solutions with water. In the Figure 5.9, it could be seen that with the addition of PA in the casting solution, the miscibility are of the system was reduced means that the PA added solution needed less water for the phase separation than the binary solution of NMP and PSf.

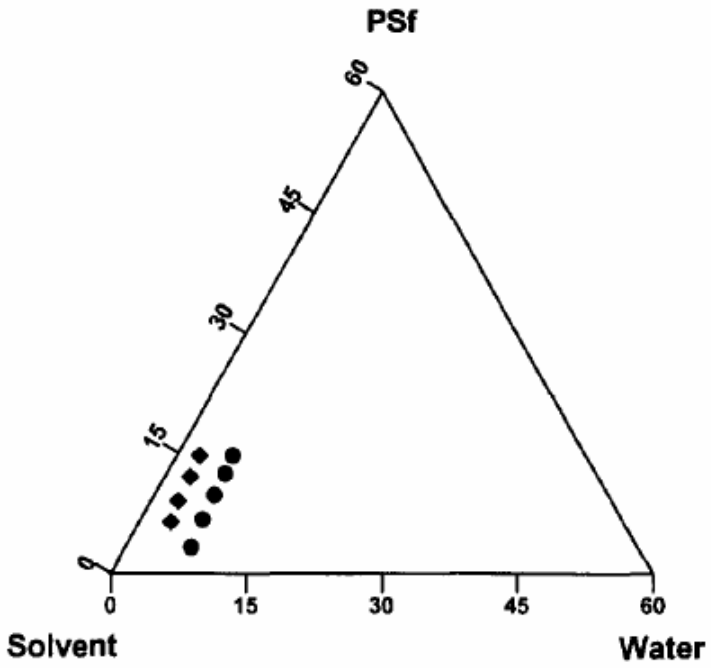

Figure 5.9. Cloud point data for PSf-NMP-water and PSf-(NMP+PA)-water system (● NMP; ◆ NMP+PA) (Source: Han et al. 1999)

5.5. Previous Studies on Determination of Cloud Point Curves for PMMA/Solvent/Nonsolvent Systems

In the study of Lai et al. (1998), the ternary phase diagrams of PMMA/n-butyl-acetate/n-hexane, PMMA/acetone/water and PMMA/acetone/n-hexane were constructed by theoretical calculation and experimental measurement. Experimental cloud points were measured by titrating the PMMA solutions with water until the onset of turbidity and binodal curves were calculated by using Flory Huggins theory for three-component systems.

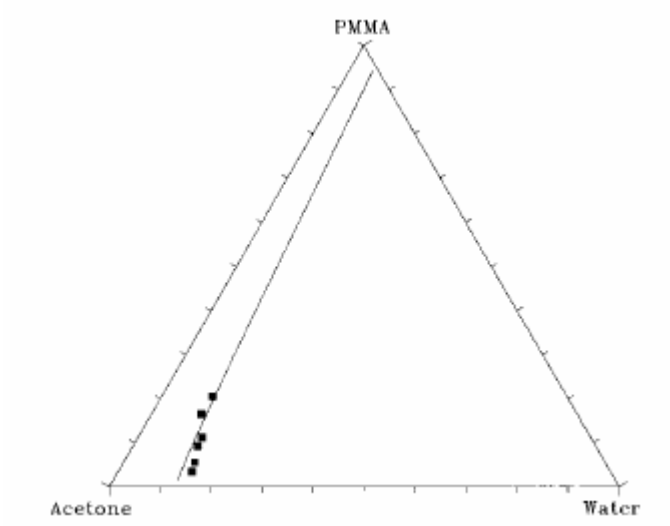

Figure 5.10. Comparison between the calculated and experimental binodal curves for PMMA/acetone/water system at 25°C (Source: Lai et al. 1998)

Good agreement was obtained between the calculation and the measurement by using concentration-dependent water/acetone and acetone/PMMA interaction parameters and constant water/PMMA interaction parameters as shown in Figure 5.10. χ_{13} (water-PMMA interaction parameter) was determined as 2.34 by using swelling-equilibrium measurements. g_{23} (acetone-PMMA interaction parameter) at different concentrations was measured as $g_{23} = 0.48 + 0.23\nu_3$ by Cahn microbalance. The concentration of polymer solution was determined by measuring the amount of solvent absorbed by PMMA. g_{12} (water-acetone interaction parameter) was calculated by using the data of excess Gibbs free energy or activity coefficients obtained from literature sources and found as $g_{12} = 0.661 + 0.417 / (1-0.755u_2)$.

CHAPTER 6

MODELING OF SORPTION PROCESS

The transport behavior of small molecules in polymers strongly depends on the polymer structure and mobility. Diffusion in polymers is one of the fundamental problems associated with a variety of industrial applications including controlled drug release systems, packaging and separation technologies.

"When a penetrant diffuses into a polymer film, the macromolecules rearrange toward a new configuration with a relaxation rate that depends on temperature as well as on solvent concentration". The nature of the transport process is determined by the relative timescales of the diffusion and relaxation processes (Rodriguez 2003).

In the next sections, typical sorption kinetics and model equations to describe these kinetics are given. These models are combined with experimentally measured sorption curves to determine diffusion coefficients and relaxation times. The diffusion regimes and features of diffusion in glassy polymers are also discussed.

6.1. Typical Sorption Kinetics

Results of the typical sorption experiments are generally presented by plots of mass uptake as a function of square root of time ($t^{1/2}$). The response of the polymers in the presence of a penetrant can be categorized into different classes based on the rates of penetrant diffusion and relaxation of the polymer. Sorption kinetics as categorized according to the shape of the mass uptake (M_t/M_∞) as a function of $\sqrt{t}$ as shown in Figure 6.1.

6.1.1. Case I Sorption (Fickian Sorption)

This type of diffusion occurs when the rate of diffusion is significantly slower than the rate of relaxation of the polymer chains (Ghi et al. 2000). When the fractional mass uptake is plotted as a function of square root of time, the Fickian sorption curves exhibit the following behavior:

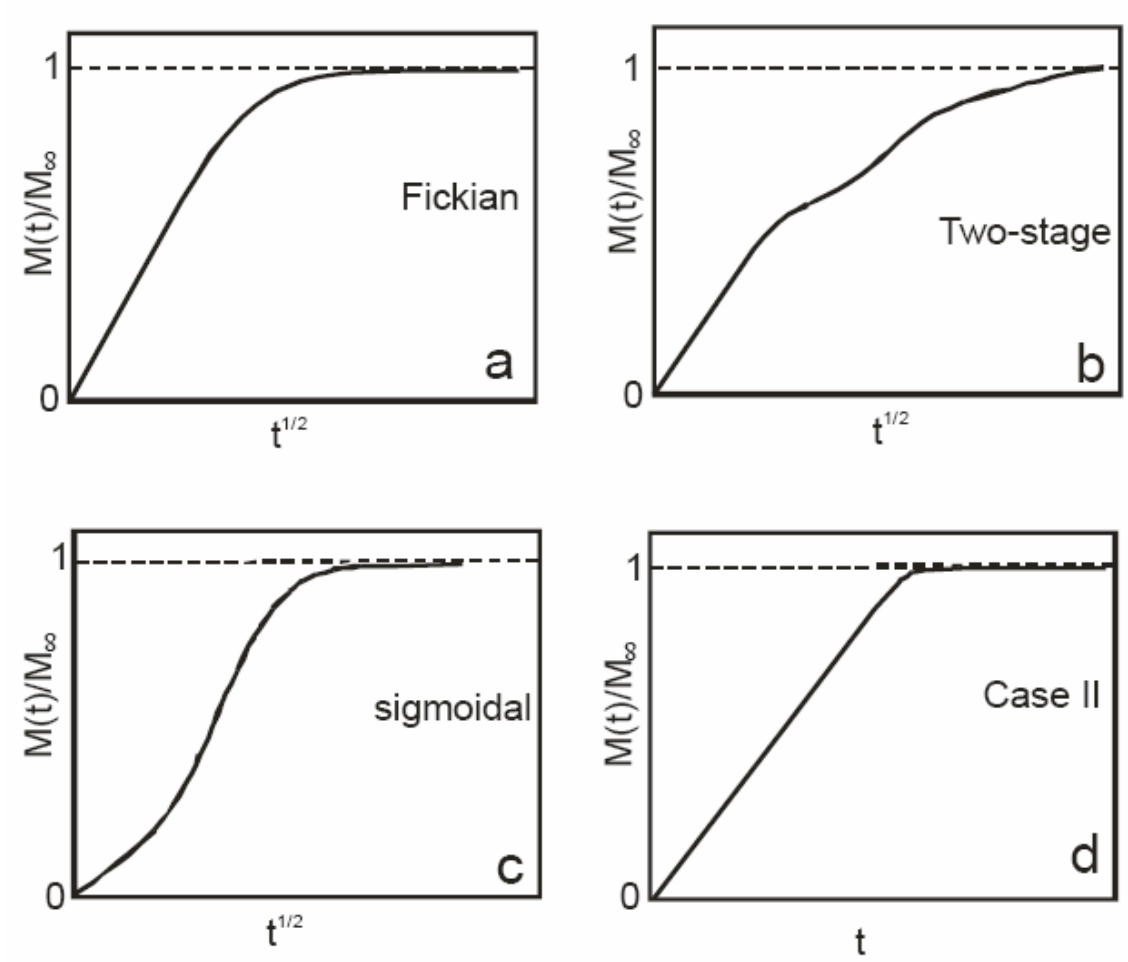

Figure 6.1. Typical sorption kinetics: (a) Fickian; (b) Two-stage; (c) Sigmoidal; (d) Case II (Source: McDonough 2004)

1. In the initial stages of the sorption process, the sorption curve becomes linear.
2. This linear region extends up to 60% of the uptake ($M_t/M_\infty = 0.6$).
3. Above the linear portion, the sorption curve becomes concave with respect to the $t^{1/2}$ axis.
4. The sorption curves obtained for different values of the film thicknesses when plotted as M_t / M_∞ versus $t^{1/2} / L$ coincide with each other.
5. The sorption and desorption curves at the same temperatures coincide with each other.

Penetrant diffusion through rubbery polymers is generally Fickian. The polymers in the rubbery state respond rapidly to changes in their condition. If they are above their glass transition temperature, the polymer chain adjust so quickly in the presence of penetrant that they do not show diffusion anomalies (Crank 1975). This

sorption behavior is also observed in glassy polymers at low penetrant activities (Dhoot 2004).

If Fickian diffusion controls the penetrant uptake in a polymer film of uniform thickness, then the time required to reach equilibrium is determined by the diffusivity of penetrant in the polymer film (Crank, 1975):

$$t_{eq} \approx \frac{L^2}{D} \tag{6.1}$$

In order to determine diffusivity of penetrant in the polymer film for Case I sorption, unsteady-state process is modeled using following assumptions:

1. The diffusion process is one dimensional transport process in a polymer film of thickness L
2. Diffusion process is a viscous Fickian process
3. There is no chemical reaction between the penetrant and the polymer film.
4. The diffusion process is isothermal
5. The vapor phase is essentially pure
6. The mutual diffusion coefficient D is independent of concentration during each step of the sorption process

Under these assumptions, sorption process is described by the following equation

$$\frac{\partial C}{\partial t} = D \frac{\partial^2 C}{\partial x^2} \tag{6.2}$$

Initially, the concentration of the penetrant, C_0, in the polymer is same everywhere;

$$t = 0 \rightarrow C = C_0 \tag{6.3}$$

At times t > 0, the concentration of the penetrant at the surface is constant and equal to its equilibrium concentration, C_{eq}

$$t > 0 \rightarrow x = L \quad C = C_{eq} \tag{6.4}$$

and concentration gradient at the lower surface is zero since this surface is impermeable to penetrant vapor

$$t > 0, \; x = 0, \; \partial C/\partial x = 0 \tag{6.5}$$

Analytical solution of equation (6.2) through equation (6.5) is given by Crank (1975) as:

$$\frac{C - C_0}{C_1 - C_0} = 1 - \frac{4}{\pi} \sum_{n=o}^{\infty} \frac{(-1)^n}{2n+1} \exp\left\{- D(2n+1)^2 \pi^2 t / L^2\right\} \cos \frac{(2n+1)\pi x}{L} \tag{6.6}$$

Equation (6.6) is integrated from x = 0 to x = + L, then the dimensionless uptake is obtained as follows;

$$\frac{M_t'}{M_\infty'} = \frac{M_t - M_0}{M_\infty - M_0} = 1 - \frac{8}{\pi^2} \sum_{m=0}^{\infty} \frac{1}{(2m+1)^2} \exp\left\{- D(2m+1)^2 \pi^2 t / L^2\right\} \tag{6.7}$$

where M_t and M_∞ are the penetrant mass uptake at time t and at equilibrium, respectively; while M_0 is the mass of the polymer film at the beginning of each sorption step; D is the diffusion coefficient; and L is the film thickness (Crank 1975). Diffusivity can be estimated by minimizing the difference between experimental fractional mass uptake data and theoretical ones calculated from Equation 6.7.

Crank (1975) has shown that at short times, $t \rightarrow 0$, Equation (6.7) can be simplified as follows;

$$\frac{M_t'}{M_\infty'} = \frac{2}{\sqrt{t}} \left(\frac{Dt}{L^2} \right)^{1/2} \tag{6.8}$$

Equation (6.8) indicates that at short times, uptake curve becomes linear and diffusion coefficient can be easily calculated from the slope of the plot of M_t' / M_∞' versus $t^{1/2}$.

6.1.2. Case II Sorption

Case II sorption is considered as a typical non-Fickian behavior (Figure 6.1d). This type of diffusion occurs when the rate of penetrant diffusion is greater than the rate of relaxation of the polymer chains (Ghi et al. 2000), and is strongly depend on swelling kinetics (Chin et al. 1999). The main feature of Case II sorption is a sharp diffusion front separating a swollen penetrated distance from a glassy core. In addition, the penetrant weight uptake is proportional to time rather than the square root of time, as in other cases (McDonough 2004).

Hopfenberg and Frisch (1969) rewrote the Fick's second law (Equation 6.2), incorporating a term to describe the constant velocity movement of a penetrant front.

$$\frac{\partial C}{\partial t} = \frac{\partial}{\partial x}\left(D\frac{\partial C}{\partial x} - \nu C \right) \tag{6.9}$$

According to Hopfenberg and Frisch, anomalous penetrant uptake could be expressed by the motion of the solvent front described by a linear combination of the two effects:

$$\nu = N_a k_a t^{1/2} + N_b k_b t \tag{6.10}$$

where ν is the front velocity, N_a and N_b are the mole fraction of each component and k_a, k_b are uptake rate constants for pure liquid a or b.

Thomas and Windle observed that methanol absorption in PMMA obeys Case II sorption. They assumed that diffusion of the solvent in a swollen element is much faster than in a glassy element. When solvent molecules enter the element, they clear the way for following molecules; the plasticizing effect causes next molecules to enter more rapidly. Accumulation is initially faster than transport to the next element and this result in a sharp front (van der Wel and Adan 1999).

6.1.3. Case III Sorption

Case III sorption or anomalous diffusion occurs in the transition region between Case I and Case II sorption, when the rates of polymer relaxation and penetrant

diffusion are comparable. There are two types of anomalous diffusion, two-stage sorption and sigmodial sorption.

6.1.3.1. Two-Stage Sorption

Two-stage sorption is generally defined as anomalous type of absorption. It is named ′two-stage' sorption because the sorption curve appears to be composed from two different parts: (1) fast Fickian sorption; (2) slow non-Fickian. The sorption curve is Fickian from the start until it starts to level off. Instead off reaching the equilibrium level which is typical for Fickian sorption, the curve is extended through a non-Fickian part. Finally equilibrium is reached for all instances (van der Wel and Adan 1999). General appearance of two-stage sorption is shown in Figure 6.1b. This type of diffusion behavior is often observed for organic vapor sorption in glassy polymers such as benzene in PET, acetone in PET, ethyl benzene in polystyrene (Dhoot et al. 2001).

A theory, describing the features of 'two-stage' sorption, has been proposed by Berens and Hopfenberg in 1978 (Berens and Hopfenberg 1978). According to their diffusion-relaxation model, sorption process is composed of two phenomenologically independent contributions: a diffusion part $M_F(t)$ governed by Fick's laws and a structural part $M_R(t)$, resulting from polymer relaxations. The total weight gain at time t is then expressed as the linear superposition of these contributions:

$$M(t) = M_F(t) + M_R(t) \tag{6.11}$$

It is generally assumed that viscoelastic processes in polymers are described by a distribution of relaxation times, so $M_R(t)$ is given by:

$$M_R(t) = \sum M_{\infty,i}\left[1 - \exp(-k_i t)\right] \tag{6.12}$$

where $M_{\infty,i}$ represents the equilibrium sorption due to the *i*th relaxation process, and k_i is the first-order relaxation constant of the *i*th relaxation process. In the study of Berens and Hopfenberg (1978), this model has been developed for diffusion in spherical particles, but it has also been applied to diffusion in polymer films (van der Waal and Adan 1999).

Two-stage sorption, a non-Fickian phenomenon, has been observed by several researchers. A two-stage model incorporates Fickian diffusion at short times and protracted structural relaxation at long times (Dhoot et al. 2001). The diffusion process controls mass uptake at short times and polymer relaxation controls mass uptake at long times. The intermediate plateau region observed in each plot separates the diffusion-controlled and relaxation-controlled regimes of mass transfer. This sorption kinetics is often described using the following empirical model:

$$\frac{M_t}{M_\infty} = (1-\alpha_R)\left\{1-\frac{8}{\pi^2}\sum_{n=0}^{\infty}\frac{1}{(2n+1)^2}\times\exp\left[\frac{-D(2n+1)^2\pi^2 t}{l^2}\right]\right\} + \alpha_R\left\{1-\exp\left[\frac{-(t-t_D)}{\tau_R}\right]\right\} \tag{6.13}$$

where D is the average diffusion coefficient, α_R is the fraction of weight uptake controlled by polymer relaxation, τ_R is the time constant characterizing the long time drift in mass uptake toward equilibrium, t_D is a delay factor associated with a delay in the beginning of structural relaxation. α_R must lie between zero and one and can be determined from the intermediate plateaus which are representative of the fraction of mass uptake controlled by structural relaxation. Typical values of t_D range from 0 to l^2/D, which corresponds to the end of Fickian diffusion.

At short times, the fractional mass uptake, M_t/M_∞ increases linearly with the square root of time, which is characteristic of sorption kinetics controlled by Fickian diffusion and can be modeled as given in Equation 6.8. The average Fickian diffusion coefficient can be estimated from a best fit of data to the analytical model.

$$\frac{M_t}{M_\infty(1-\alpha_R)} = 1-\frac{8}{\pi^2}\sum_{n=0}^{\infty}\frac{1}{(2n+1)^2}\times\exp\left(\frac{-D(2n+1)^2\pi^2 t}{4l^2}\right) \tag{6.14}$$

At longer times, the mass uptake shows a protracted, non-Fickian asymptotic approach toward equilibrium. Protracted stage of uptake is associated with mass uptake controlled by the viscoelastic relaxation of the polymer chains to accommodate penetrant and can be modeled as

$$\frac{M_t}{M_\infty} = 1 - \alpha_R \exp\left[-\frac{(t - t_D)}{\tau_R}\right] \tag{6.15}$$

In the study of Dhoot et al. (2001), α_R was obtained from the plateaus, in the sorption curves while D was calculated from the slope of the initial kinetic data, which is linear in $t^{1/2}$, using the following relation:

$$\frac{M_t / M_\infty}{(1 - \alpha_R)} = 4\left(\frac{\overline{Dt}}{\pi l^2}\right) \tag{6.16}$$

The parameters τ_R and t_D were obtained by fitting the long-time kinetic data to the following equation:

$$\ln\left(1 - \frac{M_t}{M_\infty}\right) = \left(\ln \alpha_R + \frac{t_D}{t_R}\right) - \frac{t}{\tau_R} \tag{6.17}$$

Equation (6.14) clearly shows that when $\alpha_R = 0$, then Equation (6.7) is recovered which is used to analyze Fickian sorption curves.

6.1.3.2. Sigmoidal Sorption

Sigmoidal sorption curves are S-shaped, showing a point of inflection (Figure 6.1c). The transport process in the film is Fickian, but due to the slow establishment of equilibrium at the surface of the film, kinetics show anomalous behavior.

Long and Richman proposed a variable surface-concentration model to describe an anomalous, sigmoidal sorption curve. Rodriguez et al. (2003) used a simplified version model, suggested by Crank (1975). It is assumed that the diffusion process is Fickian, and that the surface concentration approaches exponentially the equilibrium concentration, C_0, at the selected activity:

$$C(L,t) = C_0\left[1 - \exp(-\beta t)\right] \tag{6.18}$$

where β is the inverse of the characteristic time for attaining saturation at the surface. If $\beta \to \infty$, the surface concentration rises instantaneously to C_0 and the curve has the characteristic initial linear portion followed by the approach to the equilibrium as seen in Fickian sorption process. The solution of Fick's second law with the boundary conditions given by Equation 6.19 and with a constant diffusion coefficient D is:

$$\frac{M_t'}{M_\infty'} = 1 - \exp(-\beta t)\left(\frac{D}{\beta l^2}\right)^{1/2} \tan\left[\left(\frac{\beta l^2}{D}\right)^{1/2}\right] - \frac{8}{\pi^2}\sum_{n=0}^{\infty} \frac{\exp\left[-D(2n+1)^2\pi^2\frac{t}{4l^2}\right]}{(2n+1)^2\left\{1-(2n+1)^2\left[\frac{D\pi^2}{\beta 4l^2}\right]\right\}} \tag{6.19}$$

Figure 6.2 shows the influence of the value of β on the shape of the sorption curves.

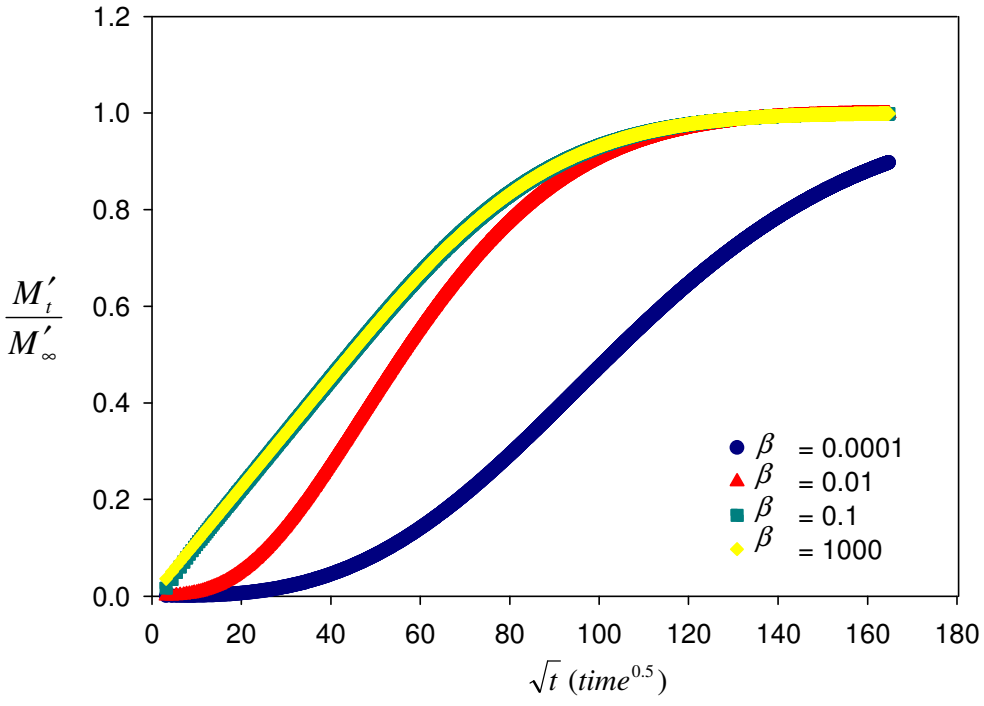

Figure 6.2. Calculation of sorption curves for different β values

6.1.4. Sorption Overshoot

In some cases, a plot of the fractional penetrant uptake M_t / M_∞ versus $t^{0.5}$ presents a characteristic maximum before attainment of the final equilibrium value. This feature of uptake kinetics is called 'sorption overshoot', and it is in general due to a rearrangement of the polymer chains following plasticization induced by a penetrant. In the literature, four possible reasons are reported for overshooting of the equilibrium penetrant concentration. First, sorption overshoots are observed during sorption of strongly interacting liquids or vapors in initially amorphous, crystallizable glassy polymers. The newly formed crystalline regions are impenetrable and part of the sorbed penetrant is expelled out thus producing the maximum in the sorption curve.

Second, a penetrant-induced melting of unstable crystals and subsequent formation of stable crystals may lead to a sorption maximum without a net change in the crystallinity fraction. Thermally induced structural reorganizations, such as primary and secondary crystallization and melting were verified by modulated differential scanning calorimetry (MDSC) in the study of Alentiev et al. (2001).

Third, sorption overshoot in rubbery and glassy polymers may occur from a slow relaxation of the polymer chains to a more compact structure. Although most of these types of effects are usually mentioned in glassy polymers, overshoots in rubbery polymers are also reported in literature (Ghi et al. 2000). In glassy polymers, the overshoot is related to the relaxation processes of the polymer chains as mentioned in Etxeberria et al. (2000). The velocity of the solvent diffusion in the polymer is faster than the chain movements at high activities. This fast sorption stresses the polymeric chains facilitating relaxation processes and accompanied by plasticization effect of the sorbed solvent. These structural rearrangements cause a decrease in the solvent solubility and existence of overshoots in the sorption kinetics. At lower activities, the solvent absorption is not very fast so the effect is expected smaller. When a slow process such as swelling partially controls the sorption kinetics, thickness of the sample becomes an important parameter (Hoyt and Balik 1996).

Finally, release of domestic components of the polymer matrix after contact with liquid may cause a maximum in kinetic sorption (Rodriguez et al. 2003).

6.2. Diffusion Regimes

When a penetrant diffuses into a polymer film, the macromolecules rearrange toward a new configuration with a relaxation rate. The relative time scales of the diffusion and relaxation processes determine the nature of the transport process (Rodriguez 2003). Vrentas defined a diffusive Deborah number, De, as the ratio of two characteristic times, relaxation time for the polymer-solvent systems (λ_m) and the characteristic diffusion time (θ_D) (Vrentas and Duda, 1979).

$$(DEB)_D = \lambda_m / \theta_D \tag{6.20}$$

where θ_D is defined as L^2 / D. When De << 1, diffusion rate is significantly slower than the relaxation rate of the polymer chain, and viscous Fickian diffusion is observed. In this case, conformational changes in the polymer take place essentially instantaneously and both solvent and polymer behave like purely viscous fluids (Vrentas and Duda 1979). When the Deborah number is sufficiently large, the diffusive process is fast compared to the molecular relaxation, and this type of diffusional transport can be denoted as elastic Fickian diffusion. There is essentially no time variation of the structure of the polymer during diffusion process. Under these conditions, a solvent molecule moves in a material which appears to have the properties of an elastic solid (Vrentas and Duda 1979). If the Deborah number is of the order of unity, the molecular relaxation and diffusive transport processes occur in comparable time scales, and rearrangement of polymer chains and movement of solvent molecules take place simultaneously. This type of diffusion transport is known as viscoelastic (anomalous) nonFickian diffusion (Vrentas 1977). Fickian behavior is expected for rubbery polymers at temperatures above the glass transition temperature, whereas anomalous sorption is more likely to occur for polymer-penetrant mixtures in the glassy state (Rodriguez 2003). The sorption curves (M_t' / M_∞' versus $t^{1/2} / L$) for films of different thicknesses give a single curve for the cases of viscous Fickian and elastic Fickian diffusion means that the binary diffusion coefficient of the polymer-solvent systems is independent of L. However, in the case of anomalous, non-Fickian diffusion, the sorption curve for films of different thicknesses may not yield a single curve, i.e., the mutual diffusion coefficient may depend on L. Anomalous features may depend on time-dependent

surface concentration and anisotropic dimensional changes in the polymer sample other than polymer relaxation (Rodriguez 2003).

6.3. Diffusion in Glassy Polymers

In glassy polymers, deviations from Fickian behavior are generally observed. These deviations are considered to arise as a consequence of the finite rate of polymer structure reorganization in response to the sorption or desorption of penetrant molecules. Anomalous effects may be related to the influence of the changing polmer structure on solubility and diffusional mobility, or they may arise from the internal stresses exerted by one part of the medium on another as diffusion proceeds (Crank 1975). When penetrant sorption is realized by swelling of the polymer, any time dependent resistance to changes in the volume of the polymer can lead to non-Fickian sorption kinetics. Non-Fickian diffusion is commonly observed in sorption of organic vapors into glassy polymers. When the penetrant swells the polymer, local stresses occur and these stresses can be quite high to cause mechanical failure in the polymer (Dhoot 2004). If the polymer chains do not deform significantly upon penetrant sorption or the chains reorganize relative to the penetrant diffusion, Fickian behavior is observed.

CHAPTER 7

EXPERIMENTAL

7.1. Materials

Polysulfone (CAS: 25135-51-7, M_w: 56,000 g/mol) and PMMA (CAS: 9011-14-7, M_w: 15,000 g/mol) used in this study were obtained from Aldrich. The physical properties of the polymers are provided in Table 7.1. For polysulfone; ultapure water and ethanol (Panreac, ρ: 0.793 g/cm^3) are used as nonsolvents, THF (Panreac, ρ: 0.636 g/cm^3), NMP (1-methyl-2-pyrrolidinone, Aldrich, ρ: 1.033 g/cm^3) and chloroform (Riedel, ρ: 1.47 g/cm^3) are used as solvents. For PMMA; ultrapure water and formamide (Aldrich, ρ: 1.134 g/cm^3) are used as nonsolvents, while acetone (Merck, ρ: 0.79 g/cm^3) and THF are used as solvents. All chemicals were used as received without further purification.

Table 7.1. Properties of polymers

Properties	Polysulfone	PMMA
M_n (g/mol)	26,000	14,286
M_w (g/mol)	56,000	15,000 by GPC
Density (g/mL)	1.24	1.17
T_g (°C)	190	82
Supplier	Aldrich	Aldrich
CAS No	25135-51-7	9011-14-7

7.2. Film Preparation Method

Preparation of a polymer film strongly influences the structure of the film formed, which plays an important role on the diffusion behavior. In glassy polymers, the film preparation method is very important and all films for the same polymer are prepared following the same procedure to standardize their histories.

7.2.1. Polysulfone Film Preparation

Firstly polysulfone was dissolved in NMP and left on a magnetic stirrer for 1 day to get a clear solution. Polymer solutions were prepared at 20 wt% concentration when 10 and 30 µm films were aimed to obtain. These films were prepared by casting the solution on a clean and smooth glass substrate by knives with exactly dimensioned slits of 120 and 300 µm, through an automatic film applicator (Sheen 1133N). When films of 1-3 µm were prepared, the polymer solutions were prepared at 5 and 10 wt%. These thin films were prepared when long terms were required to attain the equilibrium, in order to shorten the required time. The cast films were put into an oven under vacuum. The temperature of the oven was raised to 190.5°C (4.8°C/min), above the glass transition temperature of the polymer and kept in the oven for 3 day. The films were dried in a vacuum oven at 100 mb to remove the solvent completely. To obtain annealed films of reproducible quality, the oven was switched off after 3 days and films were cooled slowly (1.2°C/min) for one day. After removing from the oven, the films were easily detached from the glass surface with a small amount of water. The film preparation was schematically shown in Figure 6.1. The dry-film thicknesses were measured using a micrometer (Testo) at different locations. The accuracy of the micrometer was ±0.03 mm. And the film thicknesses were measured accurately with Scanning Electron Microscope (SEM) to check the results. The thicknesses of the samples were measured from several different points and the average were used for subsequent calculation. The prepared films were kept in desiccator. Differential scanning calorimetry and thermal gravimetric analysis were used to ensure full removal of the solvent.

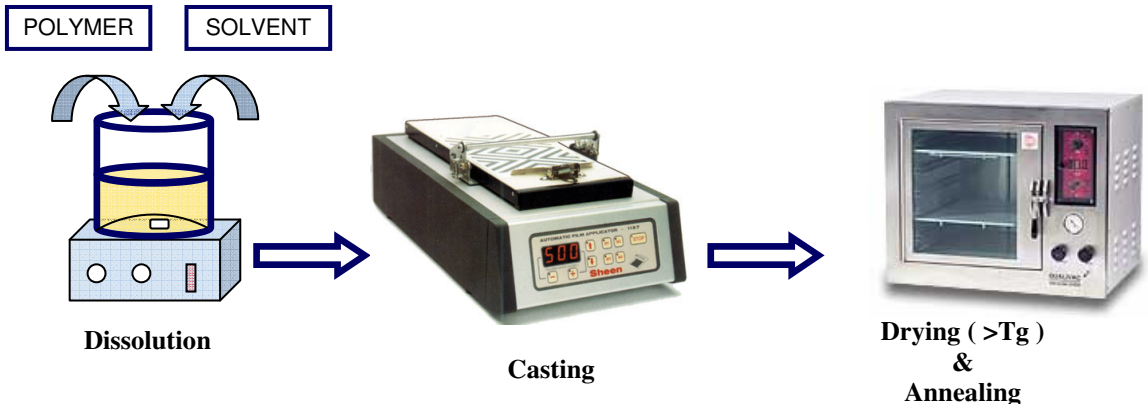

Figure 7.1. Schematic representation of film preparation procedure

Pieces in the size of approximately 11 × 11 mm were cut from the raw films. The latter size was used to fit the film onto the trays of the small stainless steel sample holder.

7.3. Characterization Studies

7.3.1. Scanning Electron Microscope (SEM) Analysis

Scanning Electron Microscope (Philips, XL-30SF6) was used to investigate the morphology of the films prepared and to measure the average thicknesses of the films. In the preparation stage, the film samples were coated with a thin gold layer to enable the transport of electrons from the electron beam that were not reflected or transformed to secondary electrons. The samples were placed in a sample holder and evacuated. Then the SEM pictures were obtained at certain magnifications to see the details of the films.

7.3.2. Differential Scanning Calorimetry (DSC) Analysis

Differential Scanning Calorimetry (Shimadzu DSC 50) was used to be ensure the full removal of the solvent from the polysulfone films. The boiling point of NMP used in film preparation is 220°C, as a result the ensurement was achieved by DSC analysis. 3.1 mg polysulfone film sample was placed in an aluminum pan and heated at a constant rate from 20°C to 500°C with a heating rate of 1°C/min until 30°C and 5°C/min above 30°C using nitrogen as a purge gas with a flow rate of 40 mL/min.

7.3.2. Thermal Gravimetric Analysis (TGA)

Thermal gravimetric analysis (TGA) was performed to prove no residual is left in the polysulfone films. Analysis was performed with Shimadzu TGA51 under nitrogen flow at a rate of 30 mL/min. 11.07 mg polysulfone film was placed in an aluminum pan and heasted continuously from 20°C to 600°C at a rate of 10°C/min.

7.4. Determination of Cloud Point Curves

The cloud point curves were determined by the titration of homogeneous polymer solutions with nonsolvents until the onset of turbidity. The concentration of polymer solutions was varied between 8-22 w %. Quantities of polymer was determined by using an electronic balance capable of reading up to ±0.0001 g and put into HPLC vials (10 mL) with its solvents. The flasks were capped tightly with a rubber septum stopper to avoid evaporation, and left in a fast-acting thermostat bath for one day in order to obtain homogeneous solutions (Figure 7.2). Afterwards, nonsolvents were added to the clear polymer solutions by a microsyringe (Agilent) with an accuracy of ±0.001 mL, through the septum until turbidity was observed. During titration, the solutions were well stirred and kept at a constant temperature by a fast-acting thermostat bath. The composition at which permanent turbidity first occurred is called the cloud point, which represents the composition where the phase transition occurred and was determined by measuring the amount of nonsolvent added.

Figure 7.2. Fast-acting thermostated bath

7.5. Magnetic Suspension Balance Analysis

7.5.1. Experimental Set-up and Operating Procedure

Magnetic suspension balance used for sorption measurements consists of four groups as main sorption unit, control unit, computer and supporting units (constant temperature baths, cold trap, heating tape, temperature controller, pressure transducer, tubings, fittings and ball valves) as shown in Figure 7.3.

Figure 7.3. Digital photograph of experimental set-up in laboratory. 1, balance; 2, sorption cell; 3, circulating water bath; 4, water bath; 5, pressure transducer; 6, vacuum pump; 7, cold trap; 8, heating tape; 9, temperature controller; 10, control unit; 11, computer

The resolution of the balance is 1 μg, the maximum load is 5 g, and the reproducibility of the measurements is ±2 μg. The magnetic suspension balance can withstand to high pressures up to 150 bars and temperatures up to 250°C. Housing of copper chrome zirconium is used to separate the measuring room between the suspension magnet and the electromagnet and its the inner surface is gold plated. The lower part of the housing is made of stainless steel. The sealing between the measuring cell and the weighing instrument is metal seal coated with gold. In order to protect the permanent magnet, it is completely sealed in a stainless steel housing. The entire interior volume of the magnetic suspension balance is thermostated to the sample temperature by means of double walled thermostated jacket which completely surrounds the measuring cell (Figure 7.4).

Figure 7.4. Double walled jacket for thermostating measuring cell with a circulating fluid (Source: WEB_2 2007)

A water bath (Polyscience, 3) with an accuracy of ±0.5°C and the operating range between 5°C above the room temperature and 100°C is used to circulate the fluid through the jacket. A thermocouple probe inserted into the column just below the sample holder, measures the temperature of the fluid in the column. The polymer films are put into a stainless steel sample holder and it is suspended from a permanent magnet. Sample holder consists of 5 stacked trays and each tray has 11.96 × 12.46 mm dimensions. Solvent vapor is prepared in a solvent flask inserted into a constant temperature bath (Heto, 4) which works between room temperature and 100°C (accuracy ±0.5°C). The vapor pressure of the solvent is measured by a pressure transducer (Omega, 5) operating within a range of vacuum up to 1 atm with an accuracy of 0.25% full scale. Vacuum is applied to the column by using a rotary vane pump (Vacuubrand, 6) which can provide vacuum up to 10^{-4} mbar. A cold trap (7) made of pyrex is placed between the sorption column and the vacuum pump. All tubings and fittings (Swagelok) are made of stainless steel and valves (Swagelok) exposed to solvent vapor are made of teflon. Heating tape (8) is wrapped on all solvent vapor line to prevent condensation of solvent vapor. The temperature of the heating tape is controlled by a temperature controller (Love controls, 9) with an accuracy of ±0.5°C.

The magnetic suspension and weight measurements can be controlled with the MessPro software and can be operated from the control unit shown in Figure 7.5. The suspension control unit consists of a main power switch, a dial to control the suspension coupling, and another dial on the rear of the unit to check the voltages in the system. The dial on the front of the unit can be set to OFF, zero point (ZP) and measuring point (MP) positions. In zero point position, the polymer sample is set down on a support such that the balance only measures the weight of the suspension coupling. In MP, the balance lifts the basket containing the polymer sample.

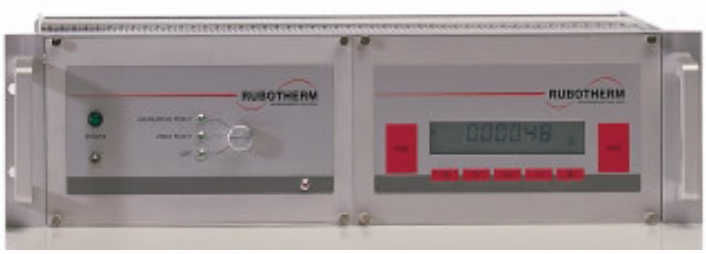

Figure 7.5. Illustration of suspension control and balance indicator units (Source: WEB_2 2007)

At the beginning of a typical experiment, five pieces in the size of approximately 11 × 11 mm are cut from the raw films. The sheets of the films are laid onto the trays of the sample holder and heated (4.8°C/min) to above the glass transition temperature of the polymer under 100 mb vacuum in a vacuum oven (Memmert) for a second time. After 2 hours at those conditions, the oven is cooled down at a rate of (1.2°C/min) for another 2 hours. The cooling process allows the film attach itself to the surface of the tray. Thus, the sorption experiment is carried as a diffusion from one side into the film. After that, sample holder is placed into the column, then the stainless steel jacket is located around the column and connected to water bath. The tubings and the fittings are heated up to 60°C by using heating tape and evacuated by a vacuum pump in order to remove water vapor condensated inside of the tubings. Then the program in the software is started and the temperature of the water bath is set 1°C above the desired temperature of the column. The system is allowed to reach equilibrium in 24 hours. After 24 hours, the column is evacuated for one hour via two connections to a vacuum pump. Then solvent line is evacuated for half an hour. When vapor-liquid equilibrium is achieved in the solvent flask at the desired temperature of the solvent, the pressure of the solvent vapor is measured by the pressure transducer and checked with the literature values. Meanwhile, the program in the software is started and measurement is taken for about every 5 seconds. After stable reading is observed, the solvent vapor is sent into the column by opening the valve. The weight change of the sample is followed as a function of time as shown in Figure 6.6. The software allows storing and drawing of all data measured.

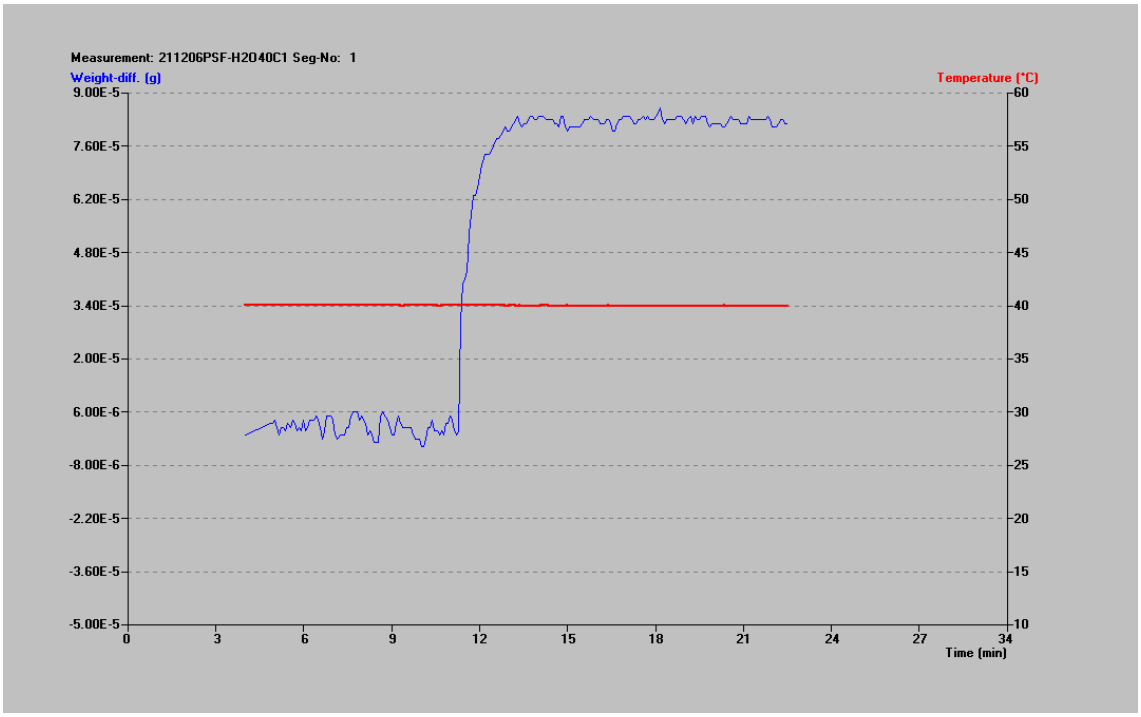

Figure 7.6. Typical computer software output obtained from sorption experiment

Once the polymer reaches an equilibrium state at a specific penetrant vapor pressure level, the valve is closed and an increase in the vapor pressure of the solvent is induced by increasing the temperature of the constant temperature bath. The step change in the column is produced by opening the valve and letting the solvent vapor at a new vapor pressure level into the column. This procedure is repeated until the temperature of the solvent vapor in the flask reaches to 5°C below the temperature of the column to avoid condensation in the column. A computer records all temperature and the weight change of the sample as a function of time automatically. The number of runs in a given series for each temperature of the column depends on the amount of the penetrant absorbed. Usually step size is adjusted to make difference between the equilibrium and initial mass of the penetrant, small. This adjustment allows assuming constant diffusivity within this range and negligible swelling of the polymer film. Schematic representation of the experimental system is shown in Figure 7.7.

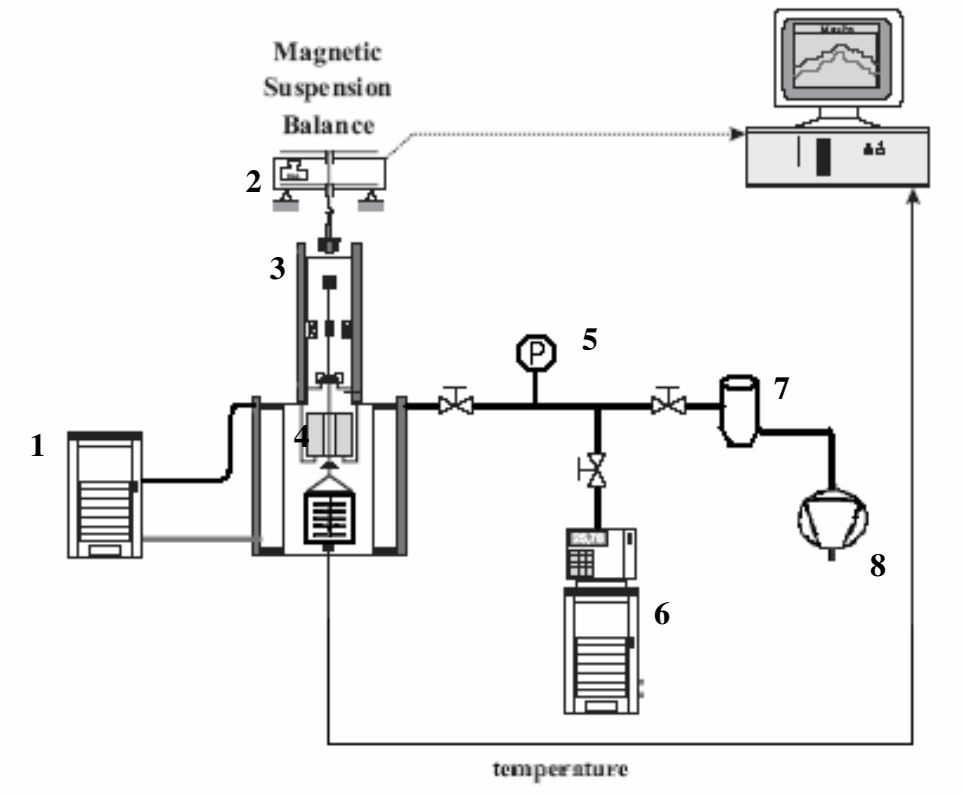

Figure 7.7. Schematic representation of the experimental system. 1, circulating liquid thermostat; 2, balance; 3, magnetic suspension coupling; 4, sorption cell; 5, pressure transducer; 6, water bath including solvent flask; 7, cold trap; 8, vacuum pump

7.5.2. Forces Affecting the System

Buoyancy of the solvent vapor in the measuring cell affects the measurement, thus, the buoyancy of the substrate at different vapor pressures and densities should be taken into account. Figure 7.8 shows all forces affecting the system. A balance of forces for the whole system in the vertical direction gives an equation for the determination of the amount of solvent vapor absorbed by the polymer.

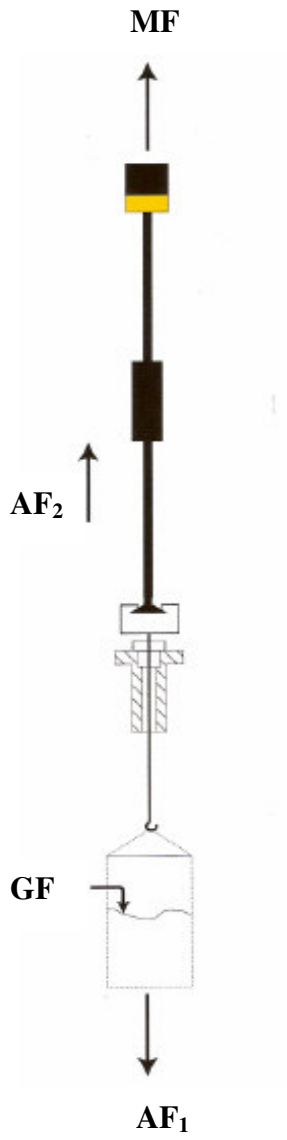

Figure 7.8. Forces affecting on the system

(Source: Rubotherm)

These forces are:

Measurement force or signal detected by the balance

$$MF = S_{MP} \cdot g \tag{7.1}$$

The force resulting from the absorption of an amount of vapor by the sample

$$AF_1 = m_{absorbed} \cdot g \tag{7.2}$$

Gravitational force affecting the system in the vacuum

$$GF = m_{vac} \cdot g \tag{7.3}$$

Ascending force affecting the system

$$AF_2 = \rho_{vapor} \cdot \left[V_{cage+hook} + V_{sample+vapor} + V_{samplecage} \right] \cdot g \tag{7.4}$$

If the balance of forces in vertical direction is written as

$$AF_1 + GF = MF + AF_2 \tag{7.5}$$

then, the absorbed amount of vapor can be determined from Equation 7.6.

$$m_{absorp} = S_{MP} + \rho_{vapor} \cdot \left[V_{cage+hook} + V_{sample+vapor} + V_{samplecage} \right] - m_{vac} \tag{7.6}$$

7.5.3. Determination of Volumes

In order to determine the ascending correction of the collected measuring data, the volume of the whole device should be determined. The explanation of the system is given in Figure 7.9. The total volume of the system as defined as follows:

$$V_{system} = V_{cage} + V_{hook} + V_{samplecage} \tag{7.7}$$

To determine these volumes, first of all, the weights of cage, hook and sample cage are measured:

$$W_{cage+hook} = 1.8260 \text{ g}$$
$$W_{sample\ cage} = 2.5852 \text{ g}$$
$$W_{suspension\ magnet} = 3.2577 \text{ g}$$

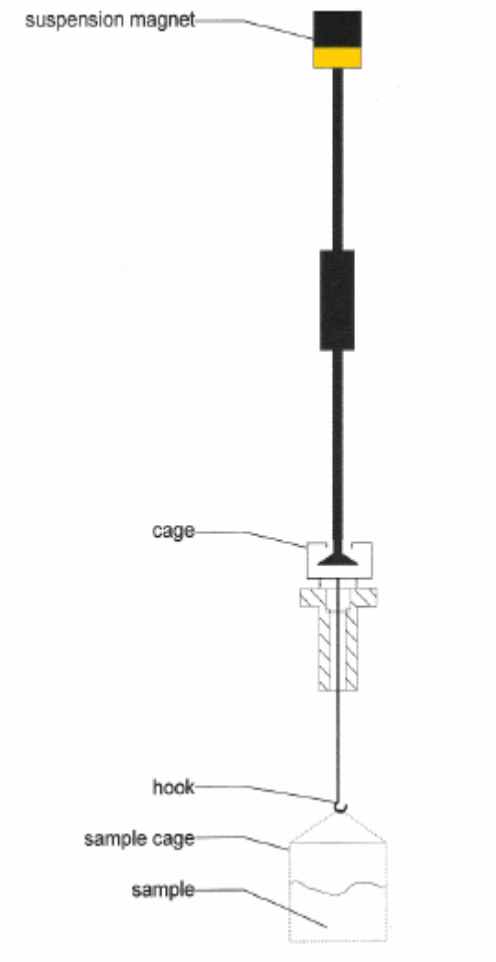

Figure 7.9. Explanation of the system

(Source: Rubotherm)

Then, these weights are corrected for bouyancy using the following equation:

$$M = W\left[\frac{1}{1-\frac{\rho_A}{\rho_{MG}}}\right] \tag{7.8}$$

In this equation; M is the buoyancy corrected weight, W is the weight displayed by the balance, ρ_A is the density of air (1.2 kg/m^3), and ρ_{MG} is the density of the material used in the balance (Stainless steel, 8000 kg/m^3).

According to this equation, buoyancy corrected weights are calculated as follows:

Bouyancy corrected weight of cage and hook:

$$M = 1.8262 \text{ g}$$

Bouyancy corrected weight of sample cage:

$$M = 2.5856 \text{ g}$$

Mass of cage, hook and sample cage:

$$1.8262 + 2.5856 = 4.4118 \text{ g}$$

Then, volume of cage, hook and sample cage:

$$V_{\text{cage+hook+sample cage}} = (2.5856 + 1.8262)/8 = 0.5514 \text{ cm}^3$$

CHAPTER 8

RESULTS AND DISCUSSIONS

8.1. Characterization of the Polymer Films

8.1.1. Determination of the Morphology and Thickness of the Polymer Films by Using Scanning Electron Microscope

Figure 8.1 shows the SEM picture of cross section of the polysulfone film. Nonporous, homogeneous film structure was observed. Using SEM pictures, thickness of each film was determined from an average of 3 or 6 measurements.

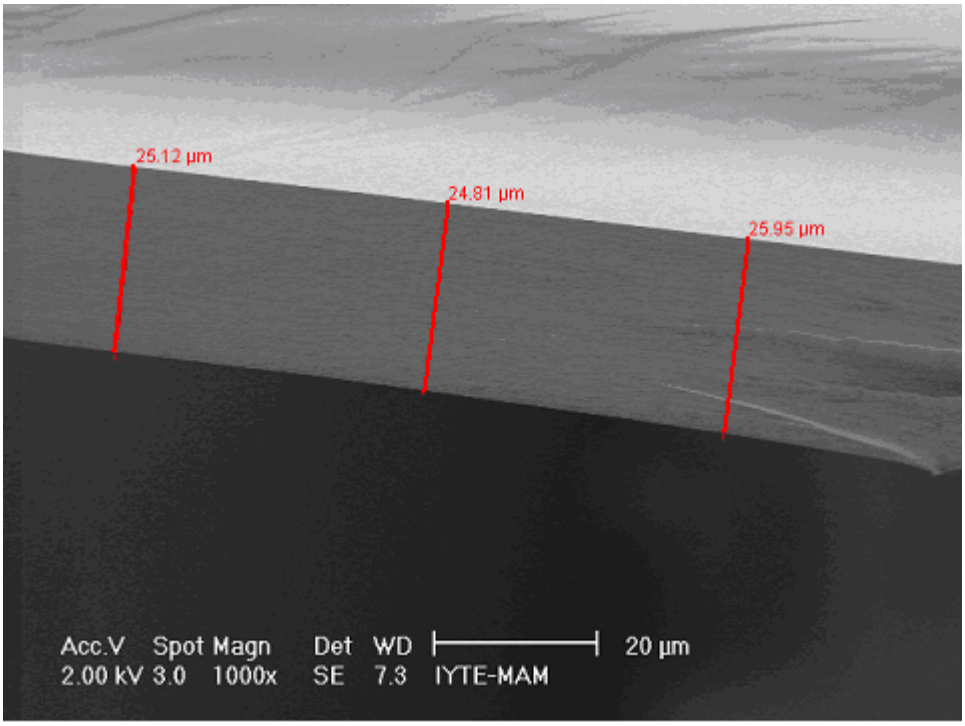

Figure 8.1. SEM picture of the cross section of polysulfone film used to measure film thickness

8.1.2. Differential Scanning Calorimetry (DSC) Analysis of the Polysulfone Films

Figure 8.2 shows the DSC curve of the polysulfone film. In DSC, energy is given to both sample and a reference material and the difference between the sample and the reference is used as a measure of thermal events. Around 190°C, a decrease in the slope of the heat flow curve was observed which corresponds to change from glassy to rubbery state. From this decrease, the glass transition temperature of the polysulfone was determined as 189°C. Amount of heat given to the sample compared to the reference increases significantly above 530°C and a negative peak was observed due to the degradation of the polymer.

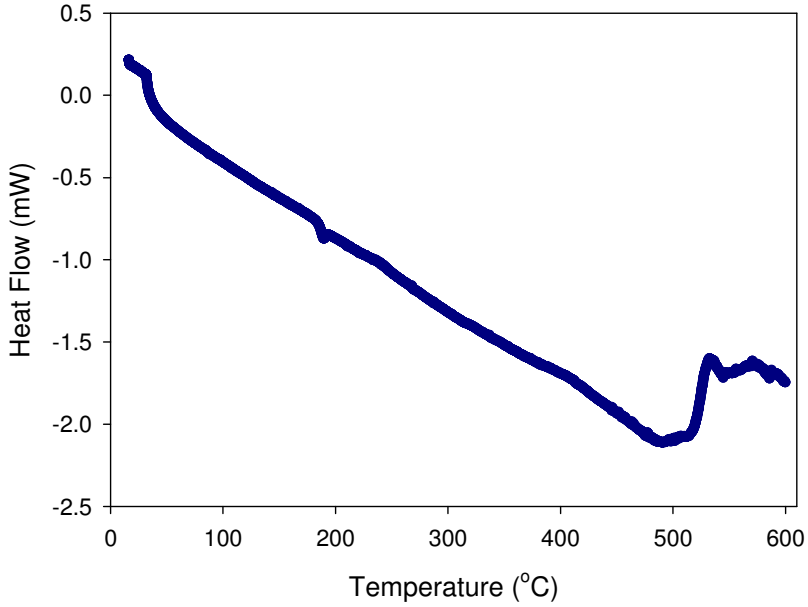

Figure 8.2. Differential Scanning Calorimetry analysis of polysulfone film

8.1.3. Thermal Gravimetric Analysis (TGA) of the Polysulfone Films

Figure 8.3 shows TGA curve of the polysulfone film. According to this figure, weight loss of the sample was observed above 281.3°C. Until 220°C (boiling point of NMP), 0.03 mg weight loss was observed which indicated that there is no significant

amount of residual NMP in the film. At 599.9°C, only 50.5% of the total weight was lost.

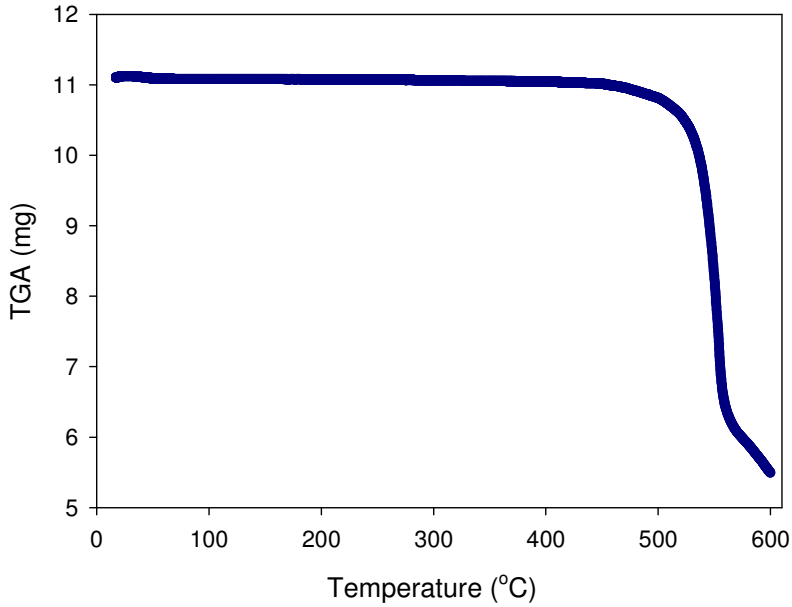

Figure 8.3. Thermal Gravimetric Analysis of polysulfone film

8.2. Determination of Cloud Points Experimentally

Figures 8.4 through 8.9 illustrate the experimental cloud points of the systems PSf/NMP/water, PSf/THF/water, PSf/NMP/ethanol, PSf/THF/ethanol, PMMA/acetone/water, PMMA/THF/water, PMMA/acetone/formamide, PMMA/THF/formamide at 40°C, which show the miscible region of polymer and solvent with nonsolvent.

8.2.1. Comparison of Experimental Cloud Points with Previous Studies

Kim et al. (1997) determined the experimental cloud points for PSf/NMP/water and PSf/THF/water systems at 15°C and 60°C by a titration method and their cloud points measured at 15°C were compared with those determined in this study. Figures 8.4 and 8.5 show that cloud point curves obtained in this study for PSf/THF/water and PSf/NMP/water are in good agreement with those reported by Kim et al. (1997). These results proved the accuracy of the experimental procedure used in this study. Kim et al. have observed that the effect of temperature on the cloud point curve is very small.

Hence, the comparison of their data collected at 15°C is reasonable with those collected in this study at 25°C.

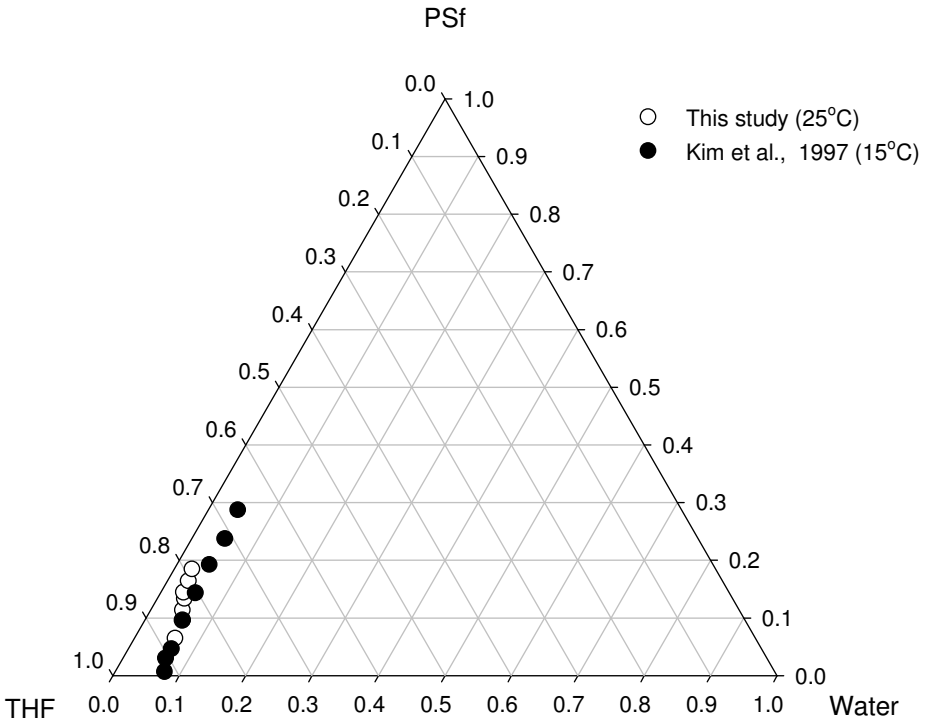

Figure 8.4. Comparison of experimental cloud point curves for PSf/THF/Water system

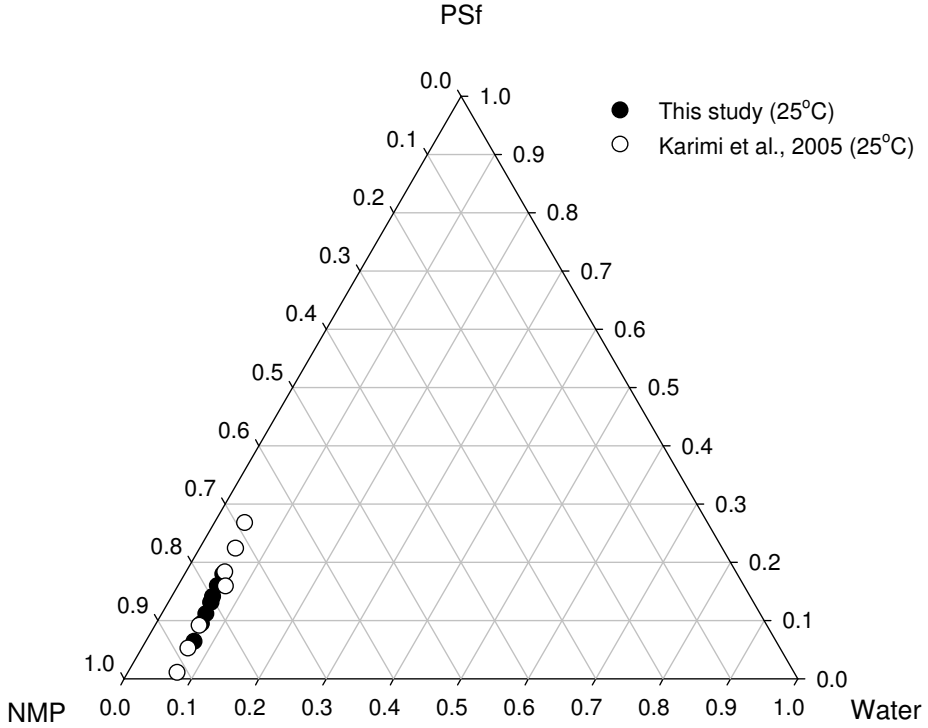

Figure 8.5. Comparison of experimental cloud point curves for PSf/NMP/Water system

8.2.2. Effect of Solvent Type on Ternary Phase Diagram

The cloud points given in Figure 8.6, show that the region of the homogeneous phase is slightly larger in the PSf/NMP/water system than in the PSf/THF/Water system at the same temperature. The influence of solvent type on the cloud points become more pronounced when ethanol is used as a nonsolvent. It was observed that homogeneous phase region is larger in the PSf/NMP/ethanol than in the PSf/THF/ethanol system at 40°C as shown in Figure 8.7.

In the case of PMMA, the homogeneous phase region is not influenced by solvent type which are acetone and THF when both water and formamide are used as nonsolvents as shown in Figures 8.8 and 8.9.

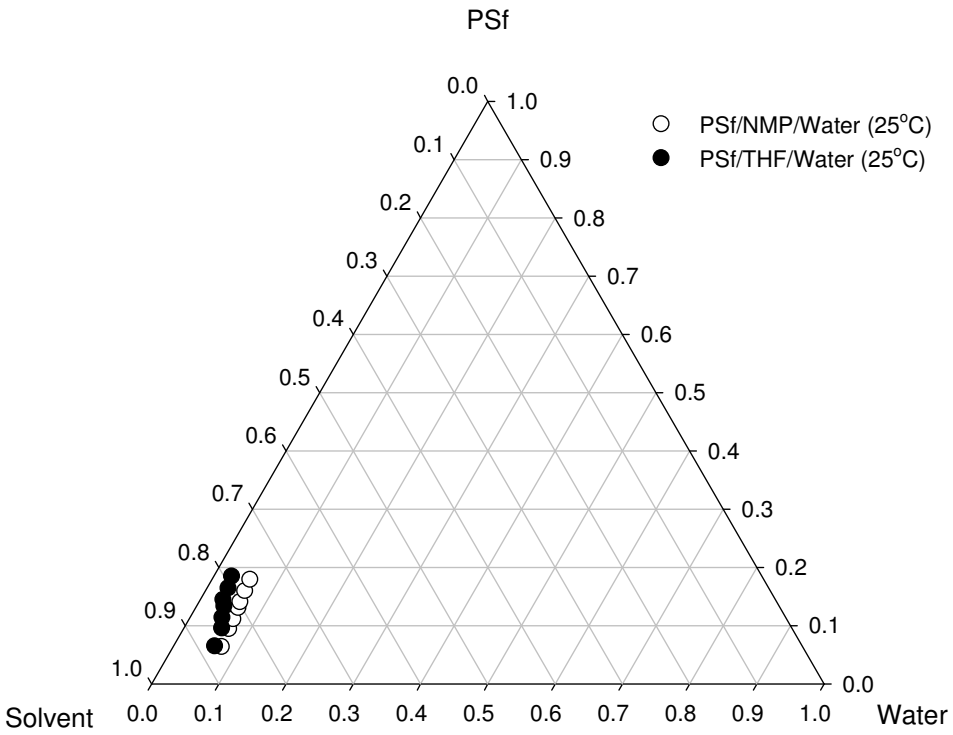

Figure 8.6. Experimental cloud points for Polysulfone/Solvent/Water system

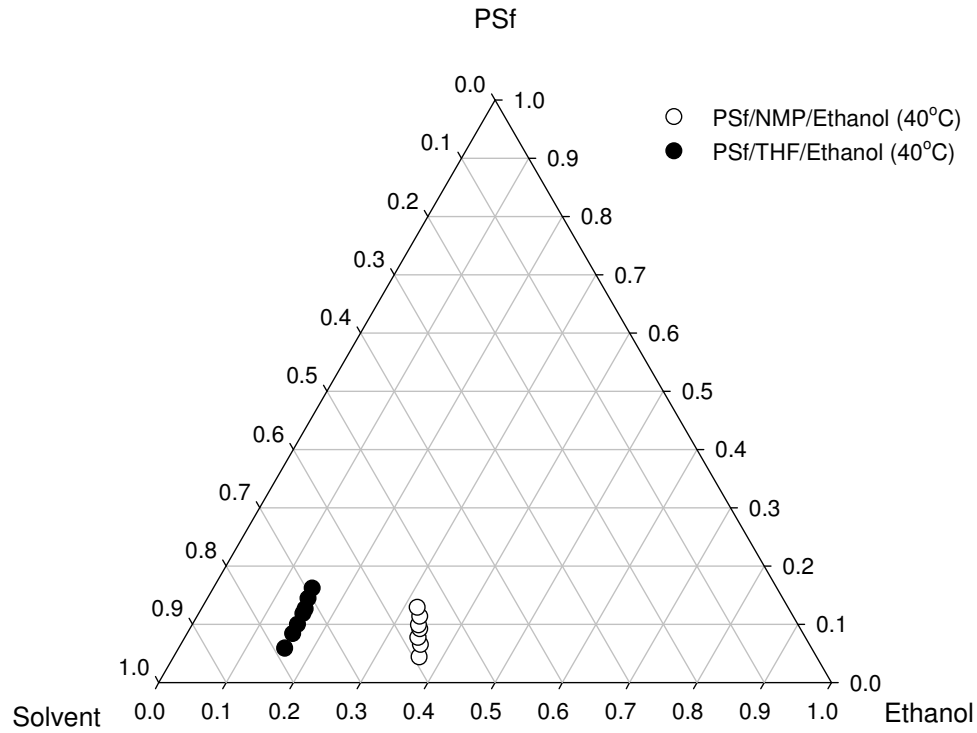

Figure 8.7. Experimental cloud points for Polysulfone/Solvent/Ethanol system

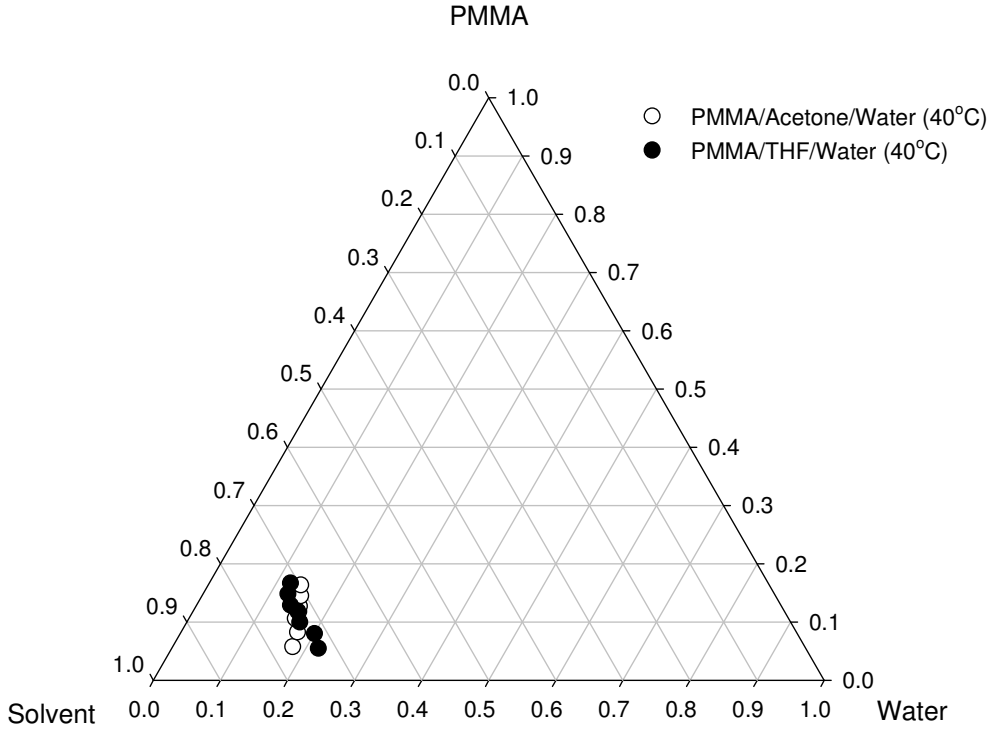

Figure 8.8. Experimental cloud points for PMMA/Solvent/Water system

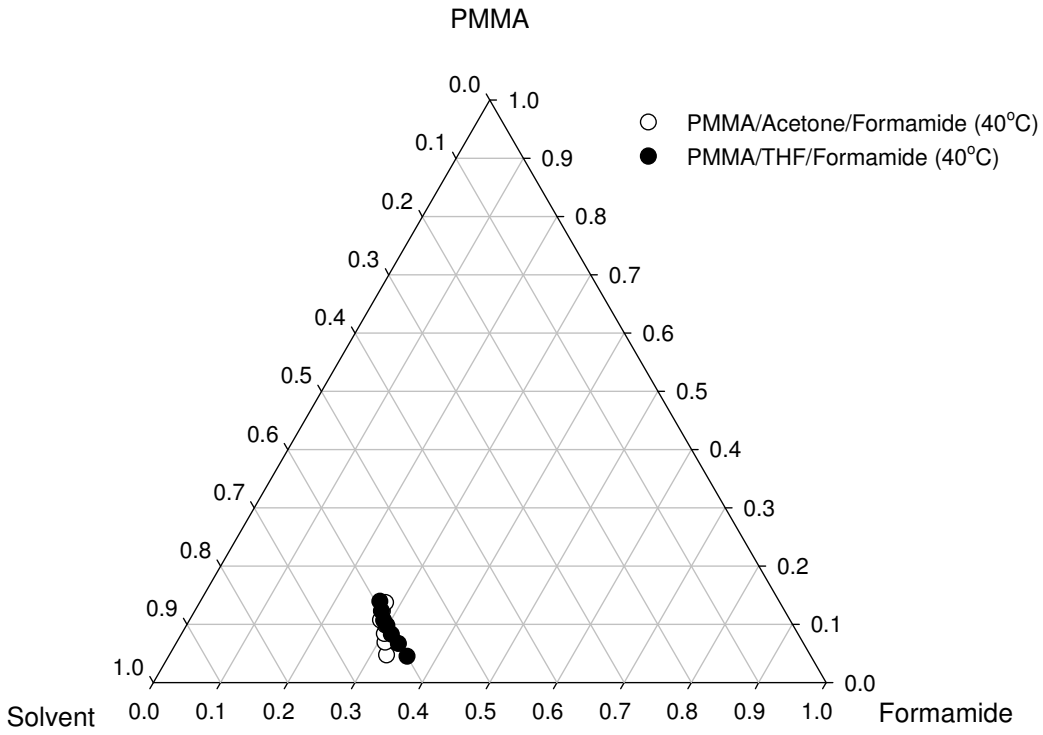

Figure 8.9. Experimental cloud points for PMMA/Solvent/Formamide system

8.2.3. Effect of Nonsolvent Type on Ternary Phase Diagram

Figures 8.10 through 8.13 show the influence of nonsolvent type on the cloud points for PSf and PMMA systems. It was observed that for each solvent (NMP and THF) when ethanol is used as nonsolvent instead of water, the homogeneous phase region enlarges as shown in Figure 8.10 and 8.11. The results indicate that smaller amount of water is required to induce phase separation, thus, nonsolvent power of water is higher than that of ethanol for PSf films.

For PMMA systems, nonsolvent power of water is higher than that of formamide when acetone and THF are used as solvents as shown in Figure 8.12 and 8.13.

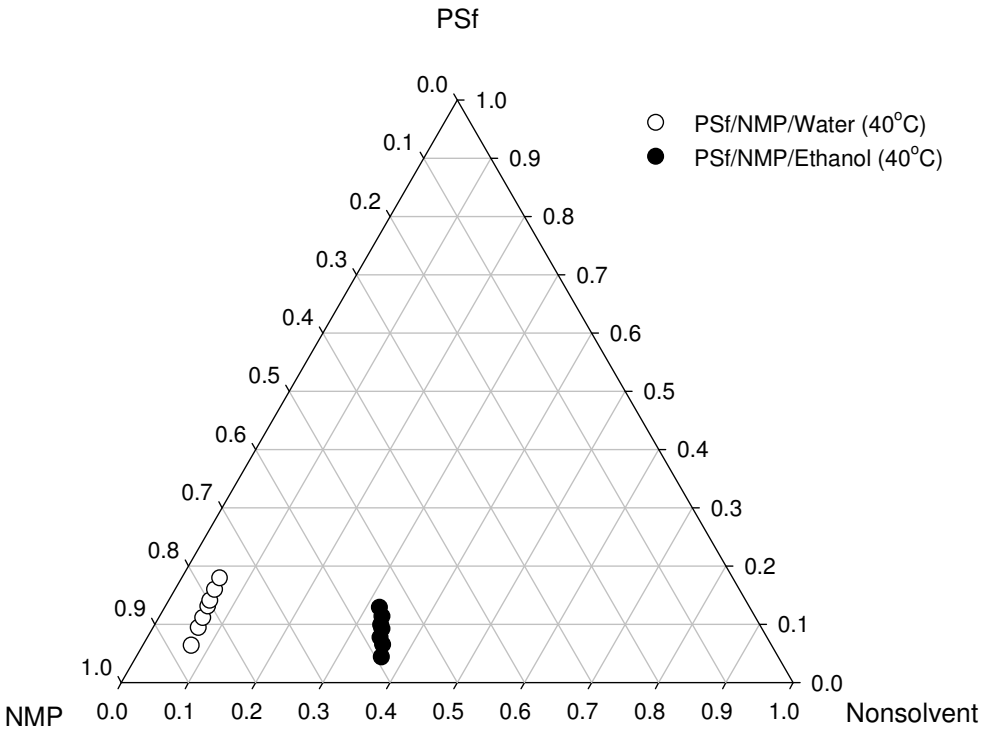

Figure 8.10. Experimental cloud points for PSf/NMP/Nonsolvent system

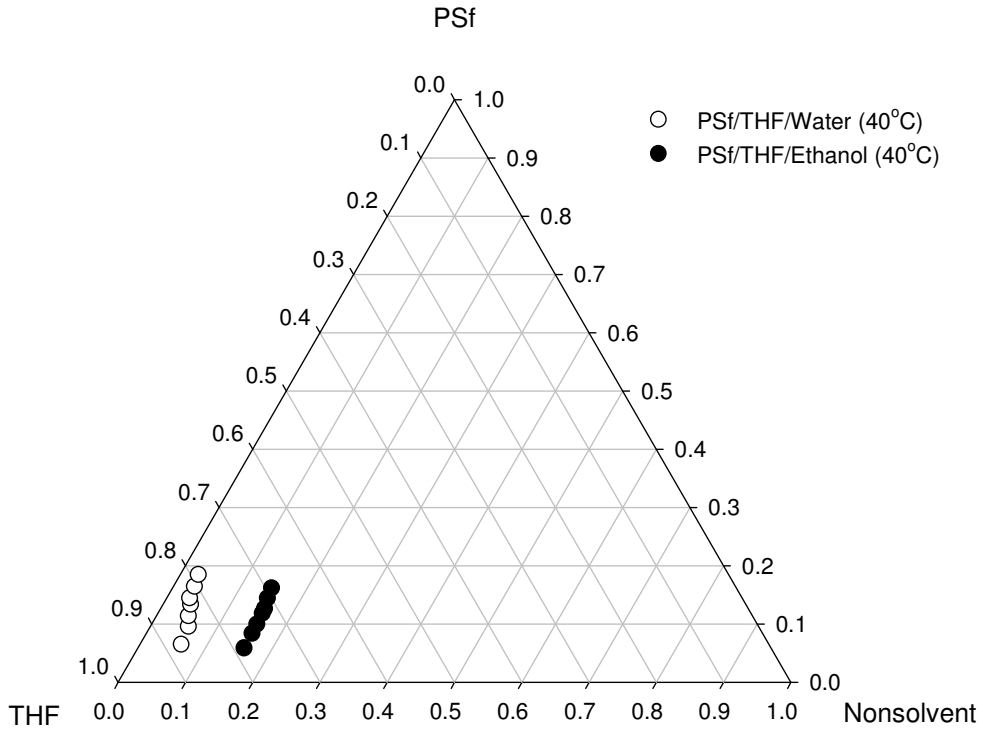

Figure 8.11. Experimental cloud points for PSf/THF/Nonsolvent system

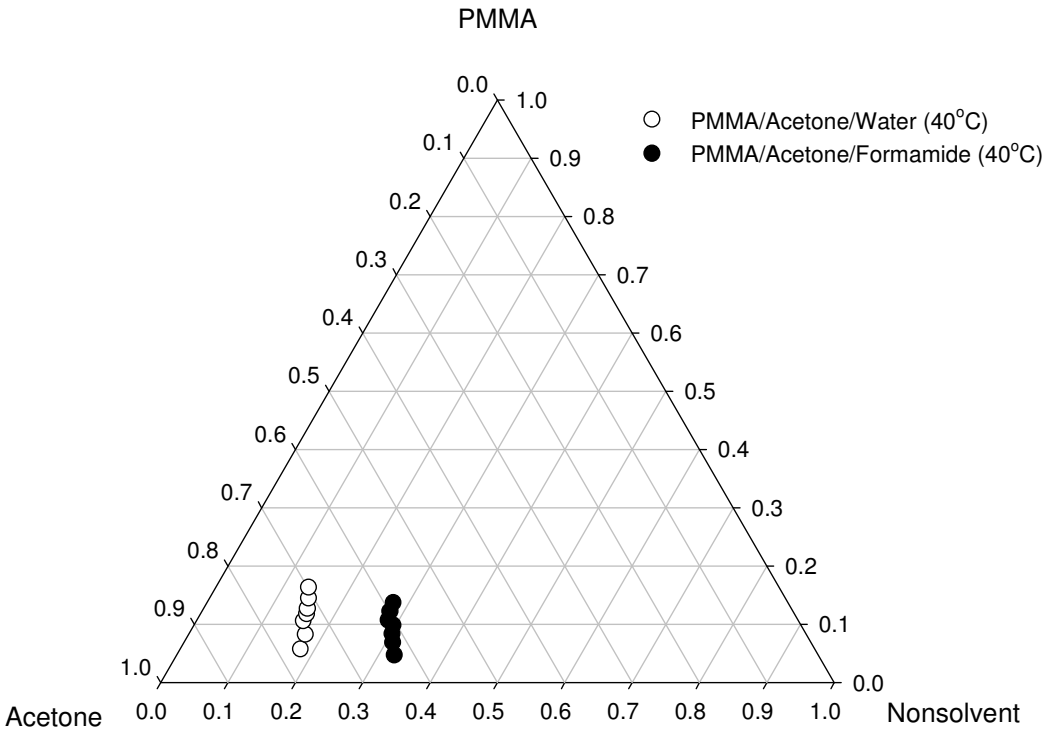

Figure 8.12. Experimental cloud points for PMMA/Acetone/Nonsolvent system

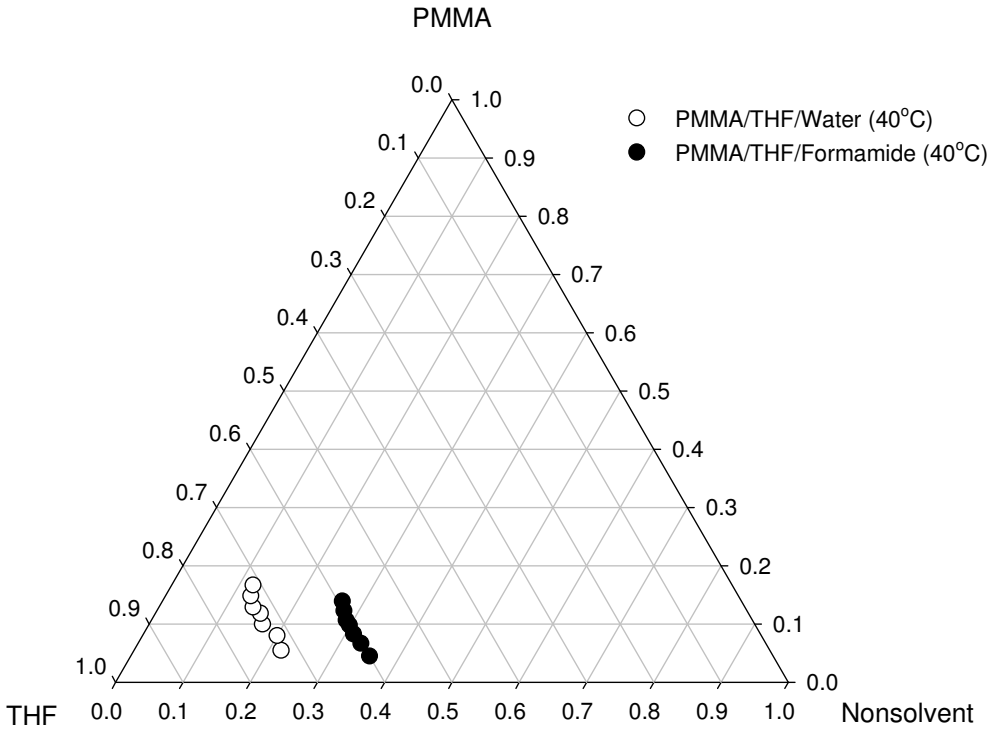

Figure 8.13. Experimental cloud points for PMMA/THF/Nonsolvent system

8.2.4. Effect of Temperature on the Phase Diagram

The cloud point experiments were performed for PSf/NMP/Water and PSf/THF/Water systems at 25°C and 40°C. Figure 8.14 shows that the effect of temperature on the cloud points is relatively small. Similar results have been obtained by Kim et al. (1997) for the same systems. They have observed that the region of homogeneous phase is slightly enlarged with increasing temperature.

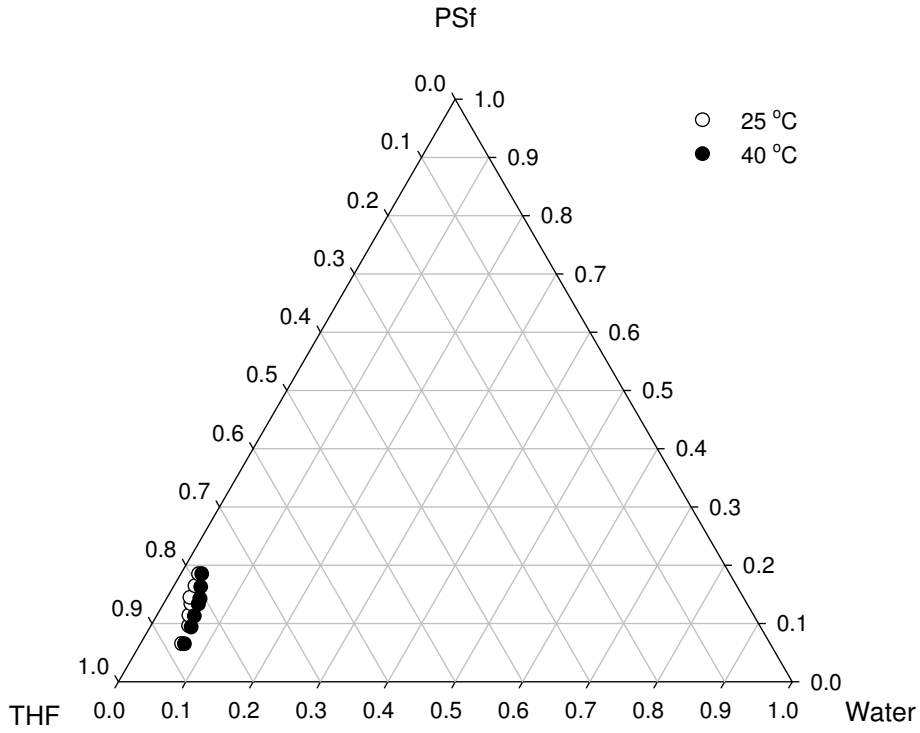

Figure 8.14. Effect of temperature on the experimental cloud points for PSf/THF/Water system

8.3. Comparison Between the Theoretical and Experimental Binodal Curves

In order to construct ternary phase diagrams theoretically, three Flory-Huggins interaction parameters (χ_{13}, χ_{23}, χ_{12}) and molar volumes of polymer, solvent and nonsolvent should be known. The nonsolvent/polymer interaction parameters (χ_{13}) were either obtained from the literature (Kim et al. 1997, Lai et al. 1998) or determined from swelling experiments. The solvent/polymer interaction parameters (χ_{23}) were also obtained from the literature or calculated from Equation (5.13) using solubility

parameters (Brandrup et al. 1999). Except for acetone-water pair, the solvent/nonsolvent interaction parameters (χ_{12}) were regressed by minimizing the difference between experimental and theoretical cloud point curves. The interaction parameters used in the calculations are listed in Table 8.1. It was attempted to determine a proper value of χ_{13} in the PSf/solvent/water system since we had failed to fit the calculated binodal with our experimental cloud point curve with a reported value of 3.7 (Altena and Smolders 1982). It was chosen 2.7 from the study of Kim et al. (1997). By using the numerical code developed, the theoretical ternary phase diagrams of PSf/NMP/water, PSf/THF/water, PSf/NMP/ethanol, PSf/THF/ethanol, PMMA/acetone/water and PMMA/THF/water were constructed as shown in Figure 8.15 through 8.20. Very good agreement was obtained between the theoretical and experimental results for the systems PSf/NMP/water, PSf/THF/water, PSf/NMP/ethanol and PSf/THF/ethanol, indicating that the extended Flory-Huggins theory developed by Tompa (1956) is a very powerful tool for predicting the liquid-liquid demixing behavior in a ternary system when suitable interaction parameters are known. For the system, PMMA/acetone/water and PMMA/acetone/formamide, the experimental cloud points didn't agree well with the theoretical binodal curves. These results can be explained by the inaccuracies in interaction parameters obtained from different sources.

Table 8.1. Flory Huggins interaction parameters

System	χ_{12}	χ_{23}	χ_{13}
PSf/NMP/water	1.2 (regression)	0.24 (Kim et al. 1997)	2.7 (Kim et al. 1997)
PSf/THF/water	1.2 (regression)	0.46 (Allen et al. 1969)	2.7 (Kim et al. 1997)
PSf/NMP/ethanol	1.4 (regression)	0.24 (Kim et al. 1997)	1.8 (swelling exp)
PSf/THF/ethanol	1.2 (regression)	0.46 (Allen et al. 1969)	1.8 (swelling exp)
PMMA/acetone/water	1.3 (Alsoy and Ozbas 2004)	0.48 (Lai et al. 1997)	2.34 (Lai et al. 1997)
PMMA/THF/water	1.2 (regression)	0.37[a]	2.34 (Lai et al. 1997)
PMMA/acetone/formamide	1.3 (regression)	0.48 (Lai et al. 1997)	1.9 (regression)
PMMA/THF/formamide	1.5 (regression)	0.37[a]	1.6 (regression)

[a] obtained from solubility parameters (Brandrup et al. 1999)

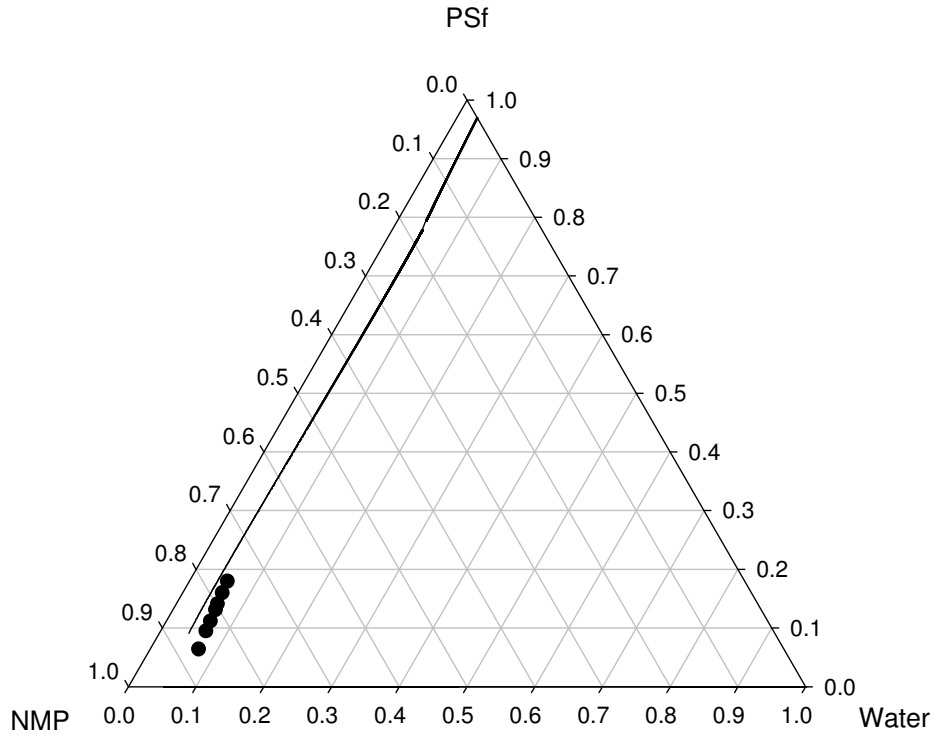

Figure 8.15. Comparison of theoretical binodal curves with experimental cloud points for PSf/NMP/water system

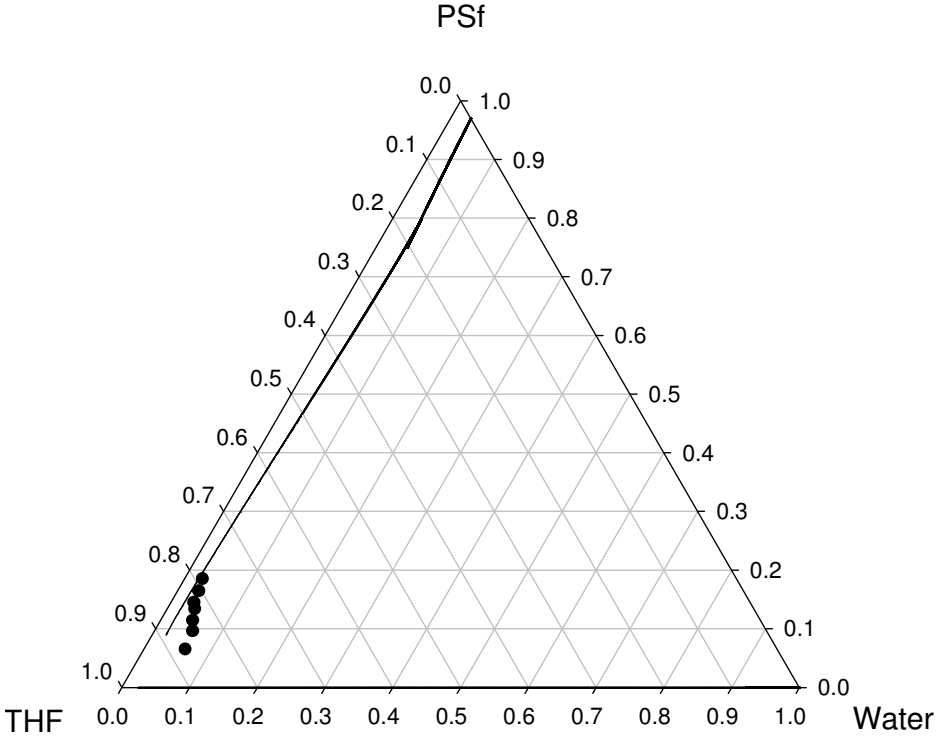

Figure 8.16. Comparison of theoretical binodal curves with experimental cloud points for PSf/THF/water system

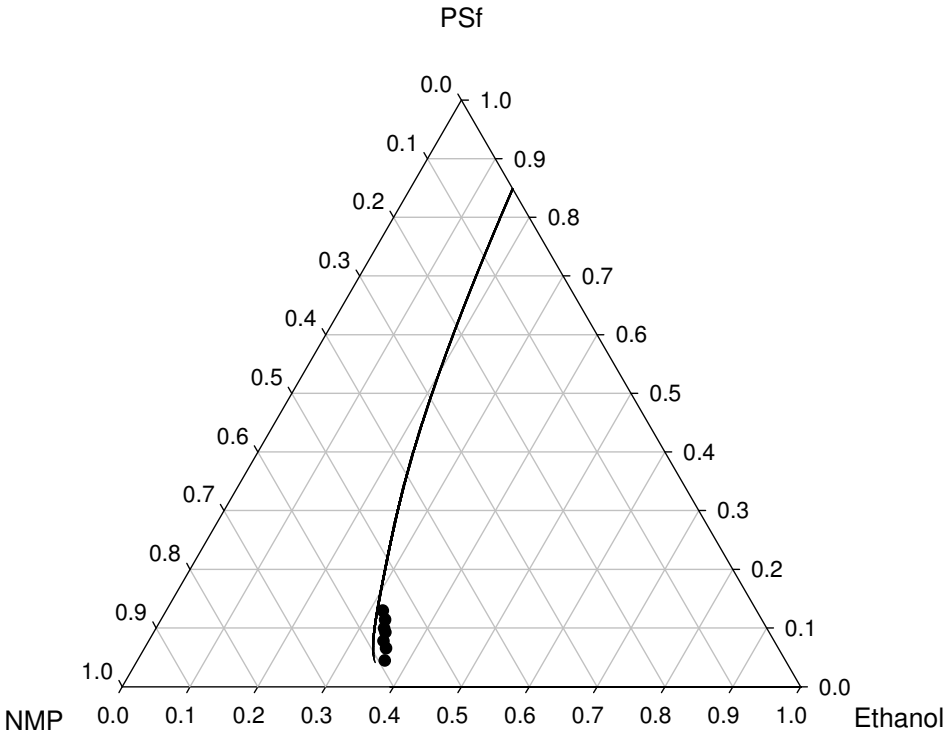

Figure 8.17. Comparison of theoretical binodal curves with experimental cloud points for PSf/NMP/ethanol system

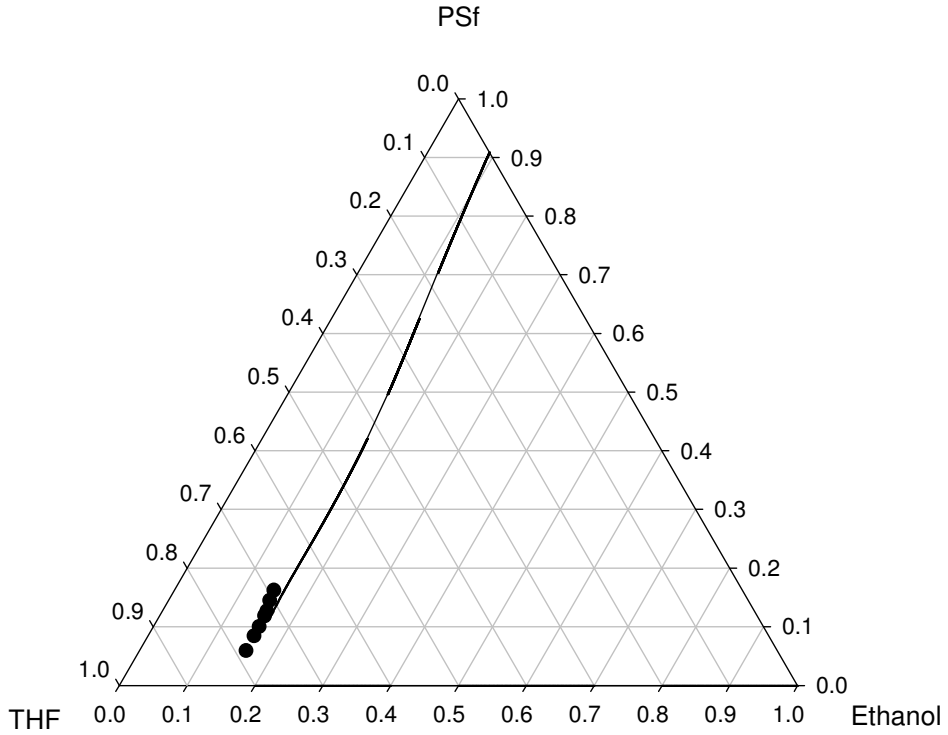

Figure 8.18. Comparison of theoretical binodal curves with experimental cloud points for PSf/THF/ethanol system

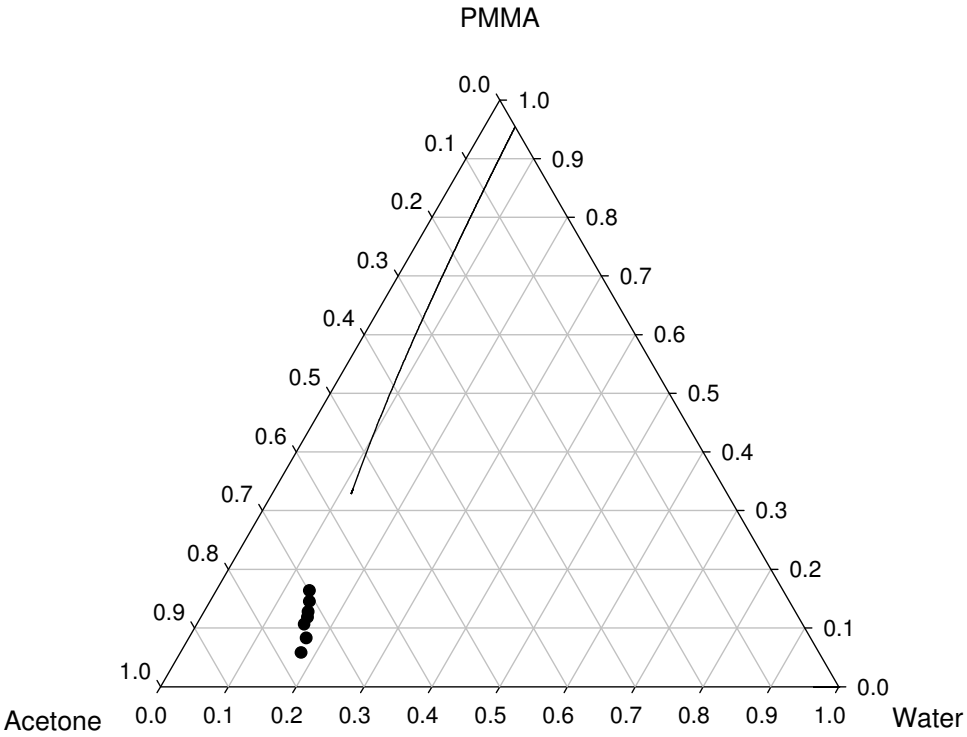

Figure 8.19. Comparison of theoretical binodal curves with experimental cloud points for PMMA/acetone/water system

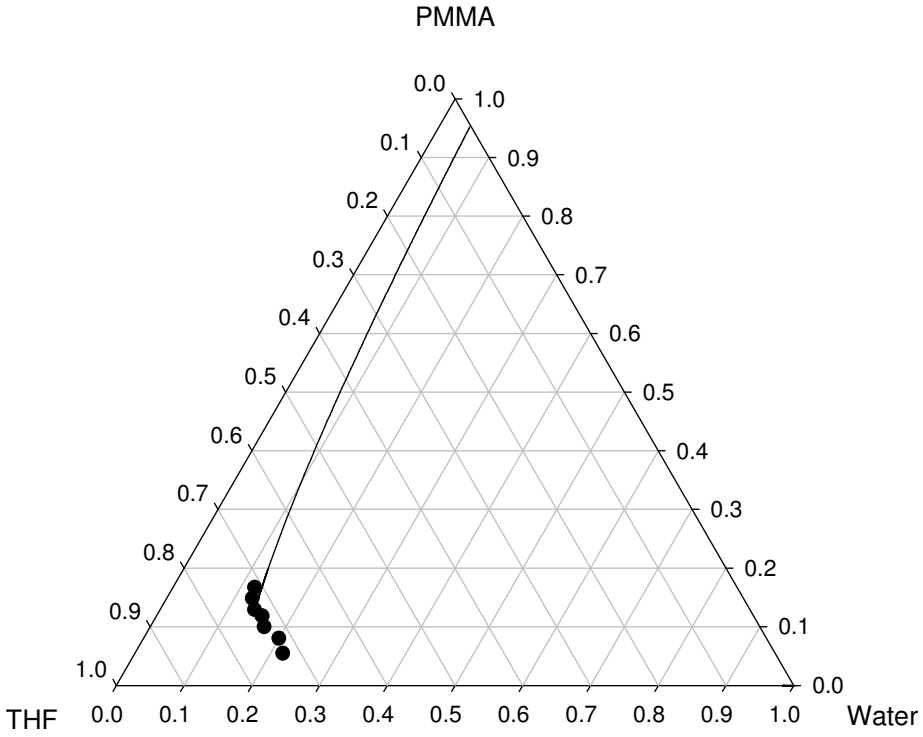

Figure 8.20. Comparison of theoretical binodal curves with experimental cloud points for PMMA/THF/water system

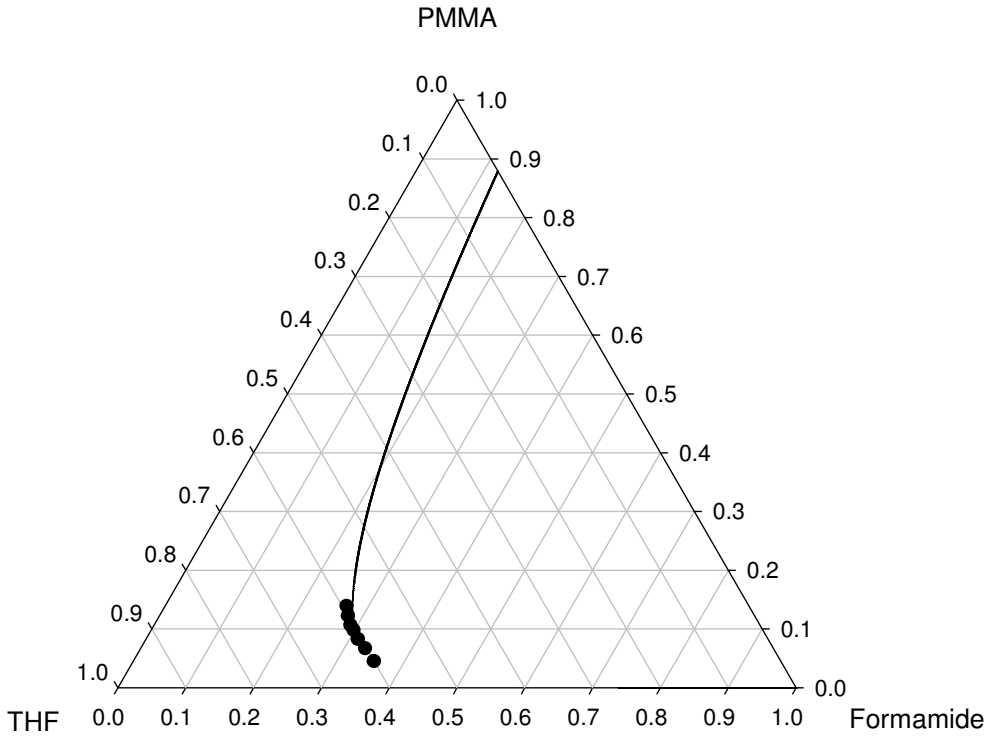

Figure 8.21. Comparison of theoretical binodal curves with experimental cloud points for PMMA/THF/formamide system

8.4. Diffusion and Equilibrium Studies of PSf/Penetrant Systems

Gravimetric sorption curves for several penetrant/PSf systems were collected. The weight change of the polymer film and the temperature inside the column were recorded by the computer for every 5 seconds. Vapor pressure of penetrant vapor followed by the pressure transducer was found to be constant during the experiments. Experimental vapor pressures were in good agreement with those calculated from a correlation given in DCAPS database (Daubert and Danner 1994). The sorption steps were chosen small enough to maintain constant diffusivity assumption during the course of a single experiment. The change in sample thickness with increased solvent loading was estimated based on the assumption of isotropic swelling.

8.4.1. Determination of Diffusion Coefficients of Polysulfone/Water System

Gravimetric sorption curves for water/PSf system were collected at 30°C, 40°C and 50°C. Weight data were corrected for buoyancy effect and normalized mass uptakes of the films, $\frac{M_t - M_0}{M_\infty - M_0}$, at each set of the experiments were drawn against the square root of time, $\sqrt{t}$, and the results are shown in Figures 8.22 through 8.24. The experimental conditions for the uptake measurements are listed in Table 8.2. The total thicknesses of the polymer including penetrant at the beginning of each sorption step and the diffusivities are also listed in Table 8.2.

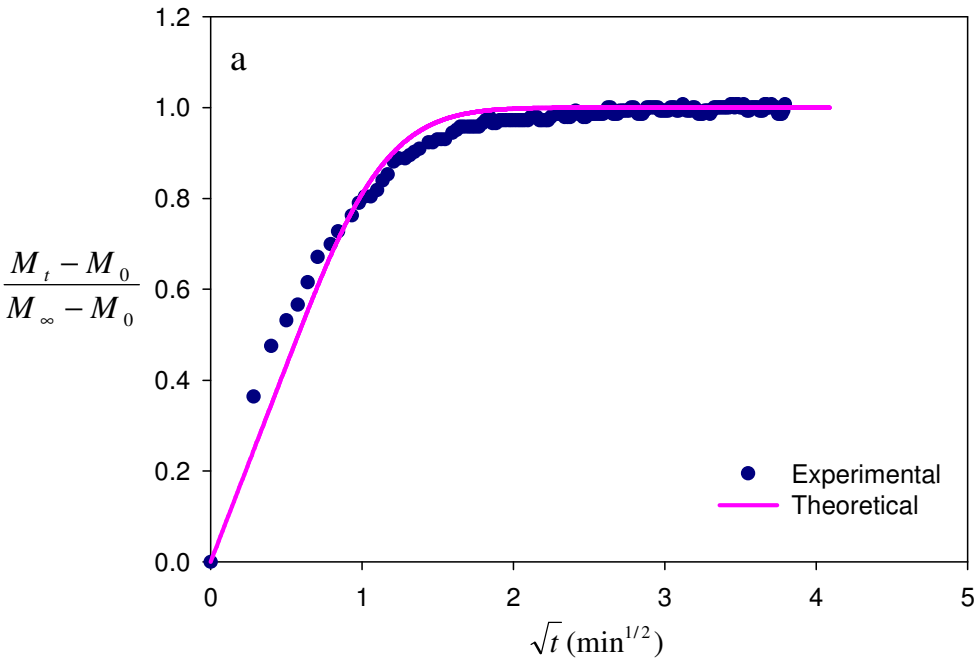

Figure 8.22. Normalized mass uptakes for the diffusion of water in polysulfone at 30°C. The solid line represents the the theoretical Fickian curve and the symbol represents the experimental sorption curve. Water vapor temperatures: a) 14°C, b) 18°C, c) 22°C, d) 26°C

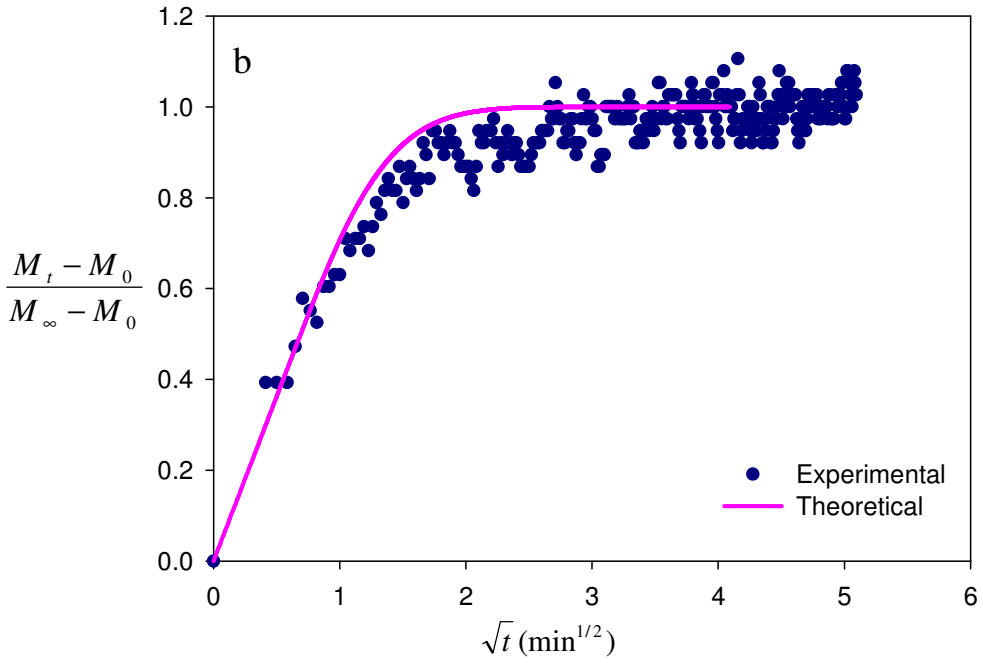

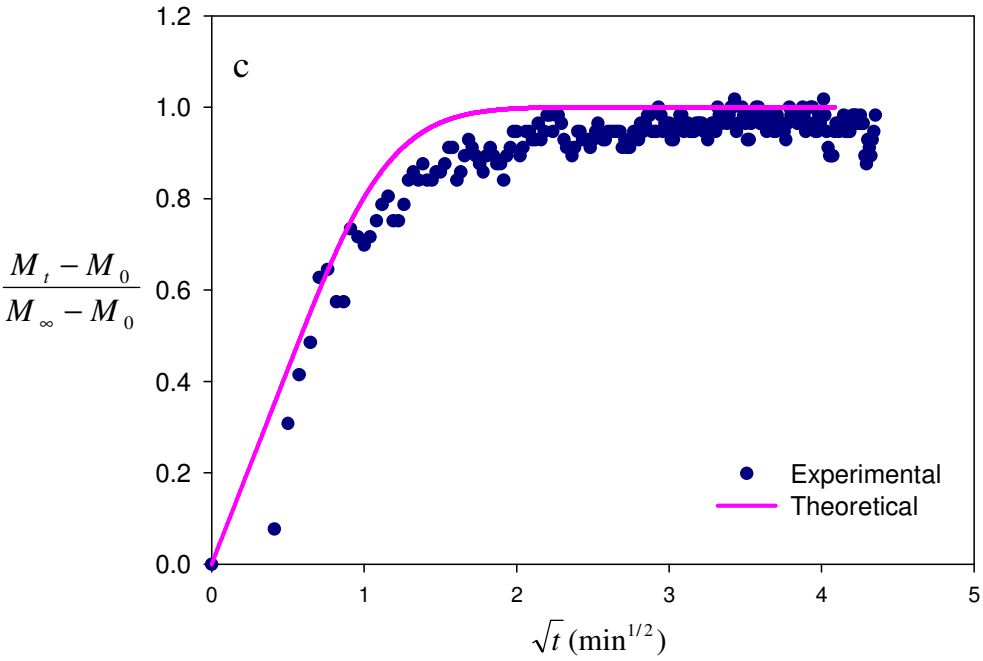

Figure 8.22. Normalized mass uptakes for the diffusion of water in polysulfone at 30°C. The solid line represents the the theoretical Fickian curve and the symbol represents the experimental sorption curve. Water vapor temperatures: a) 14°C, b) 18°C, c) 22°C, d) 26°C (Cont.)

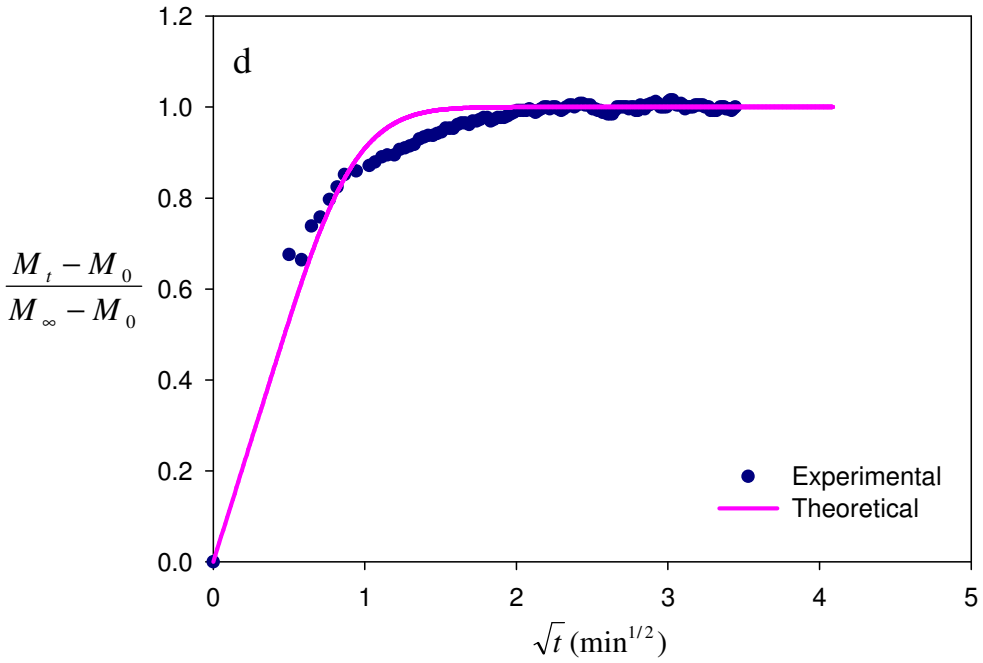

Figure 8.22. Normalized mass uptakes for the diffusion of water in polysulfone at 30°C. The solid line represents the the theoretical Fickian curve and the symbol represents the experimental sorption curve. Water vapor temperatures: a) 14°C, b) 18°C, c) 22°C, d) 26°C (Cont.)

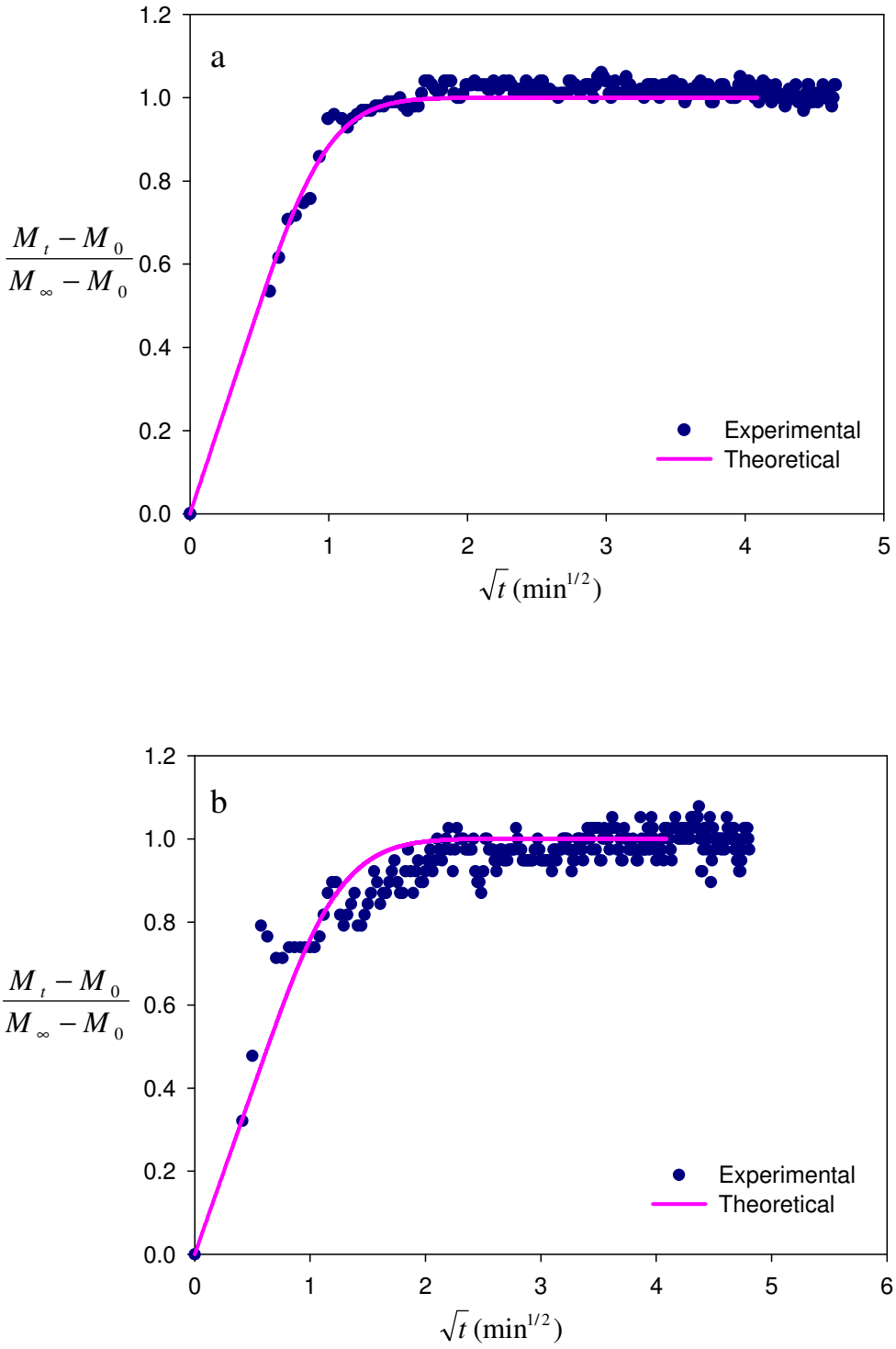

Figure 8.23. Normalized mass uptakes for the diffusion of water in polysulfone at 40°C. The solid line represents the the theoretical Fickian curve and the symbol represents the experimental sorption curve. Water vapor temperatures: a) 20°C, b) 25°C, c) 30°C, d) 35°C

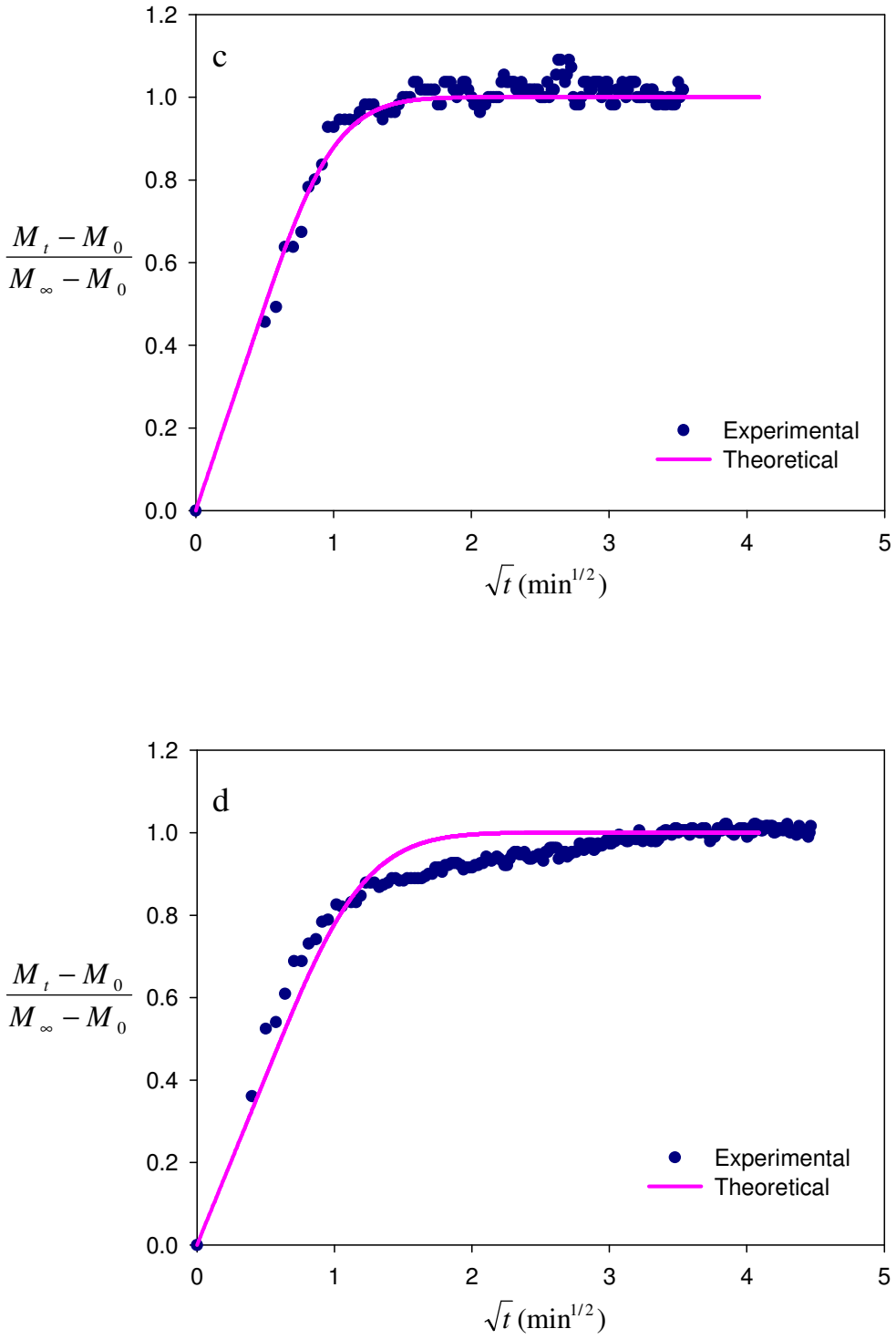

Figure 8.23. Normalized mass uptakes for the diffusion of water in polysulfone at 40°C. The solid line represents the the theoretical Fickian curve and the symbol represents the experimental sorption curve. Water vapor temperatures: a) 20°C, b) 25°C, c) 30°C, d) 35°C (Cont.)

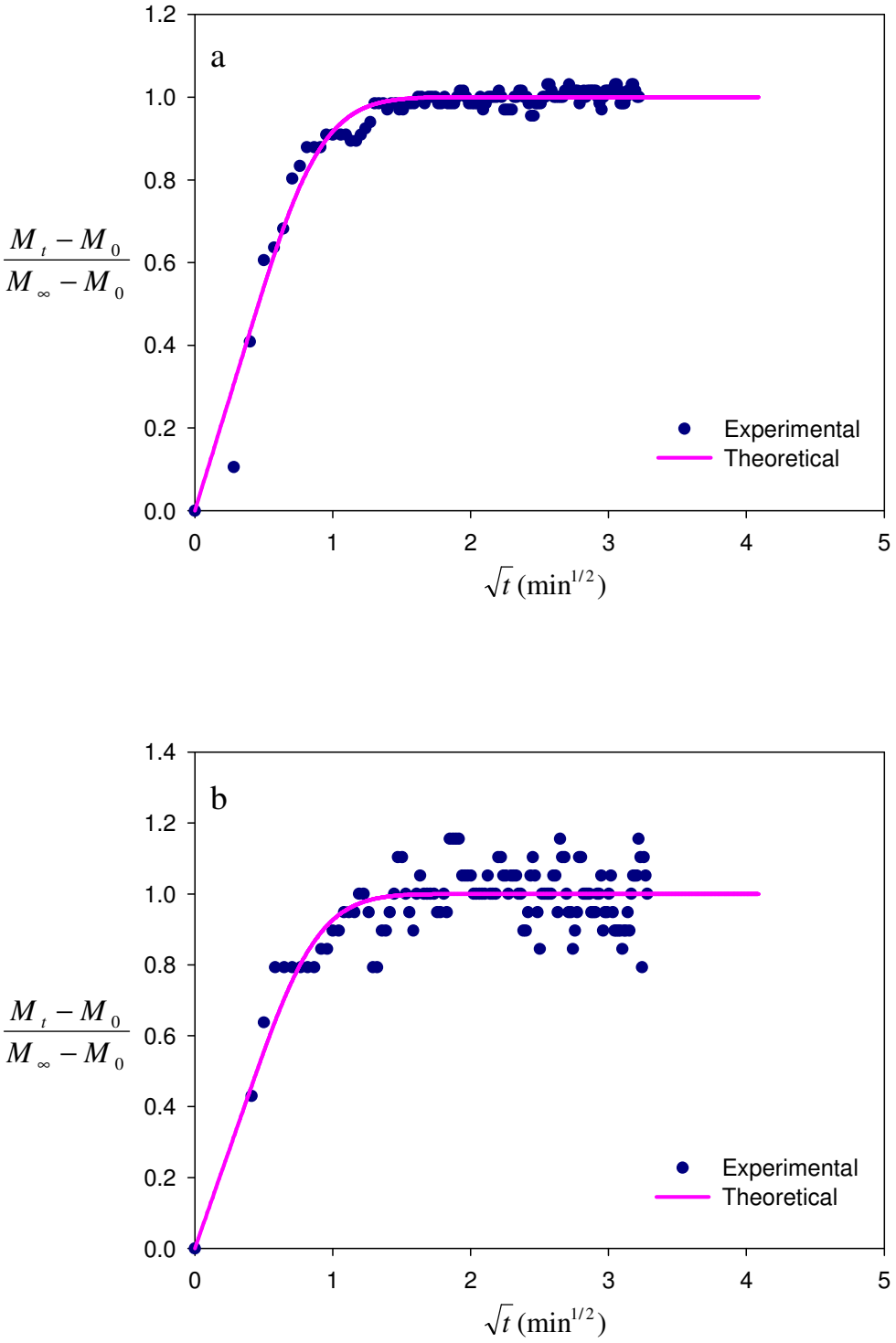

Figure 8.24. Normalized mass uptakes for the diffusion of water in polysulfone at 50°C. The solid line represents the the theoretical Fickian curve and the symbol represents the experimental sorption curve. Water vapor temperatures: a) 20°C, b) 25°C, c) 30°C, d) 35°C, e) 40°C, f) 45°C

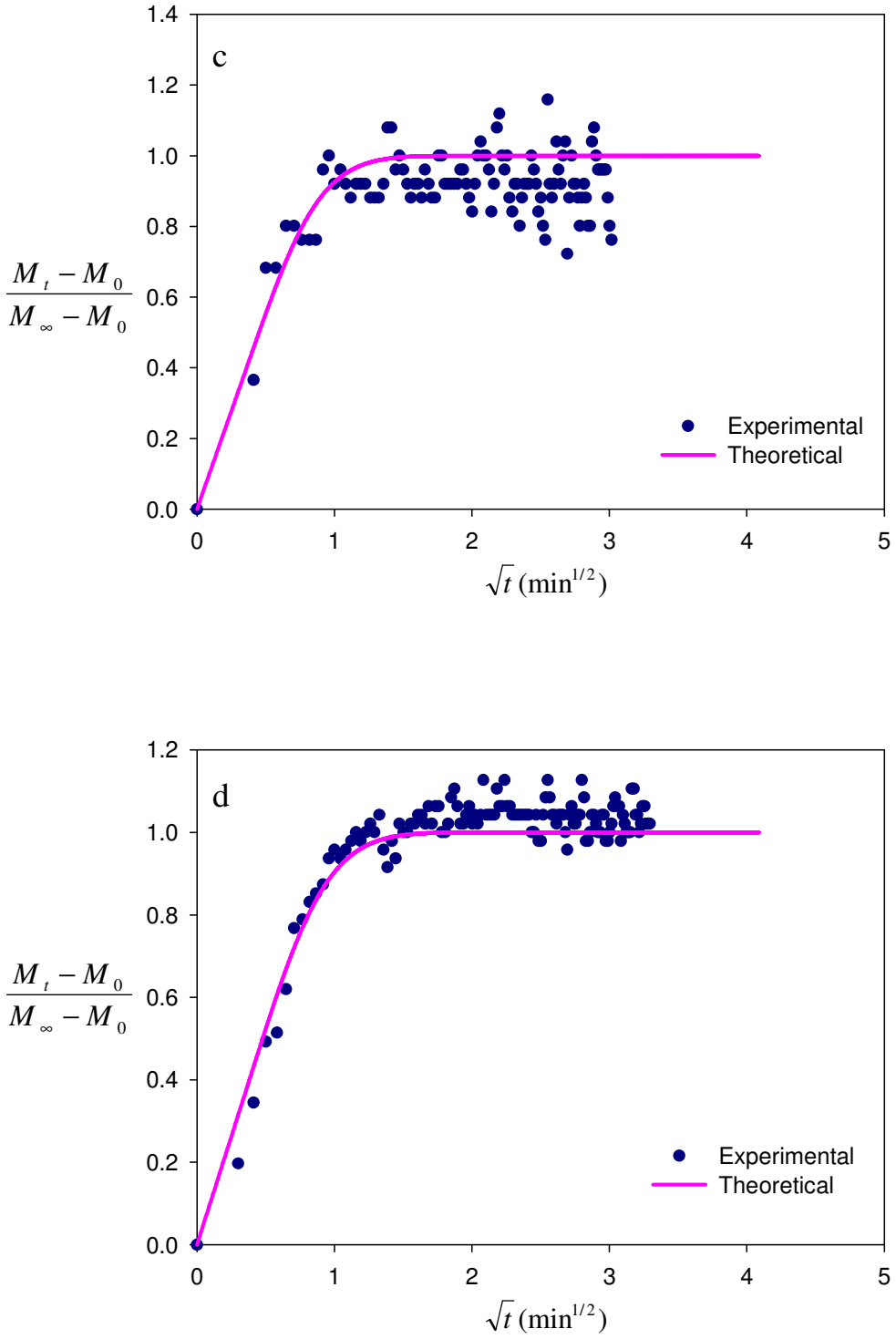

Figure 8.24. Normalized mass uptakes for the diffusion of water in polysulfone at 50°C. The solid line represents the the theoretical Fickian curve and the symbol represents the experimental sorption curve. Water vapor temperatures: a) 20°C, b) 25°C, c) 30°C, d) 35°C, e) 40°C, f) 45°C (Cont.)

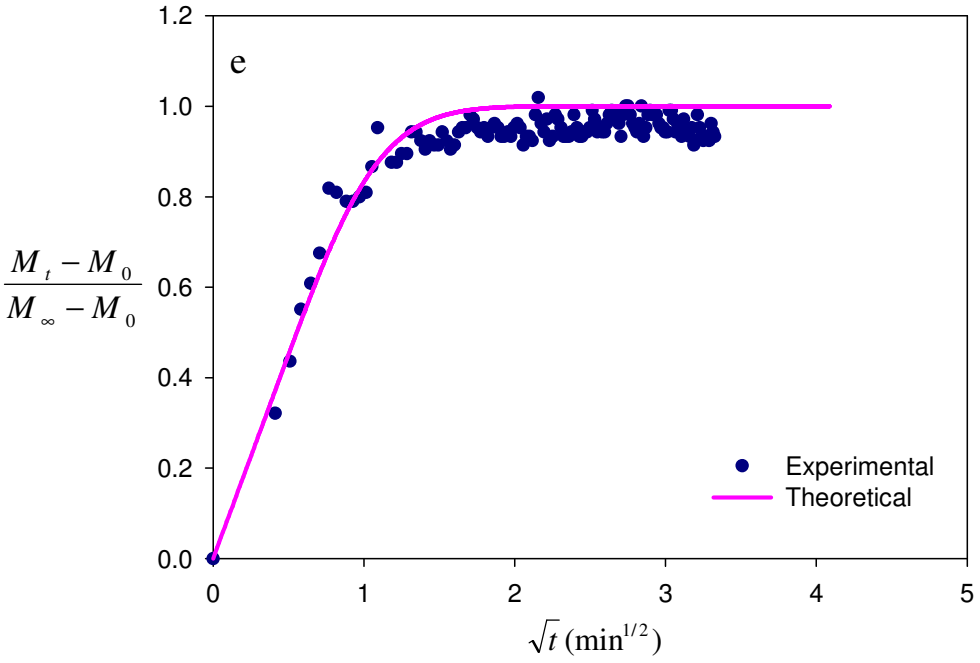

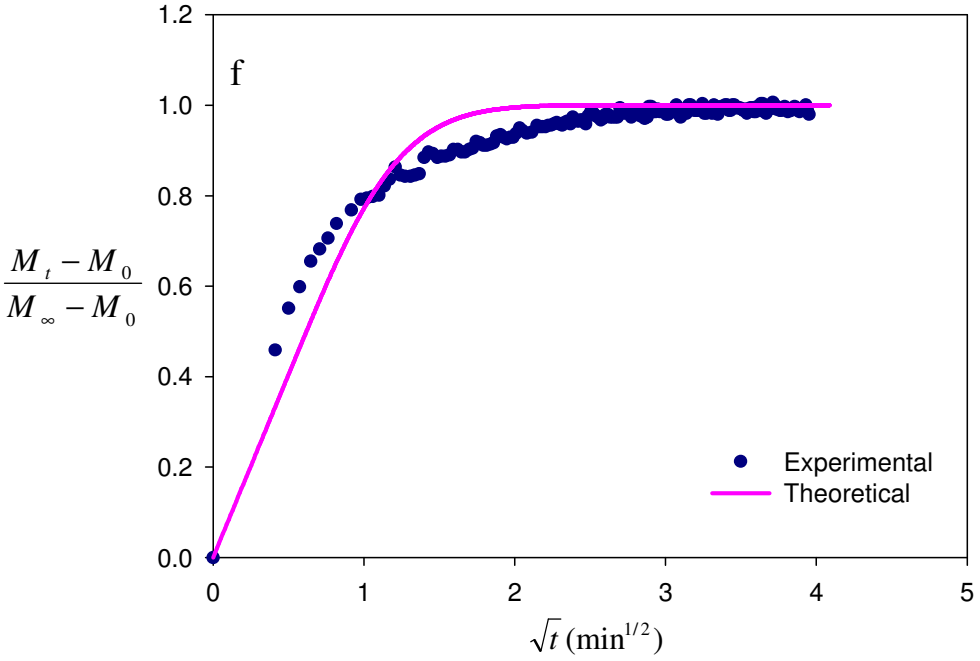

Figure 8.24. Normalized mass uptakes for the diffusion of water in polysulfone at 50°C. The solid line represents the the theoretical Fickian curve and the symbol represents the experimental sorption curve. Water vapor temperatures: a) 20°C, b) 25°C, c) 30°C, d) 35°C, e) 40°C, f) 45°C (Cont.)

The diffusivity values reported in Table 8.2 correspond to the average weight fraction of water calculated by Equation 8.1 (Hong et al. 1998):

$$\omega_{average} = \omega_{initial} + 0.7(\omega_{equilibrium} - \omega_{initial}) \tag{8.1}$$

Vrentas and Duda determined that minimal error was introduced if the average concentration was associated with 70% of the sorption interval (Vrentas and Duda 1977). Results in Figures 8.22 through 8.24 indicate that analytical solution (Equation 6.7) derived for Case 1 diffusion appropriately fits the experimental data with slight deviation in a few cases where the data were collected at high activities. It was observed that the initial trend in the normalized uptake data is linear with respect to $\sqrt{t}$ while the latter part of the curves are concave with respect to the $\sqrt{t}$ axis. This result simply suggests that sorption kinetics of water in polysulfone may follow Fickian sorption.

Table 8.2. Diffusivity data for water-polysulfone at 30°C, 40°C and 50°C

Temperature (°C)	Pressure (psia)		ω_{water}			thickness (μm)	$D\times10^8$ (cm^2/s)
	initial	Final	initial	equilibrium	Average		
30	0	0.23	0	0.00406	0.00284	27.36	7.33
	0.23	0.3	0.00406	0.00582	0.00529	27.5	5.19
	0.3	0.38	0.00582	0.00893	0.00799	27.7	7.32
	0.38	0.49	0.00893	0.01670	0.01458	28	11.6
40	0	0.34	0	0.00344	0.00240	27.36	9.82
	0.34	0.46	0.00344	0.00476	0.00436	27.48	6.16
	0.46	0.62	0.00476	0.00667	0.00609	27.64	9.79
	0.62	0.82	0.00667	0.0131	0.0112	27.87	6.79
50	0	0.34	0	0.00217	0.00152	27.36	11.5
	0.34	0.46	0.00217	0.00280	0.00261	27.43	12.2
	0.46	0.62	0.00280	0.00363	0.0034	27.53	12.2
	0.62	0.82	0.00363	0.00518	0.0047	27.65	11
	0.82	1.07	0.00518	0.00858	0.00756	27.83	8.25
	1.07	1.39	0.00858	0.01935	0.01612	28.13	6.77

The results listed in Table 8.2 indicate that diffusivity of water in PSf does not change strongly with the concentration of water in the film. The effect of temperature on the diffusivities was also found to be insignificant.

The accuracy of the diffusion measurements was controlled by performing the experiments at each temperature for 3 times. As illustrated in Figure 8.26, just for the data collected at 50°C, reproducibility of diffusivities determined at each temperature was found to be good.

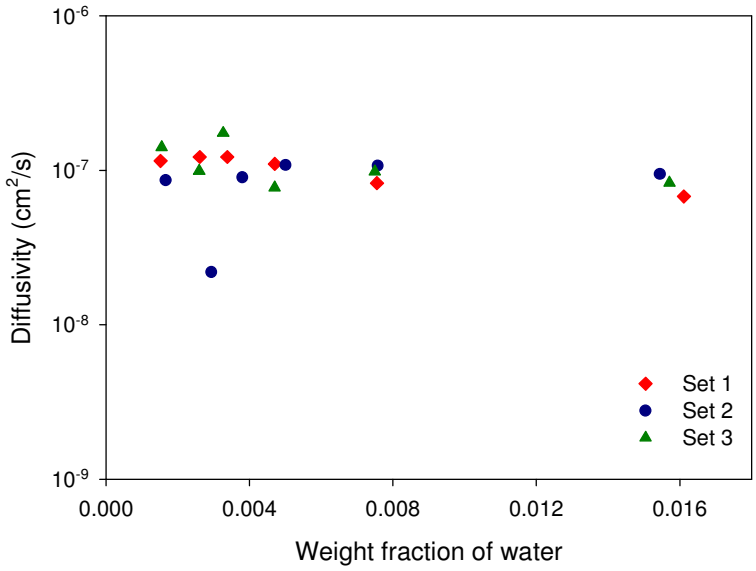

Figure 8.25. Diffusion coefficients of water in the polysulfone films as a function of its average weight fraction for 3 sets of repeated experiments at 50°C

The diffusivity data at 40°C were also compared with those obtained by Schult and Paul (1996a), as shown in Figure 8.19. Good agreement between two independent data sets also confirmed the accuracy of the measurements performed in this study.

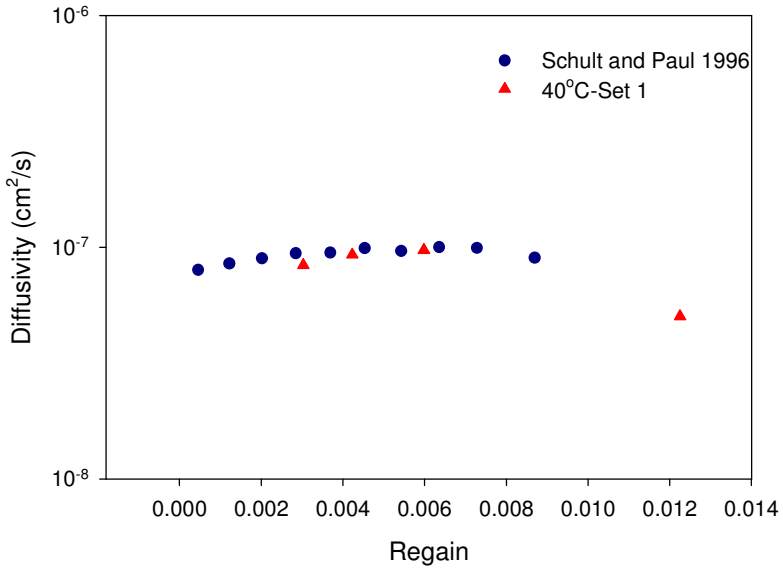

Figure 8.26. Comparison of the diffusion coefficients with the study of Schult and Paul (1996a). Regain is the weight of the water sorbed at the given activity by the dry weight of the polymer.

In the study of Swinyard et al. (1990), the diffusion coefficient of water in polysulfone was found as 7.2×10^{-8} at 40°C at unit activity which is very close to the ones found in this study and shows the agreement of the results with the literature.

8.4.2. Determination of Diffusion Coefficients of Polysulfone/ Chloroform System

Figures 8.27 and 8.28 show gravimetric sorption curves for chloroform/PSf system collected at 30°C and 40°C. The results are presented in terms of weight of the chloroform absorbed, M_t-M_0, versus the square root of the time. Experimental conditions for the uptake measurements and the total thicknesses of the polymer at the beginning of each sorption step are listed in Table 8.3.

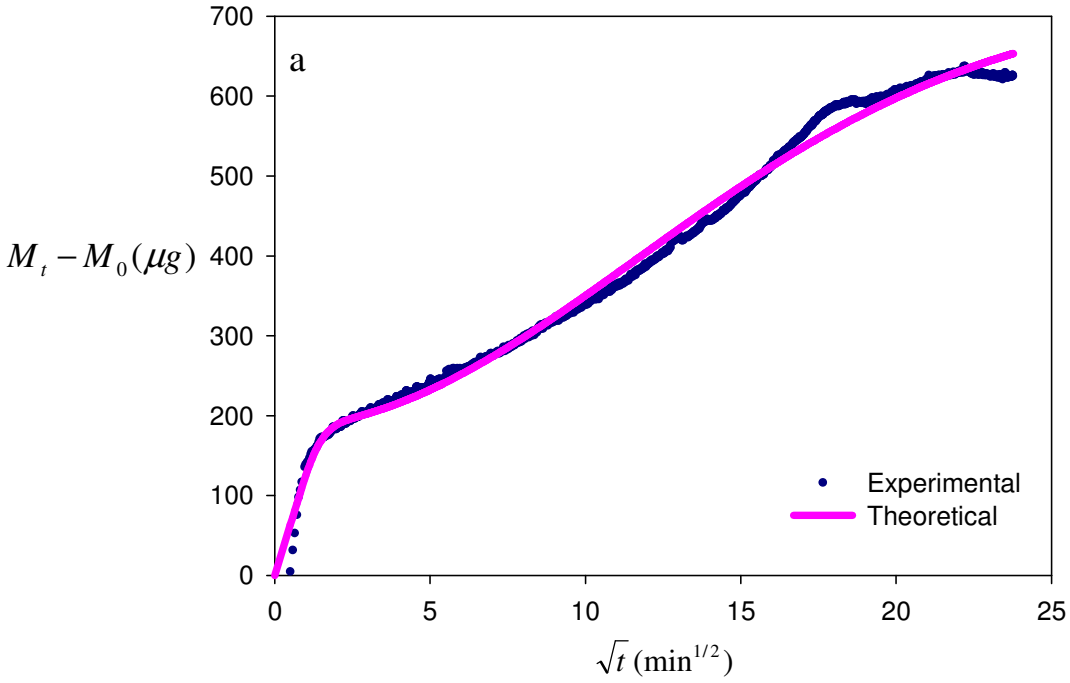

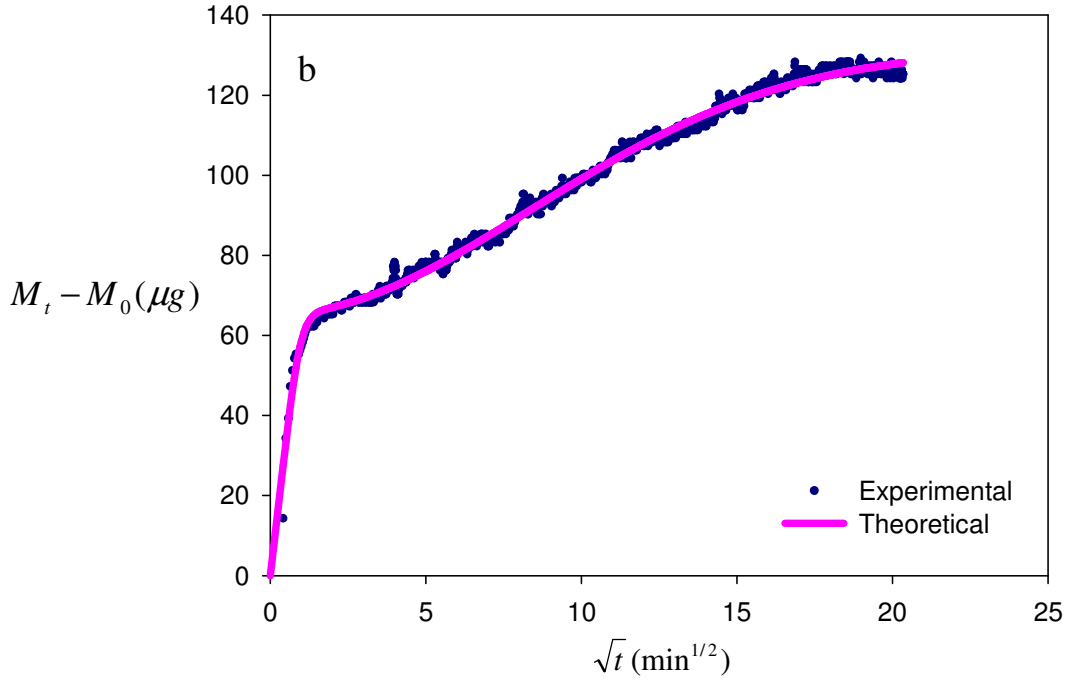

Figure 8.27. Bouyancy corrected weight difference values as a function of $\sqrt{t}$ for the diffusion of chloroform in polysulfone at 30°C. The solid line represents the theoretical curve and the symbol represents the experimental sorption curve. Water vapor temperatures: a) 9.9°C, b) 14°C, c) 18°C

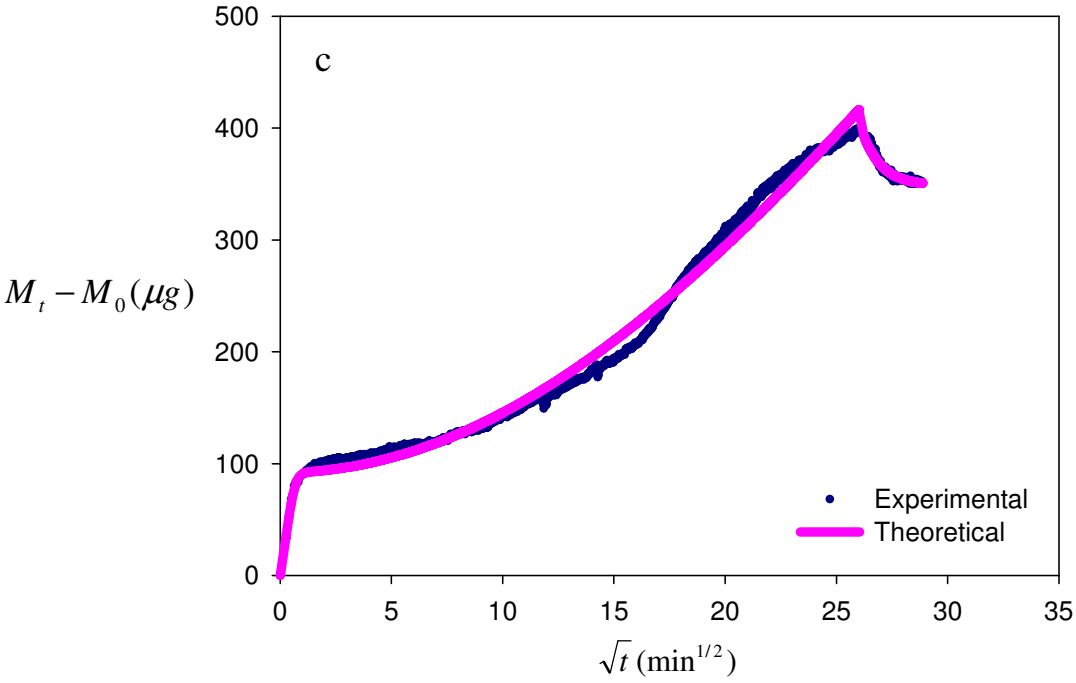

Figure 8.27. Bouyancy corrected weight difference values as a function of $\sqrt{t}$ for the diffusion of chloroform in polysulfone at 30°C. The solid line represents the theoretical curve and the symbol represents the experimental sorption curve. Water vapor temperatures: a) 9.9°C, b) 14°C, c) 18°C (Cont.)

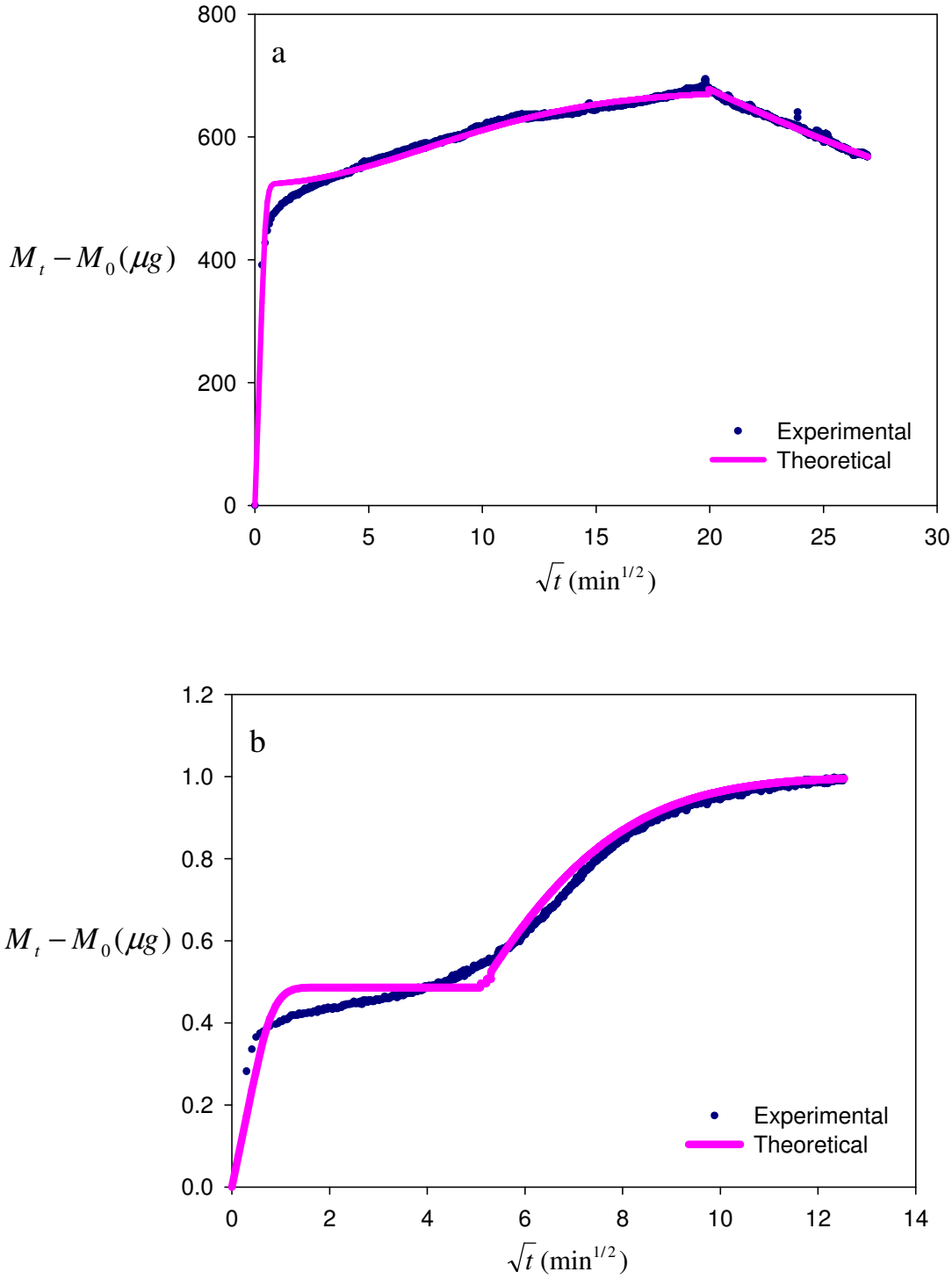

Figure 8.28. Bouyancy corrected weight difference values as a function of $\sqrt{t}$ for the diffusion of chloroform in polysulfone at 40°C. The solid line represents the the theoretical curve and the symbol represents the experimental sorption curve. Chloroform vapor temperatures: a) 11.5°C, b) 25°C, c) 30.8°C, d) 36°C

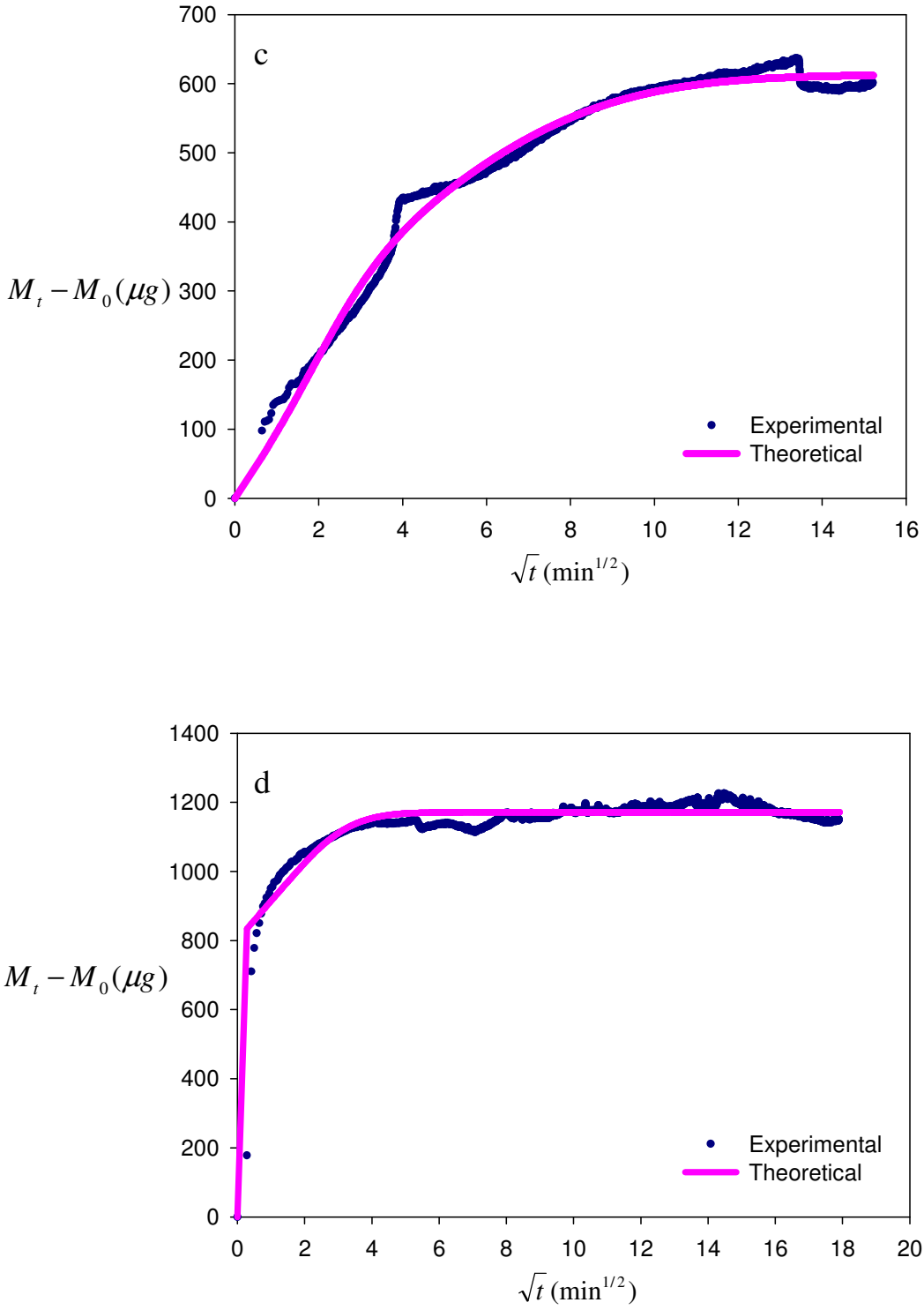

Figure 8.28. Bouyancy corrected weight difference values as a function of $\sqrt{t}$ for the diffusion of chloroform in polysulfone at 40°C. The solid line represents the the theoretical curve and the symbol represents the experimental sorption curve. Chloroform vapor temperatures: a) 11.5°C, b) 25°C, c) 30.8°C, d) 36°C (Cont.)

Table 8.3. Diffusivity data for chloroform-polysulfone at 30°C and 40°C

Temperature (°C)	Pressure (psia)		$\omega_{chloroform}$			thickness (μm)	$D\times10^9$ (cm^2/s)
	initial	Final	initial	equilibrium	average		
30	0	1.88	0	0.1855	0.1298	3.87	0.89
	1.88	2.29	0.1855	0.2146	0.2058	4.62	2.87
	2.29	2.76	0.2146	0.2864	0.2649	5.68	8.6
40	0	2.03	0	0.2233	0.1563	3.87	9.52
	2.03	3.77	0.2233	0.3164	0.2885	4.81	3.83
	3.77	4.81	0.3164	0.4169	0.3867	6.69	30.8
	4.81	5.94	0.4169	0.5458	0.5071	10.72	1.16

As shown in Figures 8.27a through 8.27c, shape of the sorption curves collected at 30°C have shown significant deviation from typical Fickian behaviour. In each case, a two stage sorption was observed with a slight overshoot in the last sorption stage (1.88-2.29 psia). Both two stage sorption and overshoot were considered as striking experimental observations for diffusion of low molecular weight solutes in glassy polymers (Kalospiros et al. 1991). For all steps, initial sorption rate is fast and increases linearly with $\sqrt{t}$ which is characteristic of sorption kinetics controlled by Fickian diffusion. At longer times, the weight increases at a much slower rate to an equilibrium value and this stage is controlled by relaxation of the polymer chains in the glassy state to accommodate the penetrant. Two stage sorption has also been observed for the sorption of vinyl chloride monomer in polyvinly chloride (Berens and Hopfenberg 1978), benzene in polyethylene terephthalate (Patton et al. 1984), methyl acetate in polymethylmethacarylate and cellulose acetate (Kishimoto et al. 1960), benzene, toluene and ethyl benzene in polystyrene (Iwai et al. 1987, Iwai et al. 1989) and acetone in cellulose nitrate (Kishimoto et al. 1960). In order to analyze the sorption curves, a mathematical proposed by Berens and Hopfenberg (1978) was used. According to this model, contributions from Fickian diffusion and relaxation processes are independent from each other, thus, they can be considered as additive. In the first two sorption steps, single relaxation time was used while in the last sorption step, relaxation was assumed to take place at two different times. The model parameters, diffusion coefficient of the penetrant (D) and the relaxation time(s) (τ_R), were regressed by minimizing the

difference between the experimental and theoretical weight uptakes calculated from Equation 6.13. Regressed values of the diffusivities and relaxation times are listed in Tables 8.3 and 8.4, respectively.

Table 8.4. Deborah numbers, τ_R and α values for chloroform-PSf at 30°C and 40°C

Tcolumn (°C)	Tpenetrant (°C)	De	τ_R
30	9.9	97.3	16234.38
	14	113	8369.73
	18	444.91	16695.87
40	11.5	2679.69	42203.94
	25	2680	1666.67
	30.8	1.96	2337.42
	36	1.01×10^{-7}	9.99×10^{-5}

The results shown in Figures 8.27a through 8.27c indicate that relaxation diffusion model is successful in analyzing the sorption curves collected at 30°C. In literature, overshoot phenomena observed in previous systems was attributed to solvent induced crystallization (Overbergh et al. 1975, Vittoria 1991), development of small microvoids (Aminabhavi and Phayde 1995, Aminabhavi et al. 1996) and slow relaxation of the polymer chains compared to the diffusion of penetrant into the polymer film (Etxeberria et al. 2000, Hoyt and Balik 1996, Kim et al. 1993). The overshoots observed in this study is caused by slow relaxation of the polymer chains to their equilibrium conformation since polysulfone used in the experiments is an amorphous polymer. The contribution of relaxation and Fickian processes on the overall sorption curve can be determined from the magnitudes of Deborah number. This dimensionless number compares the time scales for mass uptakes due to structural relaxation (τ_R) to the time scale for Fickian diffusion defined as L^2/D where L corresponds to the thickness of the film. The Deborah numbers calculated for each sorption step at 30°C and 40°C are listed in Table 8.4. At T = 30°C, Deborah number was found to increase as chloroform concentration in PSf increases. This could be attributed to presaturation of existing available sites which results in longer relaxation periods to provide redistribution of free volume elements, hence, to accommodate additional penetrant (Berens and Hopfenberg, 1978).

The sorption curves collected at T = 40°C have also shown anomalous, i.e., non-Fickian diffusion behavior as illustrated in Figures 8.28a through 8.28d. The data were analyzed successfully with the relaxation diffusion model (Equation 6.13) and the diffusivities and relaxation times regressed from these curves are listed in Tables 8.3 and 8.4, respectively. In the first step of the experiments (Figure 8.28a), an initial rapid weight gain was followed by a two stage relaxation period, in which second relaxation corresponds to decrease in amount of penetrant absorbed until its final equilibrium value was reached. A transition in sorption curve from an overshoot behavior to the two stage sorption is shown in Figure 8.28b. The shapes of the sorption curves in the last two steps become similar to that of typical Fickian curves with a slight overshoot in the third sequential step (Figure 8.28c). In contrast to the observation at T = 30°C, the Deborah numbers calculated at T = 40°C were found to decrease with the increased sorption level in the polymer. This simply indicates decreased contribution of relaxation process on the overall sorption curve due to transition from glassy to rubbery state. To determine the change in glass transition temperature of the polymer with absorption of the penetrant, following equation derived by Kelly and Bueche (1961) was used:

$$T_g = \frac{4.8\times10^{-4}(1-\phi_1)T_{g1} + \alpha_S\phi_1 T_{g2}}{4.8\times10^{-4}(1-\phi_1) + \alpha_S\phi_1} \tag{8.2}$$

In Equation 8.2, T_{g1} and T_{g2} are the glass transition temperature of the solvent and pure polymer, respectively, while α_s is the thermal expansion coefficient of the pure solvent.

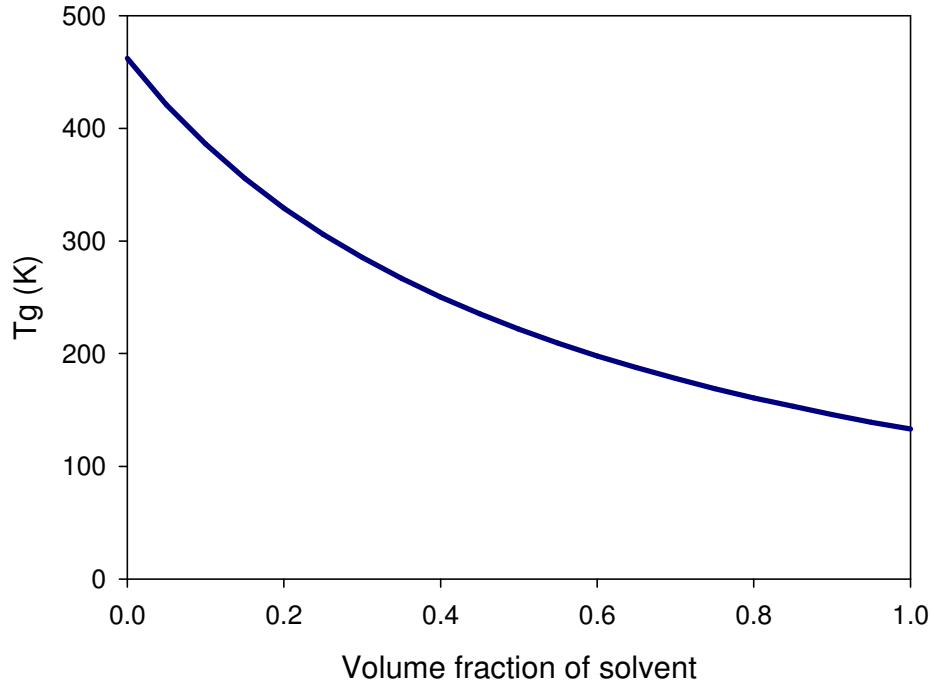

Figure 8.29. Plot of T_g as a function of volume fraction of solvent

Figure 8.29 shows that the glass transition temperature of the polymer decreases significantly with the chloroform uptake. When the weight fractions of the chloroform in the polymer are 0.31 and 0.33, the glass transition temperatures drop to 30°C and 40°C , respectively. As will be shown in the next section, at the last activity step of T = 30°C and T = 40°C measurements, the amount of chloroform absorbed in the polymer was determined as 27% and 49.5% by weight, respectively. It is clear from these results that, transition from glassy to rubbery state occurs in PSf film at T = 40°C, while the polymer is still in glassy state at T = 30°C. Transition from glassy to rubbery state results in relaxation of the polymer chains at a much faster rate, hence, the Deborah numbers calculated at T = 40°C decreases with increased chloroform sorption level in the polymer.

At T = 30°C, the diffusivity of chloform in PSf was found to increase by one order of magnitude as the weight fraction of chloroform increased from 0.13 to 0.27. On the other hand, at T = 40°C a decrease in diffusivity by almost one order of magnitude was followed by an increase at the last sorption step (4.81-5.94 psia) with significant chloroform uptake. This could be again explained by the transition from glassy to rubbery state in PSf film.

8.4.3. Determination of Diffusion Coefficients of Polysulfone/Ethanol System

Gravimetric sorption curves for ethanol/PSf system were collected at 30°C and 40°C using the films with two different thicknesses. The experimental conditions for the first uptake measurements for PSf films with 1.5 μm initial thicknesses are listed in Table 8.5.

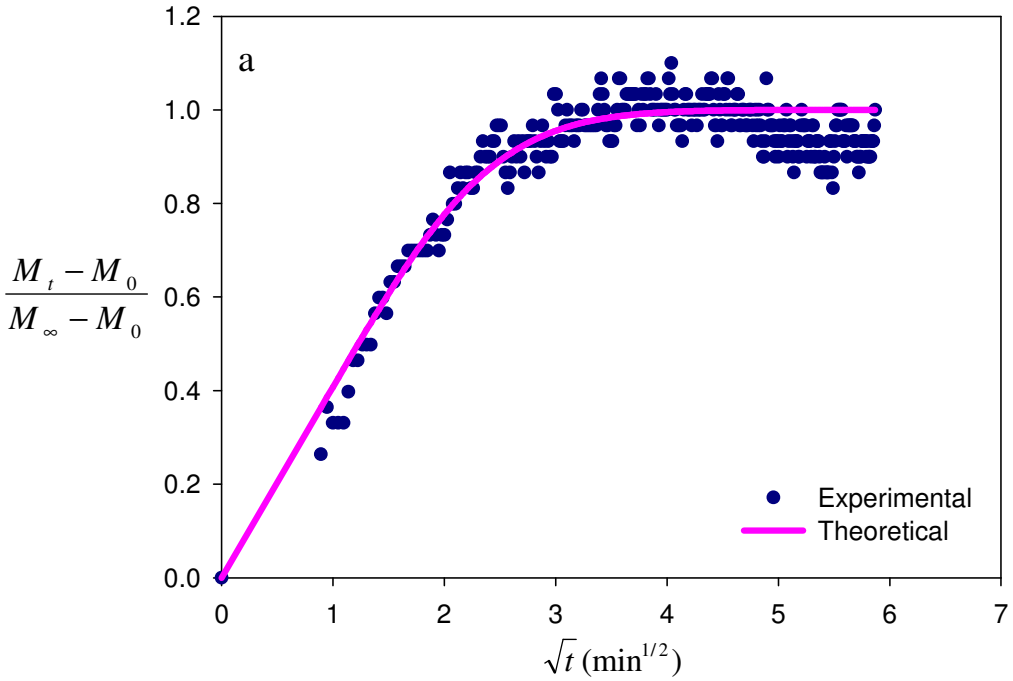

Figure 8.30. Bouyancy corrected weight difference values as a function of $\sqrt{t}$ for the diffusion of ethanol in polysulfone at 30°C of Set 2. The solid line represents the the theoretical curve and the symbol represents the experimental sorption curve. Ethanol vapor temperatures: a) 11.9°C, b) 20°C, c) 25.6°C

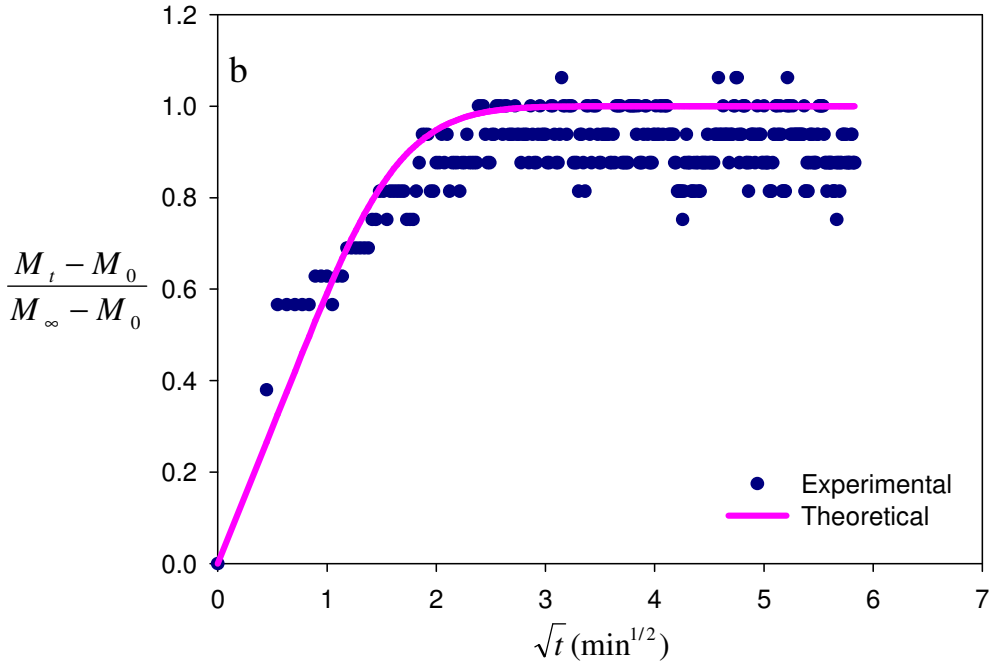

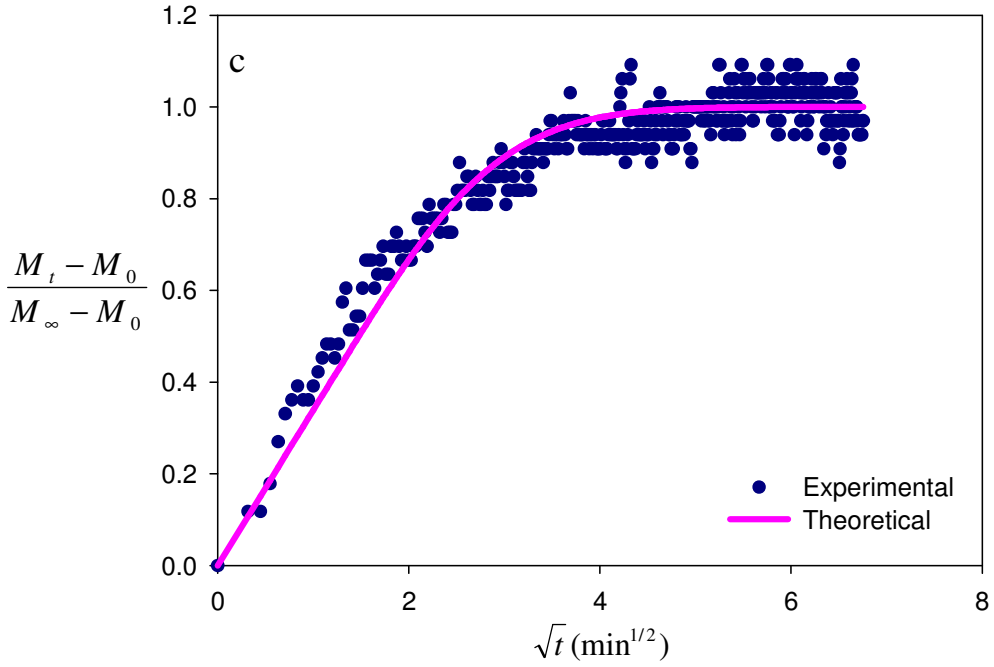

Figure 8.30. Bouyancy corrected weight difference values as a function of $\sqrt{t}$ for the diffusion of ethanol in polysulfone at 30°C of Set 2. The solid line represents the the theoretical curve and the symbol represents the experimental sorption curve. Ethanol vapor temperatures: a) 11.9°C, b) 20°C, c) 25.6°C (Cont.)

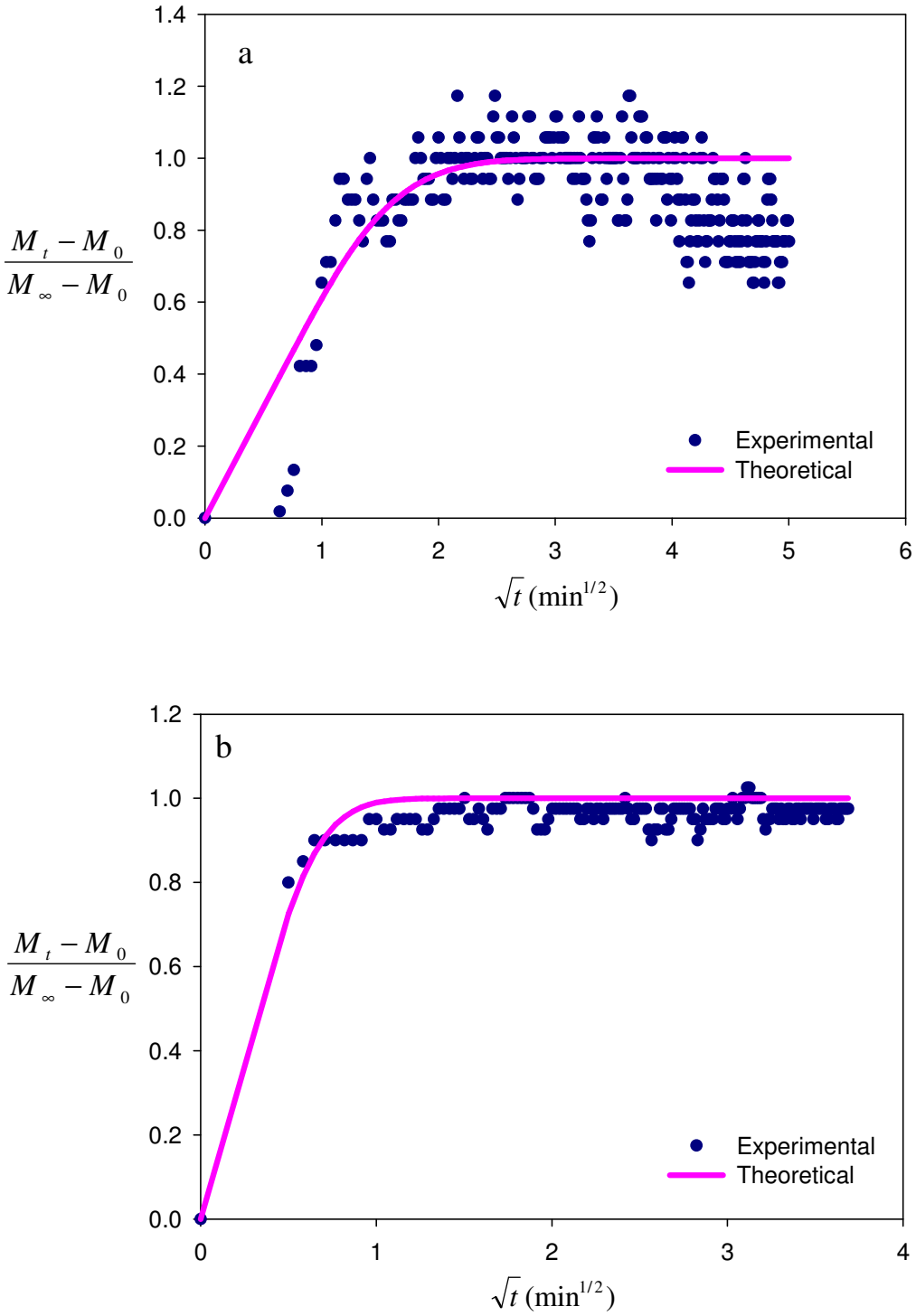

Figure 8.31. Bouyancy corrected weight difference values as a function of $\sqrt{t}$ for the diffusion of ethanol in polysulfone at 40°C of Set 2. The solid line represents the the theoretical curve and the symbol represents the experimental sorption curve. Ethanol vapor temperatures: a) 11.2°C, b) 16.2°C, c) 20.1°C, d) 30.2°C, e) 35°C

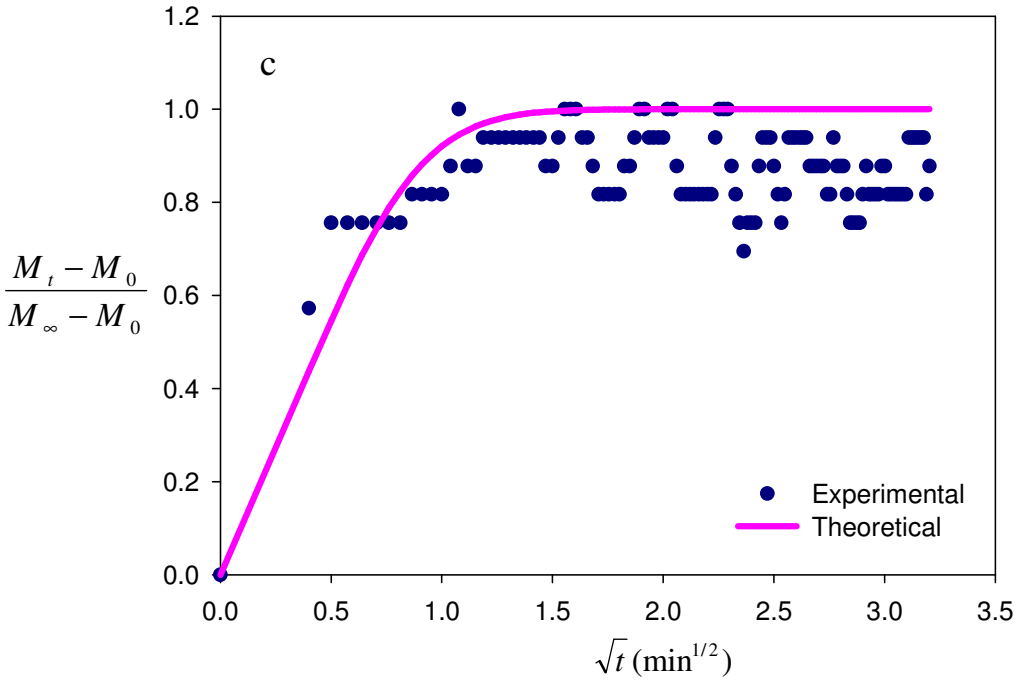

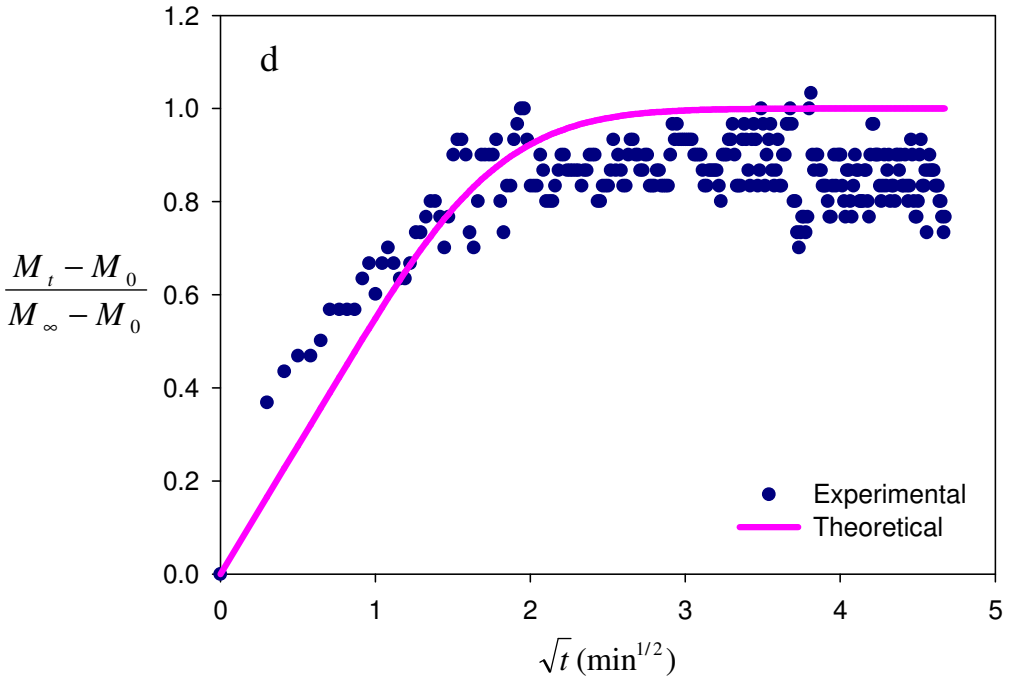

Figure 8.31. Bouyancy corrected weight difference values as a function of $\sqrt{t}$ for the diffusion of ethanol in polysulfone at 40°C of Set 2. The solid line represents the the theoretical curve and the symbol represents the experimental sorption curve. Ethanol vapor temperatures: a) 11.2°C, b) 16.2°C, c) 20.1°C, d) 30.2°C, e) 35°C (Cont.)

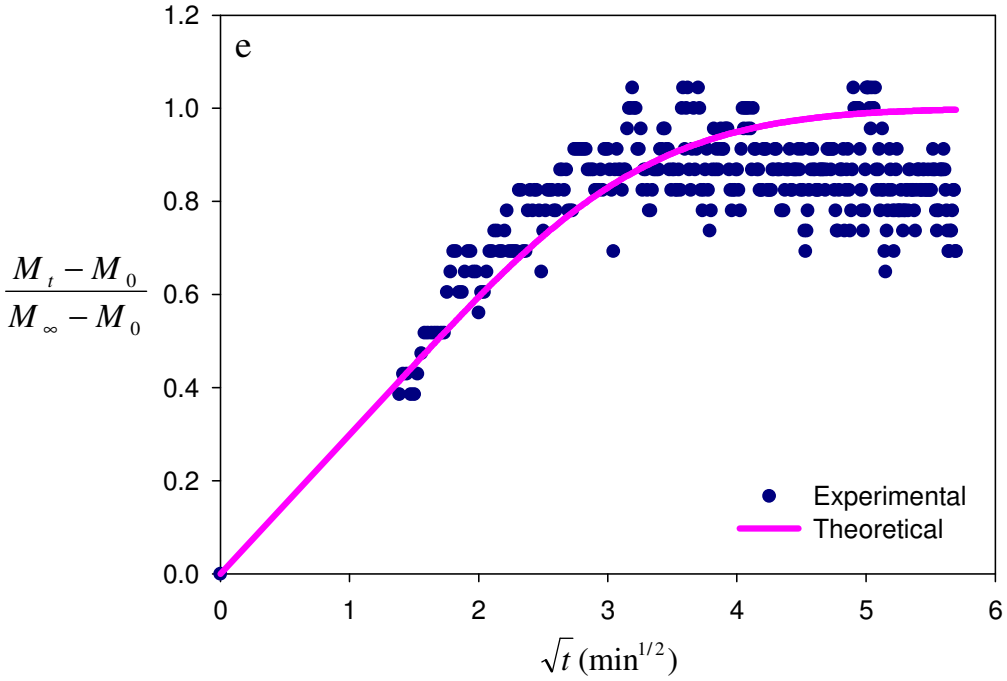

Figure 8.31. Bouyancy corrected weight difference values as a function of $\sqrt{t}$ for the diffusion of ethanol in polysulfone at 40°C of Set 2. The solid line represents the the theoretical curve and the symbol represents the experimental sorption curve. Ethanol vapor temperatures: a) 11.2°C, b) 16.2°C, c) 20.1°C, d) 30.2°C, e) 35°C (Cont.)

Table 8.5 Diffusivity data for ethanol-polysulfone at 30°C and 40°C for Set 2

Temperature (°C)	Pressure (psia)		$\omega_{ethanol}$			thickness (μm)	D×10^{11} (cm^2/s)
	initial	Final	Initial	equilibrium	Average		
30	0	0.51	0	0.0213	0.0149	1.42	4.39
	0.51	0.85	0.0213	0.0324	0.0291	1.47	10
	0.85	1.18	0.0324	0.0552	0.0484	1.55	3.6
40	0	0.49	0	0.0123	0.0086	1.42	10
	0.49	0.67	0.0123	0.0361	0.0290	1.45	65.57
	0.67	0.85	0.0361	0.0446	0.0421	1.54	36.84
	0.85	1.53	0.0446	0.060	0.0556	1.65	10.77
	1.53	1.99	0.060	0.0708	0.0677	1.81	3.84

Figures 8.30 through 8.31 show that all curves exhibit a linear initial slope while the latter part of the curves are concave with respect to $\sqrt{t}$ axis with slight overshoots and scatter around the equilibrium values. The data are analyzed with simple Fickian model (Equation 6.7) and diffusivities regressed from these analyses are listed in Table 8.5. At both temperatures, diffusivities increase to a maximum and then decrease.

Deviation from classical Fickian sorption has been observed when the sorption data were collected at 30°C and 40°C with PSf films of 9.8 μm as shown in Figures 8.32 and 8.33. At both temperatures, a transition from Fickian type to two stage sorption was observed. The curves were analyzed with the diffusion-relaxation model (Equation 6.13) and the diffusivities and relaxation times determined from nonlinear regression analyses are listed in Tables 8.6 and 8.7, respectively. The change in Deborah numbers with increased ethanol uptake in the films indicate that the contribution of relaxation process on the overall sorption increases at T = 30°C, while opposite trend is determined at T = 40°C.

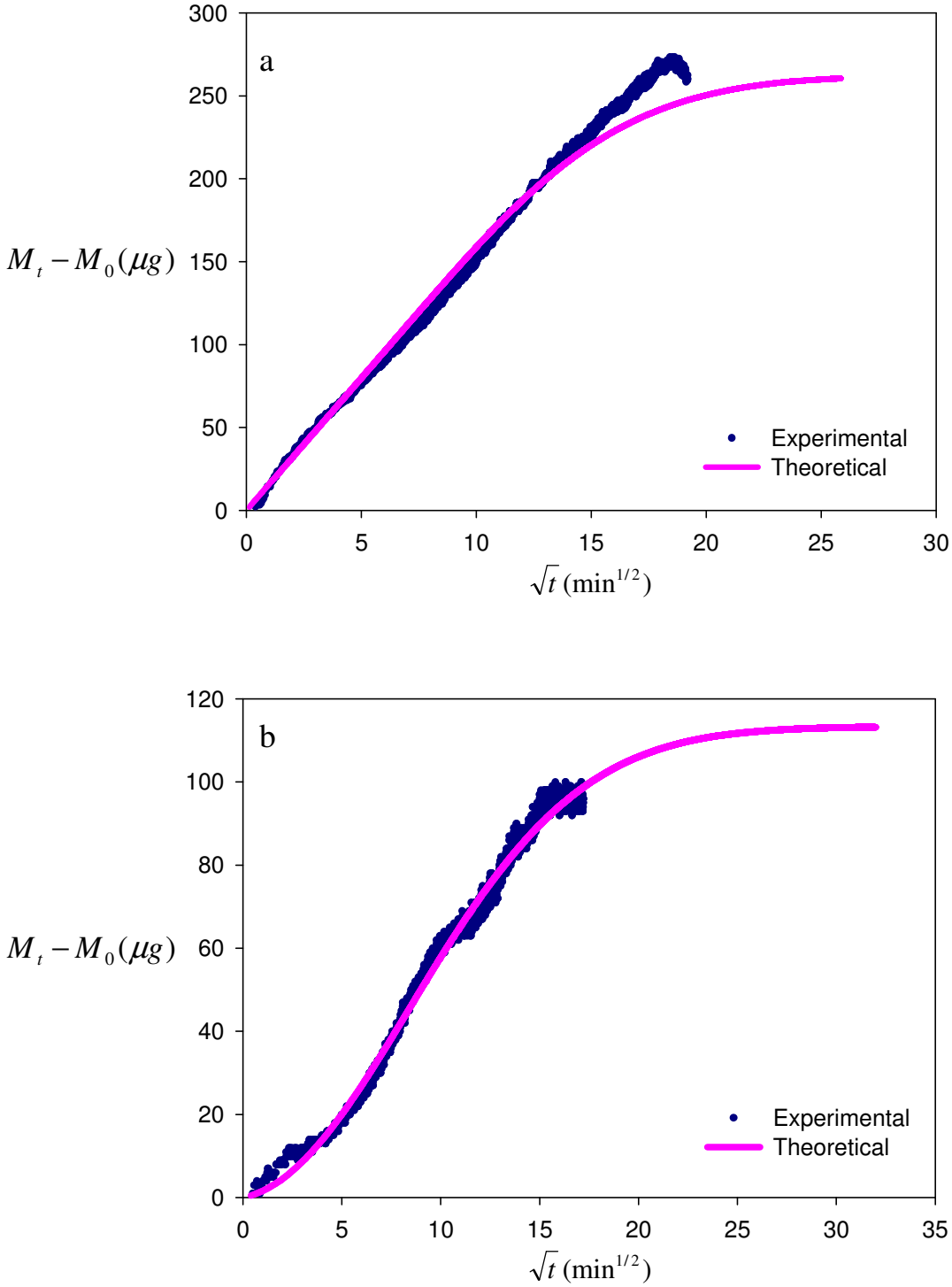

Figure 8.32. Bouyancy corrected weight difference values as a function of $\sqrt{t}$ for the diffusion of ethanol in polysulfone at 30°C for Set 1. The solid line represents model predictions and the symbol represents the experimental sorption curve. Ethanol vapor temperatures: a) 11.7°C, b) for 15.9°C, c) 20.1°C, d) 25.1°C

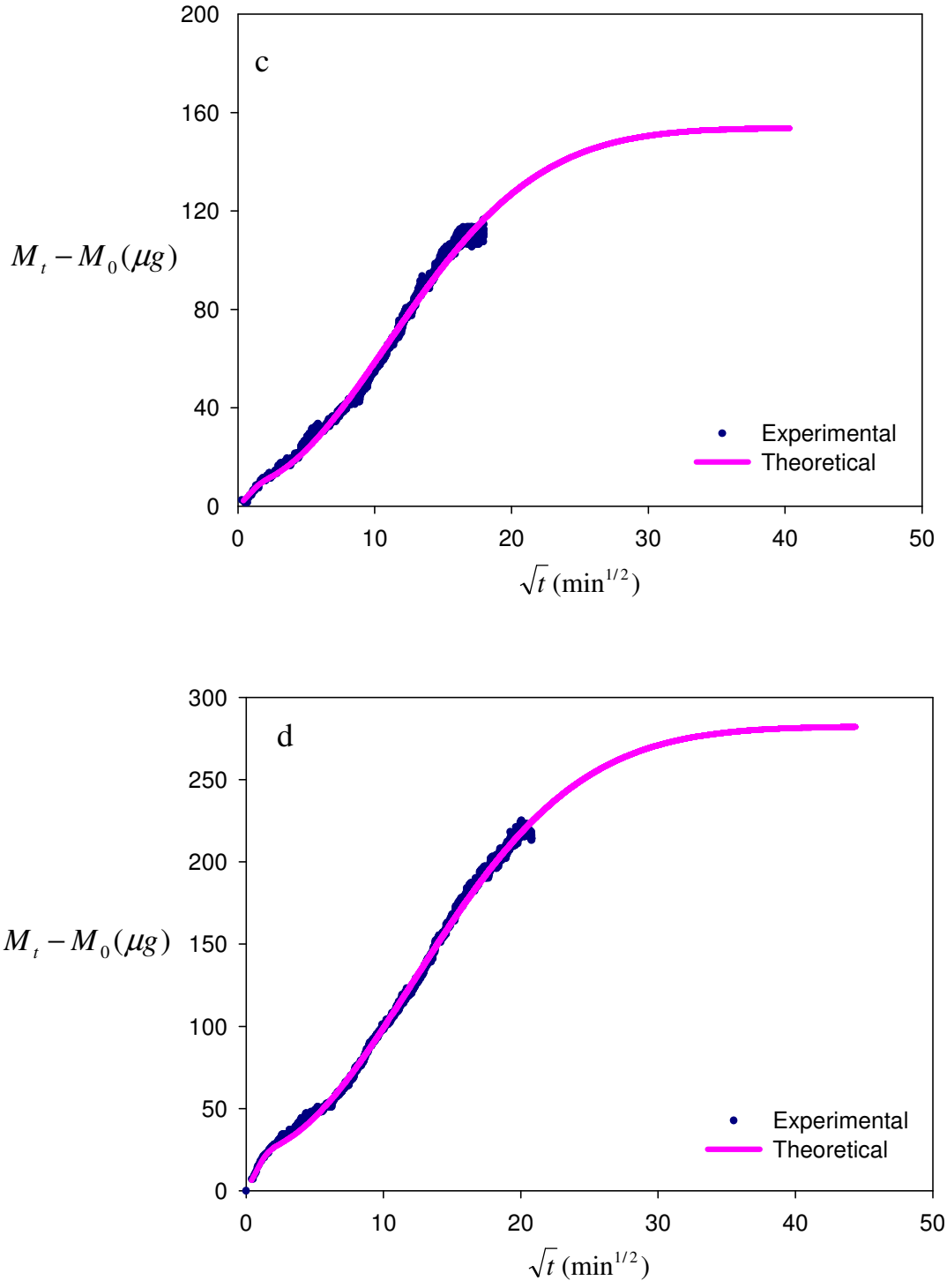

Figure 8.32. Bouyancy corrected weight difference values as a function of $\sqrt{t}$ for the diffusion of ethanol in polysulfone at 30°C for Set 1. The solid line represents model predictions and the symbol represents the experimental sorption curve. Ethanol vapor temperatures: a) 11.7°C, b) for 15.9°C, c) 20.1°C, d) 25.1°C (Cont.)

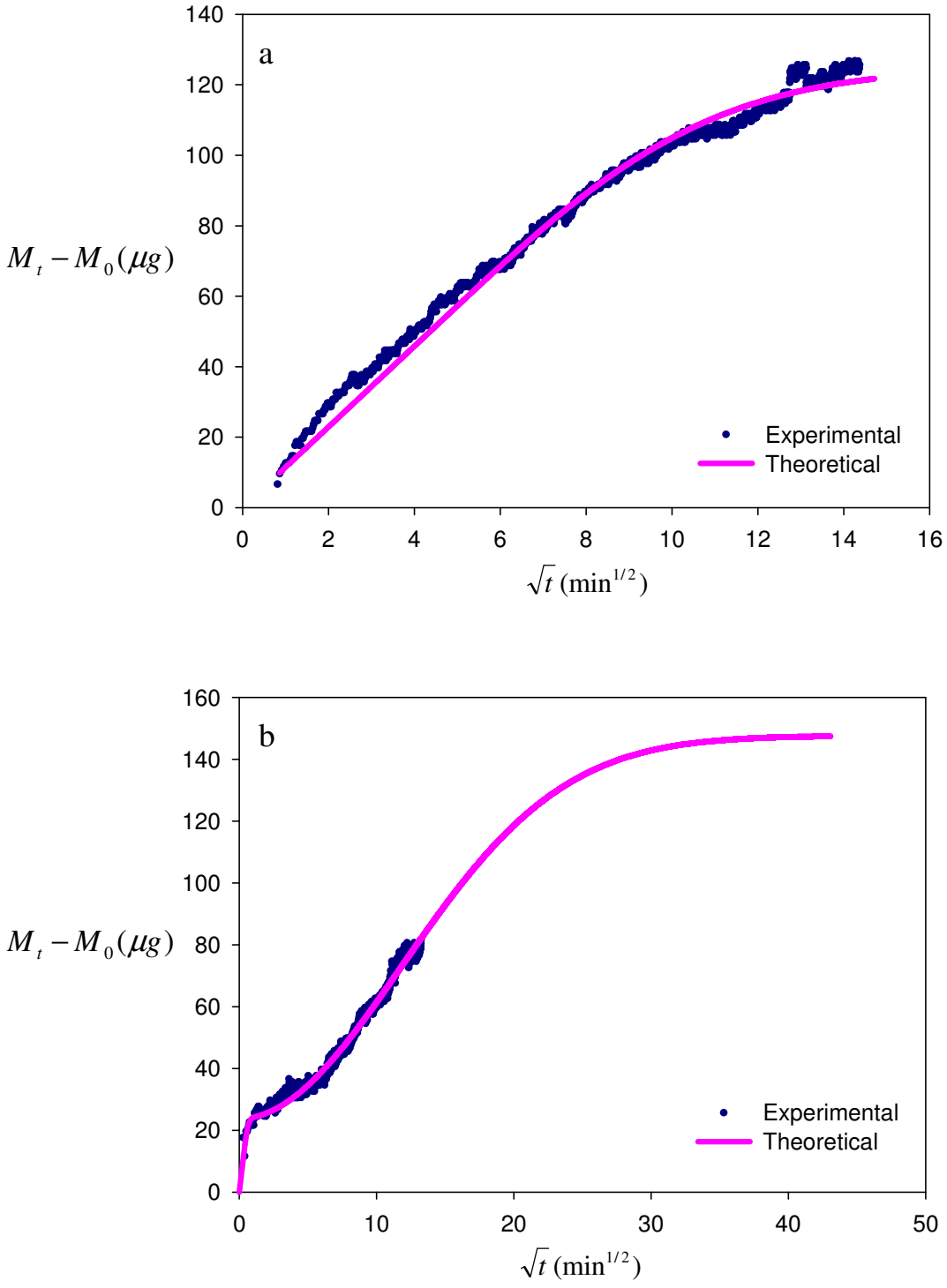

Figure 8.33. Bouyancy corrected weight difference values as a function of $\sqrt{t}$ for the diffusion of ethanol in polysulfone at 40°C for Set 1. The solid line represents model predictions and the symbol represents the experimental sorption curve. Ethanol vapor temperatures: a) 14.3°C, b) 25°C, c) 30°C, d) 35°C

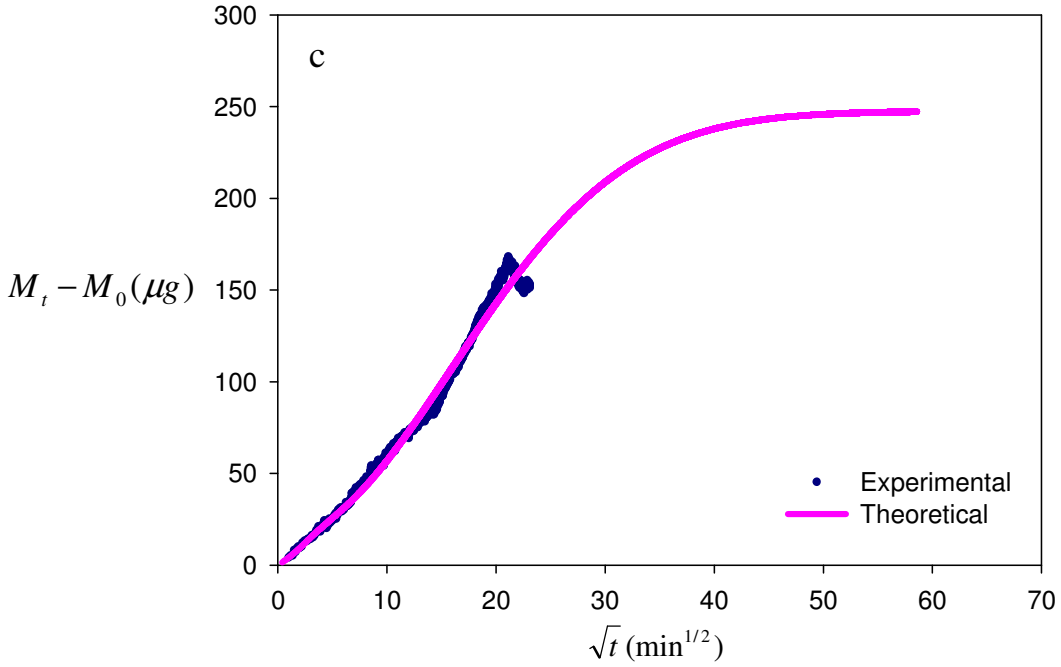

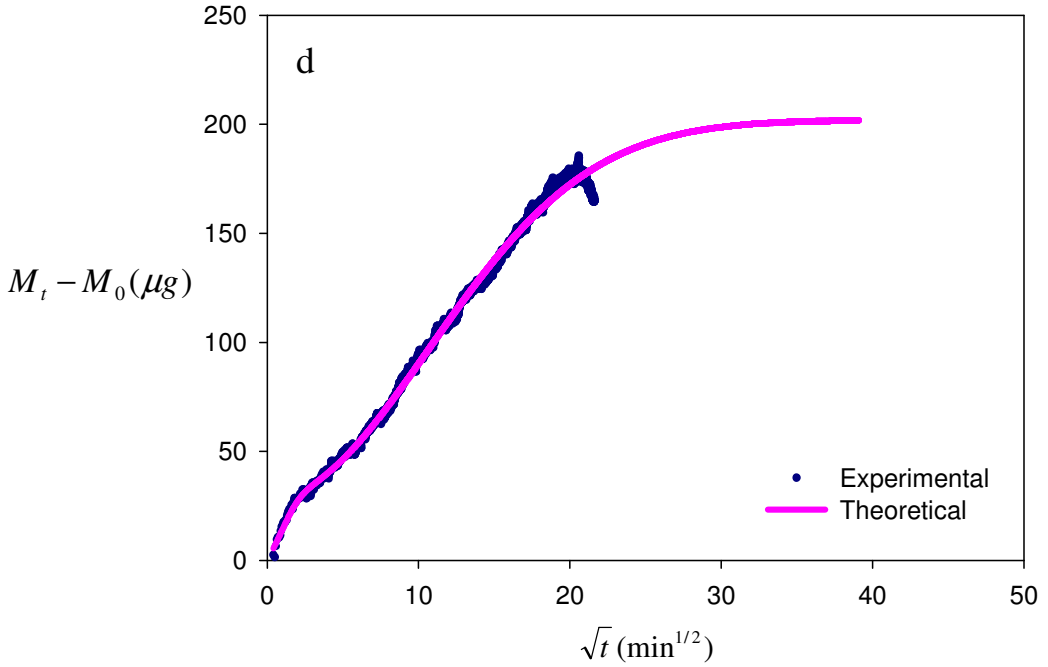

Figure 8.33. Bouyancy corrected weight difference values as a function of $\sqrt{t}$ for the diffusion of ethanol in polysulfone at 40°C for Set 1. The solid line represents model predictions and the symbol represents the experimental sorption curve. Ethanol vapor temperatures: a) 14.3°C, b) 25°C, c) 30°C, d) 35°C (Cont.)

Table 8.6. Diffusivity data for ethanol-polysulfone at 30°C and 40°C of Set 1

Temperature (°C)	Pressure (psia)		ω_{water}			thickness (μm)	$D\times10^{11}$ (cm^2/s)
	Initial	Final	initial	equilibrium	average		
30	0	0.5054	0	0.01579	0.01105	9.88	4.76
	0.5054	0.6595	0.01579	0.02231	0.02035	10.13	6.94
	0.6595	0.8529	0.02231	0.03102	0.02841	10.47	575.6
	0.8529	1.1459	0.03102	0.04662	0.04194	10.93	659.7
40	0	0.5965	0	0.0081	0.00564	9.88	10.77
	0.5965	1.1393	0.0081	0.01743	0.01462	10	3320
	1.1393	1.5138	0.01743	0.0327	0.02815	10.21	84
	1.5138	1.99	0.0327	0.0449	0.04125	10.65	330.7

Table 8.7 Deborah numbers, τ_R and α values for ethanol-polysulfone at 30°C and 40°C

Tcolumn (°C)	Tpenetrant (°C)	De	τ_R
30	15.9	0.153	9023.04
	20.1	18.62	14192.38
	25.1	23.85	17277.66
40	25	137	16485.74
	30	6.04	29994.14
	35	9.98	13527.67

In order to further illustrate anomalous diffusion of ethanol in glassy PSf films, normalized mass uptake curves were plotted against $\frac{\sqrt{t}}{L}$ using the data measured at the same activity levels as shown in Figures 8.34 through 8.36. Nonoverlap of two of these curves is considered as anomalous diffusion. Infact , sample size effect is frequently used to determine deviation from Fickian type sorption. A consequence of sample size effect hence anomalous diffusion is reflected by the change in diffusivities with the film thicknesses as reported in Table 8.8. At two activity steps (T = 30°C, a = 0.56 and T = 40°C, a = 0.76) diffusivities vary from each other by two orders of magnitude while similar diffusivities were determined for the activity level of 0.33 at T = 30°C.

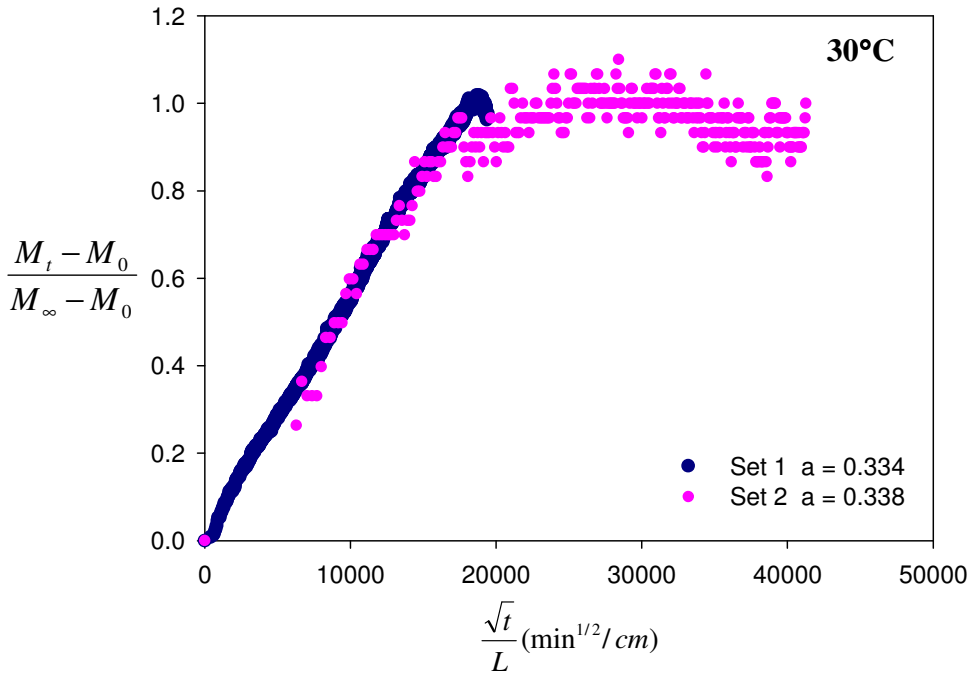

Figure 8.34. Plot of M_t/M_∞ as a function of $\sqrt{t}/L$ at activity = 0.33 for different thicknesses

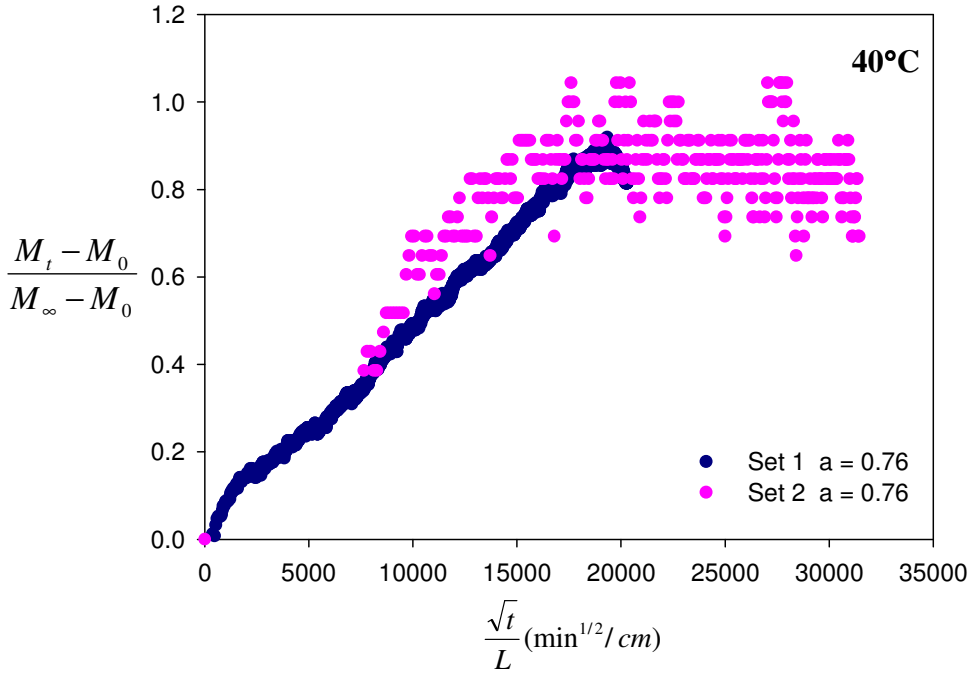

Figure 8.35. Plot of M_t/M_∞ as a function of $\sqrt{t}/L$ at activity = 0.76 for different thicknesses

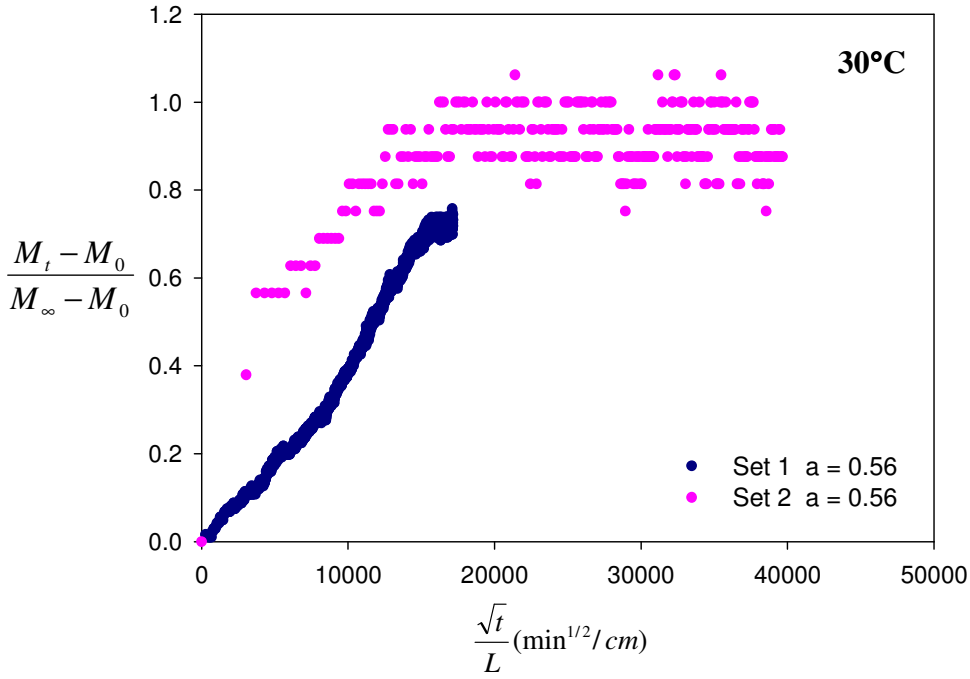

Figure 8.36. Plot of M_t/M_∞ as a function of $\sqrt{t}/L$ at activity = 0.76 for different thicknesses

Table 8.8. Diffusion coefficients of ethanol in PSf as a function of the film thickness

L (μm)	Activity	$D\times10^{-11}$
9.88	0.334	4.76
1.486	0.338	4.39
9.88	0.56	575.6
1.486	0.56	3.6
9.88	0.76	330.7
1.486	0.76	3.84

8.4.4. Equilibrium Isotherms of Penetrants in Polysulfone

Sorption isotherm of a penetrant in a polymer is usually plotted as activity of the penetrant in the vapor phase against its volume fraction in the polymer. By assuming that the penetrant vapor is ideal, activity was calculated from the ratio of the saturation vapor pressure of the penetrant at the penetrant temperature to that at column temperature as given below.

$$Activity = \frac{P_1^{\circ}(T_{penetrant})}{P_1^{\circ}(T_{column})} \tag{8.3}$$

For all penetrants, the weight fraction gravimetric sorption data were converted to volume fractions and the results are given in Tables 8.9 through 8.11 for water, ethanol and chloroform, respectively. Figure 8.37 illustrates the repeatability of the experiments with the sorption isotherm of water collected at T = 50°C.

Table 8.9. Sorption isotherms for water in polysulfone measured at the column temperatures 30°C, 40°C and 50°C

T(°C)	Volume Fraction of Water	Activity
30	0.005031	0.377
	0.007209	0.486
	0.011045	0.623
	0.020991	0.792
40	0.004259	0.317
	0.005898	0.430
	0.008251	0.575
	0.016236	0.762
50	0.002688	0.190
	0.003473	0.257
	0.004495	0.344
	0.006407	0.456
	0.010611	0.598
	0.023881	0.777

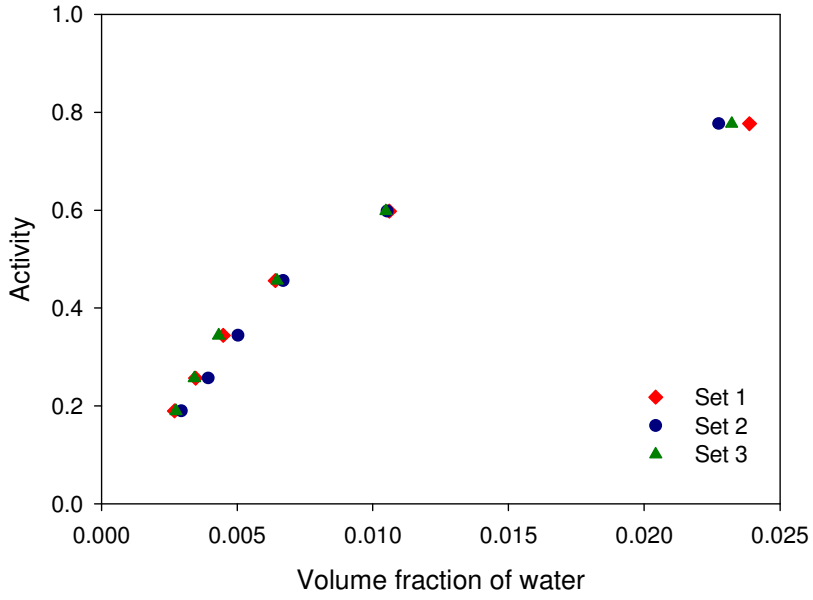

Figure 8.37. Sorption isotherms for 3 sets of repeated experiments at 50°C

Table 8.10. Sorption isotherms for chloroform in polysulfone measured at the column temperatures 30°C and 40°C

T(°C)	Volume Fraction of Chloroform	Activity
30	0.1611	0.404
	0.1873	0.492
	0.2529	0.593
40	0.1951	0.293
	0.2808	0.809
	0.3762	0.694
	0.5034	0.856

Table 8.11. Sorption isotherms for ethanol in polysulfone measured at the column temperatures 30°C and 40°C

T(°C)	Volume Fraction of Ethanol	Activity
30	0.02447	0.334
	0.03445	0.436
	0.04767	0.563
	0.07103	0.757
40	0.01254	0.230
	0.02698	0.44
	0.05027	0.585
	0.06846	0.769

8.5. Modeling of Diffusion and Equilibrium Studies

8.5.1. Modeling of the Equilibrium Isotherm

8.5.1.1. Modeling of the Equilibrium Isotherm of Water/PSf System

Equilibrium sorption isotherms of water/PSf system measured at 30°C, 40°C and 50°C were not correlated well with a constant interaction parameter. Thus, following expression for concentration dependence of the Flory Huggins interaction parameter was proposed:

$$\chi = a_0 + a_1\phi_2 \tag{8.4}$$

where a_0 and a_1 are empirical constants. These two constants were evaluated using the sorption data collected at 30°C, 40°C and 50°C, and were found to be -13.69 and 17.18, respectively. Figure 8.38 shows that Flory Huggins theory along with proposed concentration dependence of the Flory-Huggins interaction parameter successfully correlates the sorption isotherms of water/PSf system. The average value of the Flory Huggins interaction parameter within the volume fraction range from 0 to 1 was determined as 3.15. The value of average χ greater than 0.5 simply indicates that water acts as a nonsolvent for PSf.

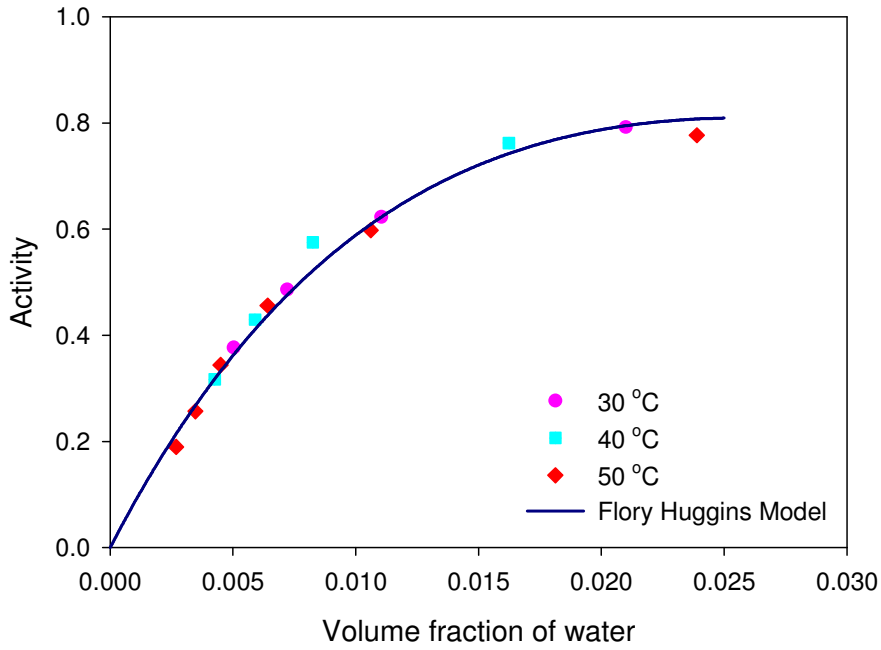

Figure 8.38. Sorption isotherm of water-polysulfone system

8.5.1.2. Modeling of the Equilibrium Isotherm of Chloroform/PSf System

Equilibrium sorption isotherms of chloroform/PSf system measured at 30°C and 40°C were correlated well with a constant Flory Huggins interaction parameter as shown in Figure 8.39. From the nonlinear regression analysis, the Flory Huggins interaction parameter was determined as -0.03. The negative sign of the χ parameter indicates strong interaction between polysulfone and chloroform. In addition, very small value of χ compared to the limiting value of 0.5 simply proves that chloroform is a very good solvent for polysulfone.

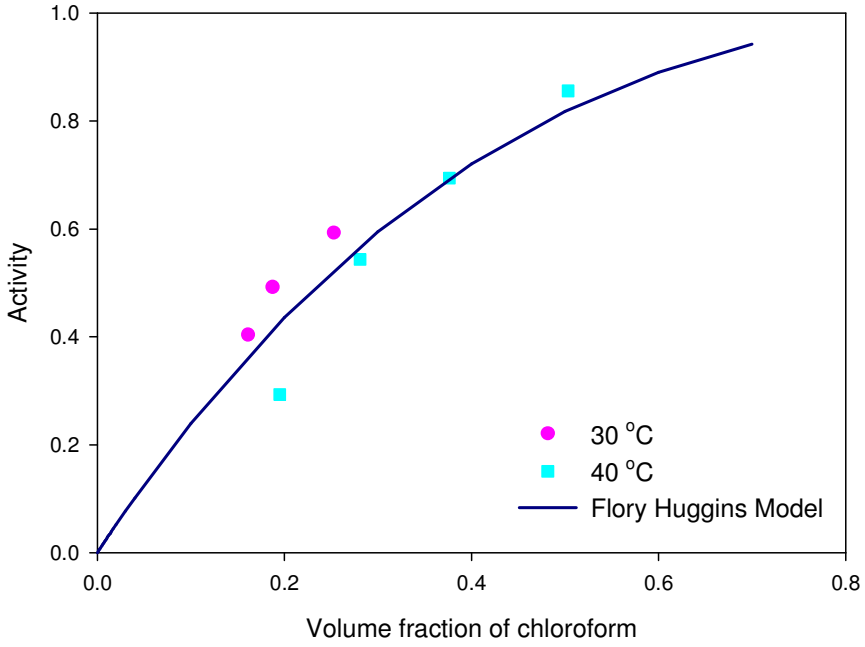

Figure 8.39. Sorption isotherm of chloroform-polysulfone system

8.5.1.3. Modeling of the Equilibrium Isotherm of Ethanol/PSf System

Equilibrium sorption isotherms of ethanol/PSf system measured at 30°C and 40°C were correlated well with a constant interaction parameter as shown in Figure 8.40. By minimizing the difference between the experimental data points and theoretical values, the Flory Huggins interaction parameter between ethanol and polysulfone was determined as 1.76. This value is close to the one obtained from swelling experiments as 1.8. The role of ethanol as nonsolvent for the production of PSf membranes is confirmed by the value of χ parameter greater than 0.5. The interaction parameter of water larger than that of ethanol simply indicates greater nonsolvent power of water for polysulfone. In other words, the homogeneous phase region is enlarged when ethanol rather than water is used as nonsolvent as shown in Figure 8.10.

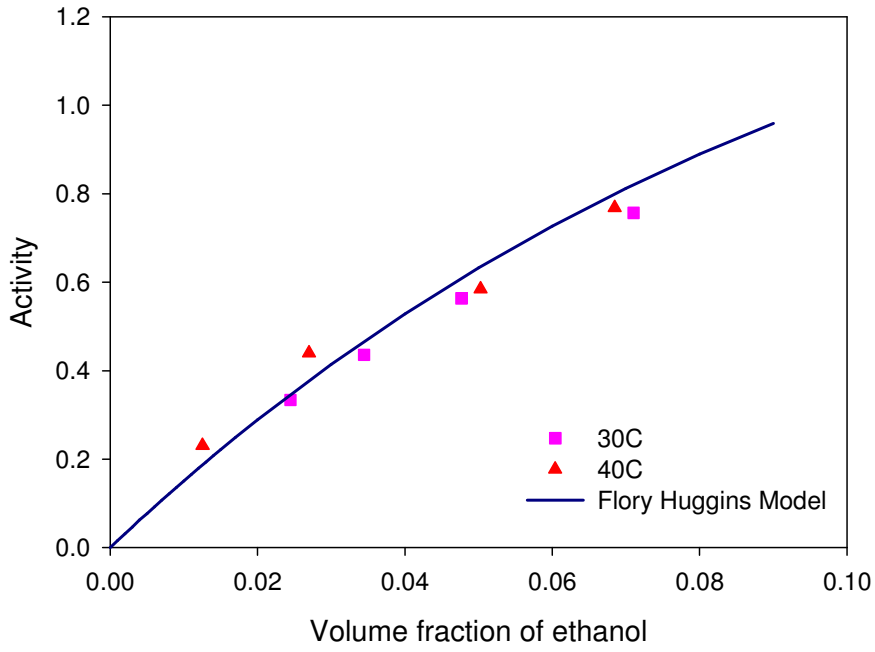

Figure 8.40. Sorption isotherm of ethanol-polysulfone system

8.5.2. Correlation and Prediction of Diffusion Coefficients

8.5.2.1. Correlation and Prediction of Diffusion Coefficients of Water/PSf system

The diffusivities of water in polysulfone were correlated with Vrentas and Duda free volume theory (Vrentas and Duda 1979). The equation used for the correlation is described by Equation 3.9 and the unknown parameters D_0 and ξ were obtained by fitting the experimental data collected at 30°C and 40°C and minimizing the following objective function using solver tool in Excel.

$$\min \sum_{i=1}^{N_{data}} \left(\ln D_{experimental} - \ln D_{theoretical} \right)^2 \tag{8.5}$$

The other free volume parameters required in Equation 3.9 were taken from the study of Yip et al. (2006) and Alsoy Altinkaya and Ozbas (2004). The free volume parameters along with the regressed parameters, D_0 and ξ are listed in Table 8.12.

Table 8.12. Free volume parameters of polysulfone and water

(Source: [a] Yip et al. 2006, [b] Alsoy and Ozbas 2004)

Parameter	PSf/water
K_{11}/γ (cm^3/gK)	0.00218[b]
K_{12}/γ (cm^3/gK)	-152.29[b]
K_{21}-T_{g1} (K)	0.00043[a]
K_{22}-T_{g2} (K)	-410[a]
$\hat{V}_1^*$ (cm^3/g)	1.071[b]
$\hat{V}_2^*$ (cm^3/g)	0.733[a]
D_0 (cm^2/s)	1.584×10^{-7} [b]
ξ	0.741[b]

Figure 8.41 shows that diffusivities calculated from Equation (3.14) by using the parameters listed in Table 8.12 are in agreement with the experimental ones. This agreement indicates that Vrentas and Duda free volume theory can correlate the diffusion behavior of water in polysulfone at 30°C and 40°C. Diffusivities obtained experimentally at 50°C are very close to the ones measured at 40°C, as a result it was observed that Vrentas and Duda free volume theory can not correlate the diffusion behavior at 50°C.

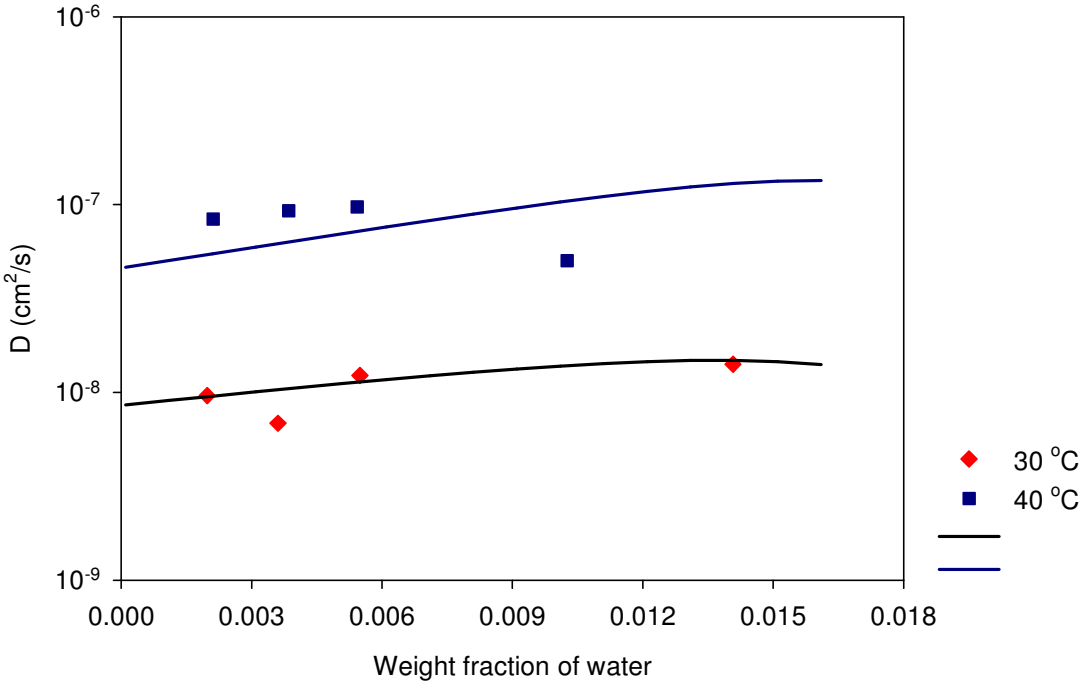

Figure 8.41. Experimental and correlated diffusivities with respect to weight fraction of water. The symbols represent the experimental data while the lines correspond to the free volume correlation.

CHAPTER 9

CONCLUSIONS

In this study, experimental cloud points for PSf/NMP (1-methyl-2-pyrrolidinone)/water, PSf/THF (Tetrahydrofuran)/water, PSf/NMP/ethanol, PSf/THF/water, PMMA (Polymethylmethacrylate)/acetone/water, PMMA/THF/water, PMMA /acetone/formamide and PMMA/THF/formamide systems were determined by the titration of homogeneous polymer solutions with nonsolvents until the onset of turbidity. In addition, sorption isotherms and diffusivity of water, ethanol and chloroform in polysulfone were measured by a gravimetric sorption technique.

The cloud point measurements have shown that the region of the homogeneous phase is slightly larger in the PSf/NMP/water system than in the PSf/THF/water system at the same temperature. The influence of solvent type on the cloud points become more pronounced when ethanol is used as a nonsolvent. It was observed that homogeneous phase region is larger in the PSf/NMP/ethanol than in the PSf/THF/ethanol system at 40°C. This indicates that nonsolvent power of water is higher than that of ethanol for PSf films. For the case of PMMA, the homogeneous phase region is not influenced by solvent type which are acetone and THF when both water and formamide are used as nonsolvents. The nonsolvent power of water is higher than formamide when acetone and THF are used as solvents. It has been observed that the effect of temperature on the cloud points is relatively small. By using the numerical code developed, the theoretical ternary phase diagrams of PSf/NMP/water, PSf/THF/water, PSf/NMP/ethanol, PSf/THF/ethanol, PMMA/acetone/water and PMMA/THF/water were constructed and very good agreement was obtained between the theoretical and experimental results for the systems PSf/NMP/water, PSf/THF/water, PSf/NMP/ethanol and PSf/THF/ethanol. For the systems, PMMA/acetone/water and PMMA/THF/water, the experimental cloud points didn't agree well with the theoretical binodal curves. These results can be explained by the inaccuracies in interaction parameters obtained from different sources.
For polysulfone/water system, sorption kinetics follows Fickian sorption. Analytical solution derived for Case 1 diffusion appropriately fits the experimental data of polysulfone/water system with slight deviation in a few cases where the data were collected at high activities. For the case of polysulfone/chloroform system, almost in

each case two stage sorption with a slow relaxation is observed. In a few cases, overshoot due to slow relaxation of polymer chains is noted. These kinetic behaviors are successfully modeled with diffusion-relaxation model. In PSf/ethanol system, Fickian type sorption is observed with the films of 1.5 μm, while two-stage sorption is seen when the film thickness is around 10 μm. The sample size effect observed for this system is attributed to relaxation of polymer chains in their glassy state.

Flory Huggins theory along with proposed concentration dependence of the Flory-Huggins interaction parameter successfully correlates the sorption isotherms of PSf/water system while for the polysulfone/ethanol and polysulfone/chloroform systems, Flory Huggins theory with constant interaction parameter is used. The Flory Huggins interaction parameter for Chloroform/PSf system is determined as -0.03 which indicates strong interaction between PSf and chloroform. The interaction parameter of water is found larger than that of ethanol which confirms greater nonsolvent power of water for PSf.

Experimental diffusivities of water in PSf collected at 30°C and 40°C is successfully correlated with Vrentas and Duda free volume theory. On the other hand, the theory fails to correlate the diffusivity data for chloroform/PSf and ethanol/PSf systems.

REFERENCES

Alentiev, A., Sanopoulou, M., Ushakov, N., Papadokostaki, K.G. 2002. "Melting and Recrystallization Processes in a Rubbery Polymer Detected by Vapor Sorption and Temperature-Modulated DSC Methods", *Polymer*. Vol. 43, p.1949.

Alfageme, J.A., Iriarte, M., Iruin, J.J., Etxeberria, A., Uriarte, C. 1999. "Water-Transport Properties in Polyetherimide Blends with a Liquid Crystal Polymer", *Journal of Applied Polymer Science*. Vol. 73, p. 323.

Allen, G., McAinsh, J., Strazielle, C. 1969. "Dilute Solution Properties of the Polyether From Bisphenol 'A' and 4,4′ Dichlorodiphenyl Sulphone", *European Polymer Journal*. Vol. 5, p. 319.

Alsoy Altinkaya, S., Ozbas, B. 2004. "Modeling of Asymmetric Membrane Formation by Dry-casting Method", *Journal of Membrane Science*. Vol. 230, p. 71.

Altena, F.W., Smolders, C.A. 1982. "Calculation of Liquid-Liquid Phase Separation in a Ternary System of a Polymer in a Mixture of a Solvent and a Nonsolvent", *Macromolecules*. Vol. 15, p. 1491.

Aminabhavi, T.M., Phayde, H.T.S. 1995. "Molecular Transport Characteristics of Santoprene Thermoplastic Rubber in the Presence of Aliphatic Alkanes Over the Temperature Interval of 25 to 70°C", *Polymer*. Vol. 36, p. 1023.

Aminabhavi, T.M., Phayde, H.T.S., Ortego, J.D. 1996. "Resistivity and Dimensional Stability of High-performance Engineering Thermoplastic Blend of Ethylene-propylene Random Copolymer and Isotactic Polypropylene Membrane in the Presence of Hazardous Haloalkanes", *Journal of Hazardous Materials*. Vol. 46, p. 71.

Areerat, S., Hayata, Y., Katsumoto, R., Kegasawa, T., Egami, H., Ohshima, M. 2002. "Solubility of Carbon Dioxide in Polyethylene/Titanium Dioxide Composite Under High Pressure and Temperature", *Journal of Applied Polymer Science*. Vol. 86, p. 282.

Balashova, I.M., Danner, R.P., Puri, P.S., Duda, J.L. 2001. "Solubility and Diffusivity of Solvents and Nonsolvents in Polysulfone and Polyetherimide", *Industrial & Engineering Chemistry Research*. Vol. 40, p. 3058.

Barth, C., and Wolf, B.A. 2000. "Quick and Realiable Routes to Phase Diagrams for Polyethersulfone and Polysulfone Membrane Formation", *Macromolecular Chemistry and Physics*. Vol. 201, No.3, p. 365.

Baschetti, M.G., Piccinini, E., Barbari, T.A., Sarti, G.C. 2003. "Quantitative Analysis of Polymer Dilation During Sorption Using FTIR-ATR Spectroscopy", *Macromolecules*. Vol. 36, p. 9574.

Bearman, R.J. 1961. "On the Molecular Basis of Some Current Theories of Diffusion", *Journal of Physical Chemistry*. Vol. 65, p. 1961.

Berens, A.R., Hopfenberg, H.B. 1978. "Diffusion and Relaxation in Glassy Polymer Powders: 2. Separation of Diffusion and Relaxation Parameters", *Polymer*. Vol. 19, p. 489.

Brandrup, J., Immergut, E.H., Grulke, E.A., 1999. *Polymer Handbook*, (John Wiley & Sons Inc.)

Bristow, G.M., Watson, W.F. 1958. "Cohesive Energy Densities of Polymers: Part 1.- Cohesive Energy Densities of Rubbers by Swelling Measurements", *Trans. Faraday Society*. Vol. 54., p. 1731.

Chang, S-M., Muramatsu, H., Nakamura, C., Miyake, J. 2000. "The Principle and Applications of Piezoelectric Crystal Sensors", *Materials Science and Engineering*. Vol. C 12, p. 111.

Chaudhary, B.I., Johns, A.I. 1998. “Solubilities of Nitrogen, Isobutane and Carbon Dioxide in Polyethylene”, *Journal of Cellular Plastics*. Vol. 34, p. 312.

Cheng, J-M., Wang, D-M., Lin, F-C., Lai, J-Y. 1996. “Formation and Gas Flux of Asymmetric PMMA Membranes”, *Journal of Membrane Science*. Vol. 109, p. 93.

Chin, J.W., Nguyen, T., Aouadi, K. 1999. “Sorption and Diffusion of Water, Salt Water, and Concrete Pore Solution in Composite Materials”, *Journal of Applied Polymer Science*. Vol. 71, p.483.

Cohen, M.H., Turnbull, D. 1959. “Molecular Transport in Liquids and Glasses**”**, *Journal of Chemical Physics*. Vol. 31, p. 1164.

Crank, J., 1975. *The Mathematics of Diffusion*, Third Edition, (Oxford Science Publications, Oxford), p.2.

Crank, J., Park, G.S., 1968. “Methods of Measurement”, in *Diffusion in Polymers*, (Academic Press Inc., New York), p.1.

Danner, R.P., High, M.S., 1993. *Handbook of Polymer Solution Thermodynamics,* (American Institute of Chemical Engineers, New York).

Davis, P.K., Danner, R.P., Duda, J.L., Romdhane, I.H. 2004a. “Use of Inverse Gas Chromatography to Study Binary Polymer-Solvent Systems Near The Glass Transition Temperature”, *Macromolecules*, Vol. 37, p. 9201.

Davis, P.K., Lundy, G.D., Palamara, J.E., Duda, J.L., Danner, R.P. 2004b. “New Pressure-Decay Techniques to Study Gas Sorption and Diffusion in Polymers at Elevated Pressures”, *Industrial & Engineering Chemical Research*. Vol. 23, p. 1537.

Daubert, T.E., Danner, R.P., 1994. *Physical and Thermodynamic Properties of Pure Compounds: Data Compilation*, (Taylor&Francis, New York).

Dhoot, S.N., Freeman, B.D., Stewart, M.E., Hill, A.J. 2001. "Sorption and Transport of Linear Alkane Hydrocarbons in Biaxially Oriented Polyethylene Terephthalate", *Journal of Polymer Science: Part B: Polymer Physics*. Vol. 39, p. 1160.

Dhoot, S.N. 2004. "Sorption and Transport of Gases and Organic Vapors in Polyethylene Terephthalate", M.S. Thesis. The University of Texas in Austin.

Doghieri, F., Biavati, D., Sarti, G.C. 1996. "Solubility and Diffusivity of Ethanol in PTMSP: Effects of Activity and of Polymer Aging", *Industrial & Engineering Chemistry Research*. Vol. 35, p. 2420.

Doolittle, A.K. 1951. "Studies in Newtonian Flow. II. The Dependence of the Viscosity of Liquids on Free-Space", *Journal of Applied Physics*. Vol. 22, p. 1471.

Dreisbach, F., Staudt, R., Keller, J.U. 1998. "Experimental Investigation of the Kinetics of Adsorption of Pure Gases and Binary Mixtures on Activated Carbon" in *Fundamentals of Adsorption 6*, F. Meunier Edition, (Elsevier), p. 279.

Dreisbach, F., Lösch, H.W. 2000. "Magnetic Suspension Balance For Simultaneous Measurements of a Sample and the Density of the Measuring Fluid", *Journal of Thermal Analysis and Calorimetry*. Vol. 62, p. 515.

Dreisbach, F., Seif, R.A.H., Lösch, H.W. 2002. "Gravimetric Measurements of Adsorption Equilibria of Gas Mixture CO/H_2 with a Magnetic Suspension Balance", *Chemical Engineering Technology*. Vol. 25, p. 1060.

Dubreil, A-C., Doumenc, F., Guerrier, B., Johannsman, D., Allain, C. 2003. "Analysis of the Solvent Diffusion in Glassy Polymer Films Using a Set Inversion Method", *Polymer*. Vol. 44, p. 377.

Duda, J.L., Vrentas, J.S., Ju, S.T., Liu, H.T. 1982. "Prediction of Diffusion Coefficients for Polymer-Solvent Systems", *AlChE Journal*. Vol. 28, p. 279.

Dullien, F.A.L. 1972. “Predictive Equations for Self-Diffusion in Liquids: A Different Approach”, *AlChE Journal*. Vol. 18, p. 62.

Etxeberria, A., Etxabarren, C., Iruin, J.J. 2000. “Comparison Between Static (Sorption) and Dynamic (IGC) Methods in the Determination of Interaction Parameters in Polymer/Polymer Blends”, *Macromolecules.* Vol. 33, p. 9115.

Feng, J. 2001. “Interaction and Permeability of Water with Liquid Crystalline Thermoset”, PhD Thesis. University of Florida.

Ferry, J.D., 1970. *Viscoelastic Propoerties of Polymers*, Second Edition, (Wiley, New York).

Fried, J.R., 1995. *Polymer Science and Technology*, Third Edition, (Prentice Hall PTR Englewood Cliffs, New Jersey).

Flory, P.J., 1985. *Principles of Polymer Chemistry*, (Cornell University Press, Ithaka, New York).

Ghi, P., Hill, D.J.T., Whittaker, A.K. 2000. “Water Sorption by Poly(tetrahydrofurfuryl methacrylate-co- 2-hydroxyethyl methacrylate). I. A Mass-Uptake Study”, *Journal of Polymer Science: Part B: Polymer Physics*. Vol. 38, p. 1939.

Han, M-J. 1999. “Effect of Propionic Acid in the Casting Solution on the Characteristics of Phase Inversion Polysulfone Membranes”, *Desalination*. Vol. 121, p.31.

Haward, R.N. 1970. “Occupied Volume of Liquids and Polymers”, *Journal of Macromolecular Science-Reviews in Macromolecular Chemistry*. C4, p. 191.

Hazeleger, M.C. 2006. “Understanding Adsorption in Micropores, a Study of Carbons, Soils and Zeolites”, M.S. Thesis. Universiteit van Amsterdam.

Hong, S-U. 1995. “Prediction of Polymer/Solvent Diffusion Behavior Using Free-Volume Theory”, *Industrial&Engineering Chemistry Research*. Vol. 34, p. 2536.

Hong, S.U., Laurer, J.H., Zielinski, J.M., Samseth, J., Smith, S.D., Duda, J.L., Spontak, R.J. 1998. "Morphological and Isothermal Diffusive Probe Analyses of Low Molecular-Weight Diblock Copolymers", *Macromolecules*. Vol. 31, p. 2174.

Hopfenberg, H.B., Frisch, H.L. 1969. "Transport of Organic Micromolecules in Amorphous Polymers", *Journal of Polymer Physics: Part B. Polymer Letters*. Vol. 7, p. 405.

Hoyt, M.A., Balik, C.M. 1996. "Diffusivity of a Drug Preservative in Bromobutyl Rubber", *Polymer Engineering and Science*. Vol. 36, No.14, p.1862.

Huang, Y., Liu, H., Hu, Y. 2003. "Transport of Mixed Solvents in Glassy Polymer Membrane", *Journal of Membrane Science.* Vol. 222, p. 123.

Iwai, Y., Kohno, M., Akiyama, T., Arai, Y. 1987. "Measurement and Correlation of Mutual Diffusion Coefficients for Molten Polystyrene-Hydrocarbon Systems", *Polymer Engineering Science*. Vol. 27, p. 837.

Iwai, Y., Maruyama, S., Fujimoto, M., Miyamoto, S., Arai, Y. 1989. "Measurement and Correlation of Mutual Diffusion Coefficients for Polybutadiene-Hydrocarbon Systems", *Polymer Engineering Science*. Vol. 29, p. 773.

Ju, S.T., Duda, J.L., Vrentas, J.S. 1981a "Influence of Temperature on the Diffusion of Solvents in Polymers Above the Glass Transition Temperature", *Industrial & Engineering Chemistry Product Research and Development*. Vol. 20, p.330.

Ju, S.T., Liu, H.T., Duda, J.L., Vrentas, J.S. 1981b. "Solvent Diffusion in Amorphous Polymers", *Journal of Applied Polymer Science*. Vol. 26, p. 3735.

Kalospiros, N.S., Ocone, R., Astarita, G., Meldon, J.H. 1991. "Analysis of Anomalous Diffusion and Relaxation in Solid Polymers", *Industrial & Engineering Chemistry Research*. Vol. 30, p. 851.

Kamaruddin, H.D., Koros, W.J. 2000. “Experimental Procedure Utilizing Extraction and Head-Space Analytical Method For Obtaining Methanol/MTBE Mixed-Liquid Sorption Isotherms in a Glassy Polymer”, *Journal of Polymer Science Part B: Polymer Physics*. Vol. 38, p. 2268.

Karimi, M., Albrecht, W., Heuchel, M., Kish, M.H., Frahn, J., Weigel, Th., Hofmann, D., Modarress, H., Lendlein, A. 2005. “Determination of Water/Polymer Interaction Parameter For Membrane-Forming Systems by Sorption Measurement and a Fitting Technique”, *Journal of Membrane Science*. Vol. 265, p. 1.

Kelly, F.N., Bueche, F. 1961. “Viscosity and Glass Temperature Relations for Polymer-Diluent Systems”, *Journal of Polymer Science.* Vol. 50, p. 549.

Kim, D., Caruthers, J.M., Peppas, N.A. 1993. “Penetrant Transport in Crosslinked Polystyrene”, *Macromolecules*. Vol. 26, p. 1841.

Kim, J.Y., Lee, H.K., Baik, K.J., Kim, S.C. 1997. “Liquid-Liquid Phase Separation in Polysulfone/Solvent/Water Systems”, *Journal of Applied Polymer Science*. Vol. 65, p. 2643.

Kim, J.H., Min, B.R., Won, J., Park, H.C., Kang, Y.S. 2001. “Phase Behavior and Mechanism of Membrane Formation for Polyimide/DMSO/Water System”, *Journal of Membrane Science*. Vol. 187, p. 47.

Kishimoto, A., Fujita, H., Odani, H., Kurata, M., Tamura, M. 1960. “Successive Differential Absorptions of Vapors by Glassy Polymers”, *Journal of Physical Chemistry*. Vol. 64, p. 594.

Kleinrahm, R., Wagner, W. 1986. “Measurement and Correlation of the Equilibrium Liquid and Vapour Densities and Vapour Pressure Along the Coexistence Curve of Methane”, *Journal of Chemical Thermodynamics*. Vol. 18, p. 739.

Krüger, K-M., Sadowski, G. 2005. “Fickian and Non-Fickian Sorption Kinetics of Toluene in Glassy Polystyrene”, *Macromolecules*. Vol. 38, p. 8408.

Krüger, K-M., Pfohl, O., Dohrn, R., Sadowski, G. 2006. "Phase Equilibria and Diffusion Coefficients in the Poly (dimethyl siloxane) + n-Pentane System", *Fluid Phase Equilibria*. Vol. 241, p. 138.

Kwapinski, W., Tsotsas, E. 2004. "Determination of Kinetics and Equilibria For Adsorption of Water Vapor on Single Zeolite Particles by a Magnetic Suspension Balance", *Chemical Engineering Technology*. Vol. 27, p. 681.

Lai, J-Y., Lin, S-F., Lin, F-C., Wang, D-M. 1998. "Construction of Ternary Phase Diagrams in Nonsolvent/Solvent/PMMA Systems", *Journal of Polymer Science: Part B: Polymer Physics*. Vol. 36, p. 607.

Magnetic Suspension Balances, Setup Manuel, Rubotherm Präzisionsmesstechnil Gmbh

Mamaliga, I., Schabel, W., Kind, M. 2004. "Measurement of Sorption Isotherms and Diffusion Coefficients by Means of a Magnetic Suspension Balance", *Chemical Engineering and Processing*. Vol. 43, p. 753.

Mark, H.F., 2004. "Polysulfones", in *Encyclopedia of Polymer Science and Technology*, (John Wiley, New York), Vol. 4, p. 1.

McDonough, L.A. 2004. "Microscopy and Spectroscopy of Water Uptake in Polymer Photoresists", PhD Thesis. University of Colorado.

McDowell, C.C. 1998. "Sorption and Transport of Acetone in Random Copolymers of Poly(ethylene terephthalate) and Poly(ethylene 2.6-naphthalate)", PhD Thesis. North Carolina State University.

Mohammadi, R.P. 2005. "Mechanism of Bubble Formation During the Drying of Polymer Films", PhD Thesis. The Pennsylvania State University.

Nalawade, S.P., Picchioni, F., Janssen, L.P.B.M., Patil, V.E., Keurentjes, J.T.F., Staudt, R. 2006. "Solubilities of Sub- and Supercritical Carbon Dioxide in Polyester Resins", *Polymer Engineering and Science*. Vol. 46, p. 643.

Oğuzer Ö. 2005. “Screening and Characterization of Catalytic Composite Membranes for Ethylacetate Production”, Master of Science Thesis. Middle East Technical University, Ankara.

Overbergh, N., Berghmans, H., Smets, G. 1975. “Crystallization of Isotactic Polystyrene Induced by Organic Vapors”, *Polymer*. Vol. 16, p. 703.

Ozbas, B. 2001. “Modeling of Asymmetric Membrane Formation by Dry Casting Method”, Master of Science Thesis. İzmir Institute of Technology, İzmir.

Patton, C.J., Felder, R.M., Koros, W.J. 1984. “Sorption and Transport of Benzene in Poly(ethylene terephthalate), *Journal of Applied Polymer Science*. Vol. 29, p. 1095.

Pawlisch, C.A., Macris, A., Laurence, R.L. 1987. “Solute Diffusion in Polymers. 1. The Use of Capillary Column Inverse Gas Chromatography”, *Macromolecules*, Vol. 20, p. 1564.

Piccinini, E., Baschetti, M.G., Sarti, G.C. 2004. “Use of an Automated Spring Balance For the Simultaneous Measurement of Sorption and Swelling in Polymeric Films”, *Journal of Membrane Science*. Vol. 234, p. 95.

Pfannschmidt, O., Michaeli, W. 1998. “Determination of the Solubility and Diffusivity of Gases in Polymers by Using a High-Pressure Magnet-Suspension-Balance”, Proceedings of the Annular Technical Conference of the Society of Plastics (ANTEC), Atlanta, USA, p. 1918.

Rautenbach, R., Albrecht, R., 1989. *Membrane Processes*, Third Edition, (John Wiley and Sons, Chichester).

Rodriguez, O., Fornasiero, F., Arce, A., Radke, C.J., Prausnitz, J.M. 2003. “Solubilities and Diffusivities of Water Vapor in Poly(methylmethacrylate), Poly(2-hydroxyethylmethacrylate), Poly(N-vinyl-2-pyrrolidone) and Poly(acrylonitrile)”, *Polymer*. Vol. 44, p. 6323.

Romdhane, I.H. 1994. “Polymer-Solvent Diffusion and Equilibrium Parameters by Inverse Gas-Liquid Chromatography”, PhD Thesis. The Pennsylvania State University.

Saby-Dubreuil, A.-C., Guerrier, B., Johannsmann, D. 2001. “Glas Transition Induced by Solvent Desorption For Statistical MMA/nBMA Copolymers-Influence of Copolymer Composition”, *Polymer*. Vol. 42, p. 1383.

Saleh, B., Wendland, M. 2005. “Measurements of Vapor Pressures and Saturated Liquid Densities of Pure Fluids with a New Apparatus”, *Journal of Chemical Engineering Data*. Vol. 50, p. 429.

Sato, Y., Takikawa, T., Takishima, S., Masuoka, H. 2001. “Solubilities and Diffusion Coefficients of Carbon Dioxide in Poly(vinyl acetate) and Polystyrene”, *Journal of Supercritical Fluids*. Vol. 19, p. 187.

Schneider, A., Wünsch, M., Wolf, B.A. 2002. “An Apparatus for Automated Turbidity Titrations and Its Application to Copolymer Analysis and to the Determination of Phase Diagrams”, *Macromolecules*. Vol. 203, p. 705.

Schnitzler, J.V., Eggers, R. 1999. “Changing Properties of Glassy Polymers Due to Diffusion of Supercritical CO_2”, High Pressure Chemical Engineering, Proceedings of the International Meeting of the GVC-Fachausschuβ Hochdruckverfahrenstechnik, Karlsruhe, Germany, p. 57.

Schuhmacher, E., Soldi, V., Pires, A.T.N. 2001. “PMMA or PEO in THF/H_2O Mixture: Phase Diagram, Separation Mechanism and Application”, *Journal of Membrane Science*. Vol. 184, p. 187.

Schult, K.A. and Paul, D.R. 1996a. “Water Sorption and Transport in a Series of Polysulfones”, *Journal of Polymer Science: Part B: Polymer Physics*. Vol. 34, p. 2805.

Schult, K.A. and Paul, D.R. 1996b. “Techniques for Measurement of Water Vapor Sorption and Permeation in Polymer Films”, *Journal of Applied Polymer Science*. Vol. 61, p. 1865.

Subrahmanyan, S. 2003. “An Investigation of Pore Collapse in Asymmetric Polysulfone Membranes”, PhD Thesis. Virginia Polytechnic Institute and State University.

Sugden, S. 1927. “Molecular Volumes at Absolute Zero. Part II. Zero Volumes and Chemical Composition”, *Journal of Chemical Society*. p.1786

Surana, R.K., Danner, R.P., Tihminlioglu, F., Duda, J.L. 1996. “Evaluation of Inverse Gas Chromatography For Prediction and Measurement of Diffusion Coefficients”, *Journal of Polymer Science: Part B:Polymer Physics*. Vol. 35, p. 1233.

Swinyard, B.T., Sagoo, P.S., Barrie, J.A., Ash, R. 1990. “The Tranport and Sorption of Water in Polyethersulphone, Polysulphone, and Polyethersulphone/Phenoxy Blends”, *Journal of Applied Polymer Science*. Vol. 41, p. 2479.

Tihminlioglu, F., Danner, R.P. 2000. “Solvent Diffusion in Amorphous Polymers: Polystyrene-Solvent Systems”, *Journal of Polymer Science: Part B: Polymer Physics*. Vol. 38, p. 1965.

Tihminlioglu, F., Danner, R.P., Lützow, N., Duda, J.L. 2000. “Solvent Diffusion in Amorphous Polymers: Polyvinyl Acetate-Toluene System”, *Journal of Polymer Science: Part B: Polymer Physics*. Vol. 38, p. 2429.

Tompa, H., 1956. *Polymer Solutions*, (Butterworths, London).

Tsai, H-A., Ruaan, R-C., Wang, D-M., Lai, J-Y. 2002. “Effect of Temperature and Span Series Surfactant on the Structure of Polysulfone Membranes”, *Journal of Applied Polymer Science*. Vol. 86, p. 166.

Tweddle, T.A., Kutowy, O., Thayer, W.L., Sourirajan, S. 1983. "Polysulfone Ultrafiltration Membranes", *Industrial and Enginnering Chemistry Product Research and Development*. Vol. 22, p. 320.

Tung, K-L., Lu, K-T., Ruaan, R-C., Lai, J-Y. 2006. "Molecular Dynamics Study of the Effect of Solvent Types on the Dynamic Properties of Polymer Chains in Solution", *Desalination*. Vol. 192, p.380.

Uriarte, C., Alfageme, J., Iruin, J.J. 1998. "Carbon Dioxide Transport Properties of Composite Membranes of a Polyetherimide and a Liquid Crystal Polymer", *European Polymer Journal*. Vol. 34, p. 1405.

van der Wel, G.K., Adan, O.C.G. 1999. "Moisture in Organic Coatings-A Review", *Progress in Organic Coatings*. Vol. 37, p. 1.

van de Witte, P., Dijkstra, P.J., van den Berg, J.W.A., Feijen, J. 1996. "Phase Separation Processes in Polymer Solutions in Relation to Membrane Formation", *Journal of Membrane Science*. Vol. 117, p. 1

Vittoria, V. 1991. "Solvent-Induced Crystallization of Isotactic Polypropylene in Cyclohexane at Different Temperatures", *Polymer*. Vol. 32, p. 856.

Vogel, H. 1921. "Das Temperaturabhangigkeitsgesetz Auf die Viscositat von Flussigkeiten", *Physik*. Vol. 22, p. 645.

Vrentas, J.S., Duda, J.L, 1977. "Diffusion in Polymer-Solvent Systems. I. Reexamination of the Free-Volume Theory", *Journal of Polymer Science: Polymer Physics Edition*. Vol. 15, p. 403.

Vrentas, J.S., 1977. "Diffusion in Polymer-Solvent Systems. III. Construction of Deborah Number Diagrams", *Journal of Polymer Science, Polymer Physics Edition*. Vol. 15, p. 441.

Vrentas J.S. and Duda J.L, 1979. "Molecular Diffusion in Polymer Solutions", *AlChe Journal*. Vol. 25, No.1, p.1.

Wang, P., Schneider, N.S., Sung, N-H. 1999. "Sorption and Diffusion of Organic Vapors in Two Elastomers", *Journal of Applied Polymer Science*. Vol. 71, p. 1525.

WEB_1, 2007. Pall Corporation, 05/09/2007.
www.pall.com

WEB_2, 2007. Sigma-Aldrich Co., 28/08/2007.
www.sigmaaldrich.com.tr

WEB_3, 2007. SARTORIUS's web site, 27/02/2007.
http://www.sartorius.com/fileadmin/sartorius_pdf/alle/APPL-Analytical Weighing Rubotherm-2003-e.pdf

WEB_4, 2006. RUBOTHERM's web site, 16/12/2006.
http://www.rubotherm.de/ENGL/MAINFR021.htm

WEB_5, 2006. ISOSORP's web site, 16/12/2006.
http://www.isosorp.de/startV/frame1.htm

WEB_6, 2007. INSURFACE's web site, 27/02/2007.
http://www.insurface.com/Produkte/Produkte_Anwendungen/P_ISO sorp.htm

Yilmaz, L., McHugh, A.J. 1986. "Analysis of Nonsolvent-Solvent-Polymer Phase Diagrams and Their Relevance to Membrane Formation Modeling", *Journal of Applied Polymer Science*. Vol. 31, p. 997.

Yip, Y., McHugh, A.J. 2006. "Modeling and Simulation of Nonsolvent Vapor-Induced Phase Separation", *Journal of Membrane Science*. Vol. 271, p.163.

Yossef, A.E., Marco, G.B., Timothy, A.B. 2003. “Time-Resolved Fourier Transform Infrared/Attenuated Total Reflection Spectroscopy For The Measurement of Molecular Diffusion in Polymers”, *Journal of Polymer Science: Part B: Polymer Physics*. Vol. 41, p. 2794.

Zhang, C., Cappleman, B.P., Defibaugh-Chavez, M., Weinkauf, D.H. 2003. “Glassy Polymer-Sorption Phenomena Measured with a Quartz Crystal Microbalance Technique”, *Journal of Polymer Science: Part B: Polymer Physics*. Vol. 41, p. 2109.

Zielinski, J.M. 1992. “Free-Volume Parameter Estimations for Polymer-Solvent Diffusion Coefficient Predictions”, PhD Thesis. The Pennsylvania State University.